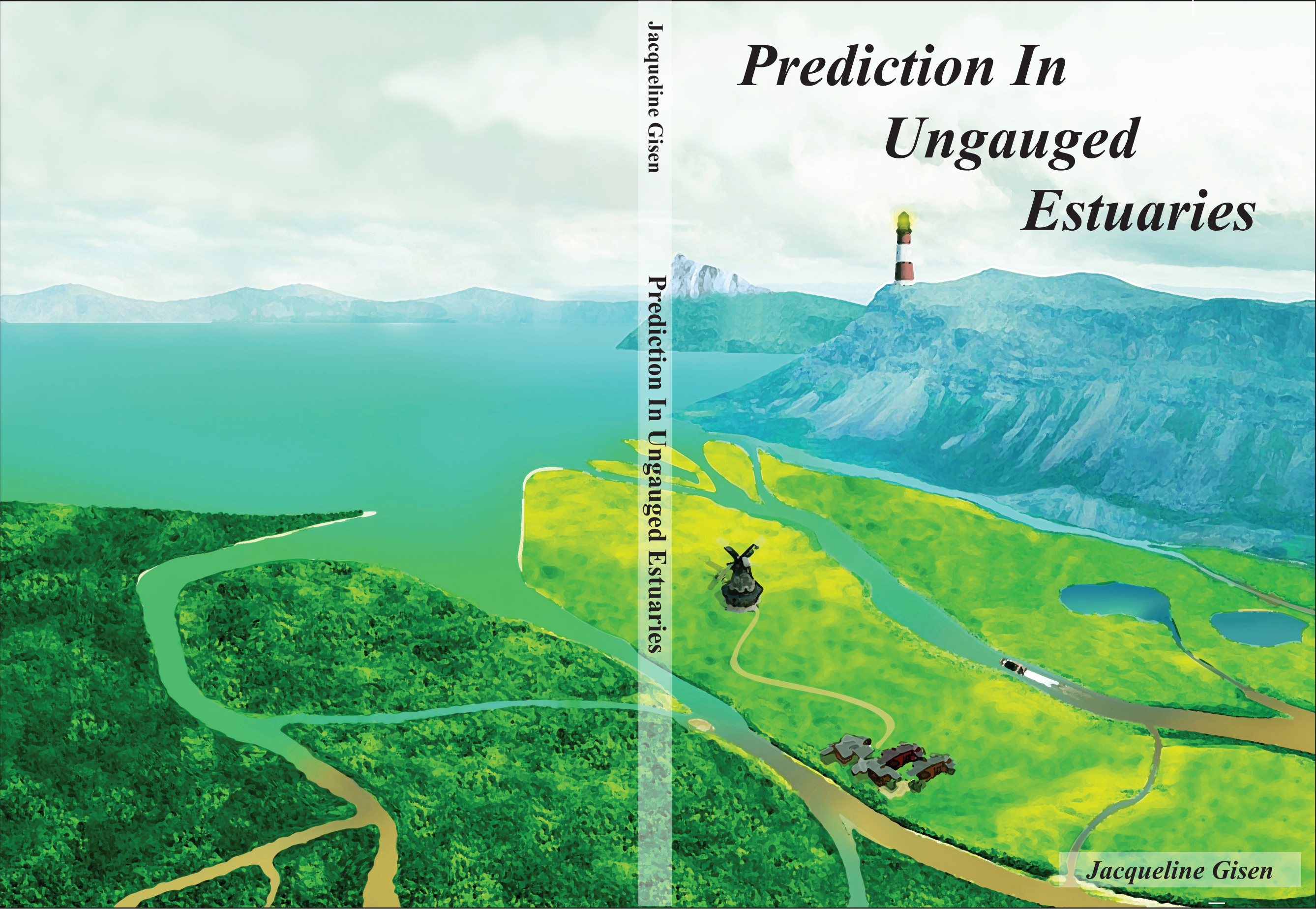


# *Prediction In Ungauged Estuaries*

Jacqueline Gisen

Prediction In Ungauged Estuaries

*Jacqueline Gisen*



# **PREDICTION IN UNGAUGED ESTUARIES**



# **PREDICTION IN UNGAUGED ESTUARIES**

## **Proefschrift**

ter verkrijging van de graad van doctor  
aan de Technische Universiteit Delft,  
op gezag van de Rector Magnificus prof. ir. K. C. A. M. Luyben,  
voorzitter van het College voor Promoties,  
in het openbaar te verdedigen op woensdag 14 januari 2015 om 12:30 uur

door

**Jacqueline Isabella Anak GISEN**

Master in Engineering (Civil - Hydrology and Water Resources), University of  
Technology Malaysia.  
geboren te Sarawak, Malaysia.

Dit proefschrift is goedgekeurd door de promotor:

Prof. dr. ir. H.H.G. Savenije

Samenstelling promotiecommissie:

Rector Magnificus,	voorzitter
Prof. dr. ir. H.H.G. Savenije,	Technische Universiteit Delft, promotor
Prof. dr. ir. Z.B. Wang,	Technische Universiteit Delft
Prof. dr. ir. J.A. Roelvink,	UNESCO-IHE Institute for Water Education
Prof. dr. H.E. de Swart,	Universiteit Utrecht
Prof. dr. P.A.G. Regnier,	Université Libre de Bruxelles
Prof. dr. A.K. Abd Wahab,	University of Technology Malaysia
Dr. A.D. Reeves,	University of Dundee
Prof. dr. ir. N.C. van de Giesen,	Technische Universiteit Delft, reservelid



*Keywords:* alluvial estuary, salinity, hydraulic geometry, predictive equations, bankfull discharge, Malaysian estuaries

*Printed by:* IPSKAMP DRUKKERS

*Front & Back:* Designed by Jacqueline Gisen and Azrol Kassim.

Copyright © 2015 by J.I.A. Gisen

ISBN 978-94-6259-512-5

An electronic version of this dissertation is available at

<http://repository.tudelft.nl/>.

*To my beloved family and friends..*



# PREFACE

**A**N opportunity always comes unexpectedly. It completely depends on us whether to take it or leave it. After working as an engineer in the civil engineering industry for three years, and getting married in between, I thought it was time to settle down. Then, suddenly the opportunity came and I was like “What?! Why now?” Still, a decision had to be made. Pursuing a PhD was never my intention, and to step out from my comfort zone was very difficult. Additionally, making the switch from the industrial sector to the field of academics was not so easy as my brain had become “rusty”. Despite all the worries, I decided to take the challenge even though I foresaw what it would be. Another challenge I needed to overcome was my research topic. I neither had any experience nor knowledge in dealing with estuaries and hence I had to start learning everything from scratch. However, I always keep to this philosophy: Once a decision is made, never regret it; take the challenge and move forward. Fortunately, I was working under the supervision of Prof. Hubert Savenije, who is a very responsible, experienced and knowledgeable researcher in the field of hydrology.

My research concerns the salt intrusion in estuaries, and the focus is to derive predictive methods to simulate the longitudinal salinity distribution. Like most quantitative research, experimental and survey data are crucial. Thus, I was required to carry out field surveys in Malaysia to collect sufficient data for calibration and verification of the salt intrusion analysis. For most people, conducting research that involves on-site measurement is difficult and time consuming. At times, uncertainty during the site investigation yielded unsatisfactory data that required additional site visits. However, I like to say that the most exciting part of doing research is stepping onto fresh ground and experiencing actual site conditions – including observing crocodiles in some of the estuaries! This is far better than simply working behind a desk measuring topographic maps.

Field work experience made me understand more about salt intrusion in estuaries. Fresh water discharge draining into the estuary from upland is the main factor determining how far the saline water intrudes into the system. However, measuring discharge accurately in the tidal region is difficult due to the tidal effect. Hence, the discharge is combined with the dispersion coefficient in the calibration process to fit the simulated salinity curve to the observed data. Dispersion is a mathematical artifact representing the mixing of fluids with different properties. Geometry data are also needed to perform the salt intrusion analysis, and apart from the cross-sectional area, an additional shape indicator is required in the salt intrusion model, known as the Van der Burgh coefficient. Similar to the dispersion coefficient, the Van der Burgh coefficient is also obtained through calibration. This implies that without measurement data, simulating salt intrusion curve is not possible. In an effort to tackle this problem, predictive equations have been developed to estimate the governing parameters (e.g. discharge, estuary depth, dispersion coefficient and Van der Burgh's coefficient) in order to determine the salt intrusion length and simulate the longitudinal salinity distribution. These equations can

become useful tools for water resources management particularly in ungauged estuaries. Moreover, it is now possible for a water manager to make a first estimate of the shape, depth, bankfull discharge, and the salinity distribution in the estuary, given a situation where data is minimal.

After spending slightly more than four years studying estuaries, I still think that I only scratched the surface of the knowledge in this field. However, I am sure that I definitely know better than those who did not study this subject. Last but not least, the life here in Delft is not just about doing research all the time. Sometimes, you need to forget about your PhD to refresh your mind. For me, I liked to visit stunningly beautiful natural sites, most importantly to destinations with less Homo Sapiens so that I could take my time to take photograph of landscapes without distraction. ♡

*Jacqueline Isabella Anak Gisen  
Delft, December 2014*

# NOMENCLATURE

$a$	Cross-sectional convergence length [L]
$a_1$	Cross-sectional convergence length of the seaward reach of estuary [L]
$a_2$	Cross-sectional convergence length of the landward reach of estuary [L]
$A$	Cross-sectional area [L <sup>2</sup> ]
$A'$	Boundary value of the cross-sectional area [L <sup>2</sup> ]
$A_0$	Cross-sectional area at estuary mouth [L <sup>2</sup> ]
$A_1$	Cross-sectional area at inflection point $x_1$ [L <sup>2</sup> ]
$b$	Width convergence length [L]
$b_1$	Width convergence length of the seaward reach of estuary [L]
$b_2$	Width convergence length of the landward reach of estuary [L]
$B$	Estuary width [L]
$B_0$	Width at estuary mouth [L]
$B_1$	Width at inflection point $x_1$ [L]
$B_b$	Bankfull stream width [L]
$B_e$	Effective storage width of estuary [L]
$B_f$	Stream width [L]
$c_0$	Classical wave celerity [L/T]
$c_x$	x-dependent wave celerity [L/T]
$C$	Coefficient of Chezy [L <sup>0.5</sup> /T]
$D$	Longitudinal dispersion [L <sup>2</sup> /T]
$D_0$	Longitudinal dispersion at estuary mouth [L <sup>2</sup> /T]
$D_1$	Longitudinal dispersion at inflection point $x_1$ [L <sup>2</sup> /T]

$D_i$	Dispersion coefficient at HWS, TA and LWS [ $L^2/T$ ]
$D_{50}$	Diameter of the bed material that is exceeded by 50% of the sample weight [L]
$E$	Tidal excursion [L]
$E_0$	Tidal excursion starting from the estuary mouth [L]
$E_1$	Tidal excursion starting from the inflection point [L]
$f$	Friction factor [-]
$f_D$	Darcy-Weisbach friction factor [-]
$F$	Froude number [-]
$F_d$	Densimetric Froude number [-]
$g$	Acceleration due to gravity [ $L/T^2$ ]
$h$	Estuary depth [L]
$\bar{h}$	Averaged estuary depth [L]
$\bar{h}_1$	Averaged estuary depth after the inflection point $x_1$ [L]
$h_0$	Estuary depth at the mouth [L]
$h_b$	Bankfull stream depth [L]
$h_e$	Effective channel depth [L]
$h_f$	Stream depth [L]
$h_{obs}$	Observed depth [L]
$h_{hyd}$	Hydraulic depth [L]
$h_{reg}$	Regime depth [L]
$h_{ideal}$	Ideal depth [L]
$H$	Tidal range [L]
$H_0$	Tidal range at estuary mouth [L]
$H_1$	Tidal range at inflection point $x_1$ [L]
$k$	Mixing mechanism [Prandle, 1981] [-]
$k_b$	Specific discharge ratio [-]
$k_s$	Sediment material coefficient [ $T^{0.5}L^{-0.5}$ ]
$K$	Dimensionless Van den Burgh's coefficient [-]
$K_m$	Dimensionless Manning's coefficient [-]
$L$	Salt intrusion length [L]

$N$	Canter-Cremers Estuary number [-]
$N_b$	Width ratio Canter-Cremers Estuary flood number[-]
$N_Q$	Discharge ratio Canter-Cremers Estuary flood number [-]
$N_r$	Estuarine Richardson number [-]
$N_{r1}$	Estuarine Richardson number with boundary condition at inflection point $x_1$ [-]
$P_b$	Bankfull wetted perimeter [L]
$P_t$	Flood volume [L <sup>3</sup> ]
$Q_b$	Bankfull discharge [L <sup>3</sup> /T]
$Q_f$	The freshet or fresh water flushing [L <sup>3</sup> /T]
$r_s$	Storage width ratio [-]
$s$	Salinity [M/L <sup>3</sup> ]
$S$	Steady state salinity [M/L <sup>3</sup> ]
$S_0$	Steady state salinity at estuary mouth [M/L <sup>3</sup> ]
$S_1$	Steady state salinity at inflection point $x_1$ [M/L <sup>3</sup> ]
$S_i$	Steady state salinity at HWS, TA and LWS [M/L <sup>3</sup> ]
$S_f$	Fresh water salinity [M/L <sup>3</sup> ]
$t$	Time [T]
$T$	Tidal period [T]
$u_0$	Velocity of the fresh water discharge at estuary mouth [L/T]
$U_b$	Velocity of the bankfull discharge [L/T]
$U_f$	Velocity of the fresh water discharge [L/T]
$x$	Distance [L]
$x_1$	First inflection point [L]
$x_2$	Second inflection point [L]
$HW$	High water
$TA$	Tidal average
$LW$	Low Water
$HWS$	High Water Slack
$LWS$	Low Water Slack

$\alpha_0$	Mixing number at estuary mouth [ $L^{-1}$ ]
$\alpha_1$	Mixing number at inflection point $x_1$ [ $L^{-1}$ ]
$\beta$	Dispersion reduction rate [-]
$\beta_0$	Dispersion reduction rate at estuary mouth [-]
$\beta_1$	Dispersion reduction rate at inflection point $x_1$ [-]
$\beta_{rev}$	Dispersion reduction rate for reversed calculation [-]
$\chi$	Friction number [-]
$\delta$	Damping number [-]
$\delta_H$	Damping rate of tidal range [ $L^{-1}$ ]
$\epsilon$	Phase lag between HW and HWS, or LW and LWS [-]
$\eta$	Tidal amplitude [L]
$\gamma$	Estuary shape number [-]
$\lambda$	Celerity number [-]
$\lambda_1$	Length of the tidal wave with boundary condition at inflection point $x_1$ [L]
$\mu$	Velocity number [-]
$\phi_u$	Phase of velocity [-]
$\phi_z$	Phase of water level [-]
$\varphi$	Natural angle of repose of sediment material characteristics [-]
$\rho$	Fluid density [ $ML^{-3}$ ]
$\Delta\rho$	Density difference over the intrusion length [ $ML^{-3}$ ]
$\omega$	Tidal frequency [ $T^{-1}$ ]
$v$	Tidal velocity amplitude [L/T]
$v_0$	Tidal velocity amplitude at estuary mouth [L/T]
$v_1$	Tidal velocity amplitude at inflection point $x_1$ [L/T]

# CONTENTS

<b>1</b>	<b>Introduction</b>	<b>1</b>
1.1	Importance of estuary. . . . .	2
1.2	The importance of estuaries in Malaysia and its main issues . . . . .	2
1.3	Formulation of the problems . . . . .	3
1.4	Objectives of the thesis . . . . .	4
1.5	Outlines of the thesis . . . . .	4
<b>2</b>	<b>Theory on estuary, tide, mixing, salinity, bankfull discharge, and hydraulic geometry</b>	<b>7</b>
2.1	Introduction . . . . .	8
2.2	Shape . . . . .	8
2.3	Tides . . . . .	10
2.4	Mixing . . . . .	12
2.5	Relationship between dispersion and salinity distribution . . . . .	13
2.6	Salinity distribution and one dimensional salt intrusion model. . . . .	15
2.7	Bankfull discharge . . . . .	17
2.8	Hydraulic geometry. . . . .	18
2.9	Conclusion . . . . .	19
<b>3</b>	<b>Establishing Database: Survey and Data</b>	<b>21</b>
3.1	Introduction . . . . .	22
3.2	Survey. . . . .	23
3.2.1	Preliminary observations . . . . .	23
3.2.2	Water level measurement . . . . .	23
3.2.3	Cross-section measurement . . . . .	24
3.2.4	Salinity measurement . . . . .	26
3.3	Discharge data . . . . .	27
3.4	Sources of database. . . . .	29
3.5	Conclusion . . . . .	31
<b>4</b>	<b>Testing a 1-D Analytical Salt Intrusion Model and its Predictive Equations in Malaysian Estuaries</b>	<b>33</b>
4.1	Introduction . . . . .	34
4.2	Study areas . . . . .	35
4.3	Background theories . . . . .	38
4.4	Results and analyses . . . . .	42
4.4.1	Geometry of the estuaries . . . . .	42
4.4.2	Salinity analysis . . . . .	44
4.4.3	Comparison with the predictive equations. . . . .	47
4.4.4	Models performance. . . . .	48

4.5	Correcting for the ungauged watersheds . . . . .	50
4.5.1	Adjustment of the river discharge . . . . .	50
4.5.2	Uncertainty of the predictive models. . . . .	53
4.6	Conclusions. . . . .	54
<b>5</b>	<b>New predictive Van der Burgh and dispersion equations and methods for their determination</b>	<b>57</b>
5.1	Introduction . . . . .	58
5.2	Existing predictive equations . . . . .	58
5.2.1	Van der Burgh's coefficient . . . . .	58
5.2.2	Dispersion coefficient . . . . .	59
5.2.3	Salt intrusion length . . . . .	60
5.3	Methods . . . . .	62
5.3.1	Selecting the dimensionless ratios . . . . .	63
5.3.2	Substitution of predictive equations in the salt intrusion model . . . . .	64
5.3.3	Data . . . . .	65
5.4	Results and analysis. . . . .	66
5.4.1	Predictive equation for the Van der Burgh coefficient $K$ . . . . .	66
5.4.2	Predictive equation for the dispersion coefficient $D$ . . . . .	67
5.4.3	Modified predictive equation for maximum salt intrusion length $L^{HWS}$ . . . . .	70
5.4.4	Longitudinal salinity profiles. . . . .	71
5.5	Discussion . . . . .	71
5.6	Conclusion . . . . .	74
<b>6</b>	<b>Estimating bankfull discharge and depth in ungauged estuaries</b>	<b>75</b>
6.1	Introduction . . . . .	76
6.2	Background theories . . . . .	77
6.2.1	Tidal dynamics analysis . . . . .	77
6.2.2	Hydraulic geometry (regime theory) . . . . .	79
6.3	Methods . . . . .	80
6.3.1	Estimating the runoff of the total drainage basin. . . . .	81
6.3.2	Estimating the depth from tidal hydraulics. . . . .	82
6.3.3	Regime equations . . . . .	86
6.3.4	Estimating the Estuarine flood number $N$ . . . . .	86
6.4	Results and discussion . . . . .	87
6.4.1	Depth estimates . . . . .	87
6.4.2	Verification of the regime theory for width. . . . .	89
6.4.3	Verification of the regime theory for depth. . . . .	89
6.4.4	Verification of the depth to width ratio. . . . .	92
6.4.5	Determining the specific discharge ratio $k_b$ from Canter-Cremers's estuary flood number $N$ . . . . .	92
6.4.6	Discussion . . . . .	94
6.5	Conclusion and recommendation . . . . .	94

---

<b>7</b>	<b>Conclusions and recommendations</b>	<b>95</b>
7.1	Conclusions. . . . .	96
7.2	Limitations and recommendations . . . . .	97
<b>A</b>	<b>Appendix</b>	<b>101</b>
A.1	Compilation of the geometry analysis for the estuaries collected from existing resources (mainly from Savenije [2005, 2012]). . . . .	101
A.2	Data used to develop the predictive equation for the dispersion coefficient $D$ . . . . .	104
A.3	Data and results of the maximum salt intrusion length $L^{HWS}$ . . . . .	106
A.4	Determining the bankfull discharge by comparing the discharge frequency of 20, 10, 2, 1.5 and 1.1 years in relation to the width hydraulic geometry theory based on Simon and Albertson [1963] . . . . .	108
	<b>References</b>	<b>109</b>
	<b>Summary</b>	<b>117</b>
	<b>Samenvatting</b>	<b>119</b>
	<b>Curriculum Vitæ</b>	<b>121</b>
	<b>List of Publications</b>	<b>123</b>



# 1

## INTRODUCTION

### 1.1. IMPORTANCE OF ESTUARY

An estuary has the characteristics of both a river and a sea [Savenije, 2005]. The geographic locations of estuaries are often strategic for the aquatic environment and navigation. Estuaries are rich in nutrients due to the natural fertilizers carried by the river flow and from agriculture activities in the upstream area. These fertilizers serve as nutrients to aquatic plants which again become food for aquatic animals and organisms. With the availability of sufficient nutrients and a calm environment, estuaries have become a superb habitat for aquatic life [Savenije, 2012; Chiras, 2013]. Moreover, the existence of mangrove eco-systems in estuaries allows aquatic animals to nest and breed between the mangroves roots [Faridah-Hanum et al., 2013].

Hence, estuaries provide food and transportation for human need. Many people living near estuaries work as fishermen or fish-farmers in small to medium scale aquaculture. Some estuaries, bays and lagoons, serve as marinas and ports for shipping [Dyer, 1997]. People living near the estuaries also use it as their source for agriculture and fresh water supply. However, the area where the water is extracted is sometimes prone to salt water intrusion [Nguyen et al., 2012; Zhang et al., 2011; Savenije, 2012].

Likewise, estuaries are also prone to pollution. The construction of harbours near the coastal area of estuaries may cause critical impact on the pollution in the area. Sediments runoff from upland areas flowing into estuaries often carry polluted substances with them. The sediments settle on the bed of the estuaries primarily in the transition from fresh to saline water [Dyer, 1997]. This phenomenon allows the pollutant to remain in the estuaries for a long time and creates a polluted situation. Recent studies on the biochemical responses have shown the pollutants such as carbon, phosphate, nitrate, metal and among others, are mainly terrestrial origin (industrial, agriculture, deforestation), which subsequently degrades the water quality particularly the oxygen level in estuaries [Bauer et al., 2013; Volta et al., 2014]. Therefore, more attention should be paid to manage the sustainability of the estuarine resources.

### 1.2. THE IMPORTANCE OF ESTUARIES IN MALAYSIA AND ITS MAIN ISSUES

In Malaysia, the main functions of estuaries are as habitat for mangrove eco-systems and for shipping (harbour development). The mangrove eco-system is very important in Malaysia due to the erosive capacity of monsoon winds (Southwest monsoon and Northeast monsoon) especially on the east coast. Roots of mangroves retain the soil on the banks of the estuaries and protect the coastal area from erosion particularly during the monsoon by attenuating the wave energy when waves pass through them. The reduction in wave energy offers a more stable environment to the estuaries. This protection is essential to keep the land area from flooding by storm surges particularly the areas with agricultural activities such as in the state of Kedah in Malaysia [Ong et al., 1991]. Mangroves also provide home to aquatic life and fireflies. In Kuala Selangor, the fireflies habitation has become a tourist attraction and subsequently contributes to the tourism industry in Malaysia [van Breemen, 2008].

The quiet wave motion in estuaries encourages the construction of harbours and ports for ships and boats to berth. Big ships require a certain depth of channel to navi-

gate, and the sea bed is shallower towards the bank. Thus, a navigation channel is constructed to deepen the bed by dredging the sediments from the estuaries. This action has led to an imbalance in the estuaries where the natural hydrodynamic behaviour between the salt and fresh water has changed [Cai et al., 2012, 2014b].

Due to dredging, saline water intrudes further upstream which may reach irrigation channels in areas where the water is utilized for agricultural purposes. As a result, crops and vegetation die due to salinization. Higher level of salinity in the mangrove swamps may affect the growth of mangroves and subsequently kill the aquatic life. Fireflies are also sensitive to changes in salinity, and this development has declined the chances for them to live and breed [van Breemen, 2008].

Another factor that leads to the depletion in the quality of the estuaries is the increasing population and activities in the developed hinterland [Ibrahim et al., 1996]. For the case of Selangor estuary, the natural condition in the estuary is weakened by the extraction of river discharge upstream to supply water to the residents in Selangor and Kuala Lumpur. Therefore, there will be less discharge of fresh water into the estuary which enhances salt water intrusion further upstream [van Breemen, 2008].

### 1.3. FORMULATION OF THE PROBLEMS

Managing estuaries can be very troublesome, especially in ungauged basins. Until today, most of the estuary basins worldwide are still ungauged except for some very large estuaries such as the Yangtze, Schelde, Elbe, Thames and others. Conducting field surveys to study an ungauged estuary is always time and energy consuming, and may be very expensive. Without substantial funding, it is almost impossible to collect the data needed to investigate the underlying hydrological processes in an estuary. Although some estuaries have been widely explored, there is still no comprehensive compilation of databases accessible for all the gauged estuaries. The only way to obtain the existing data for these estuaries is from the literature (e.g. Savenije [2005, 2012]; Toffolon and Savenije [2009]).

Information on geometry such as cross-sectional areas of an estuary often requires intensive field surveys: either self-conducted or by professional surveyors and this can sometimes be very difficult. The hydrological data such as fresh water discharge on the other hand, can be collected from the authority of the countries to which the estuaries belong. However, the available streamflow stations are commonly situated further upstream from the upper boundary of the estuaries. This has led to the underestimation of the actual fresh water discharge draining into the estuaries. In salt intrusion models, regardless of being analytical or numerical 1-D, 2-D or 3-D models, at least two (e.g. the Van der Burgh coefficient  $K$  and dispersion coefficient  $D_0$ ) or more parameters have to be calibrated to fit the salinity curve against measured salinity data. This means that the longitudinal salinity distribution can be simulated only with the presence of salinity measurements. Savenije [1993a, 2005] provided predictive equations for  $K$  and  $D_0$ , but these are subject to improvement.

Realizing the complications in conducting estuary studies, we have taken the initiative to search for possible methods to simplify the investigation process. This is done by searching for new predictive methods to enable a further understanding of the hydrological processes in estuaries of interest. Improving the existing and developing new

predictive tools would be very useful for water managers and engineers in managing estuaries.

#### 1.4. OBJECTIVES OF THE THESIS

The objectives of the research in this thesis are to seek for solutions to overcome the problems discussed in Section 1.3 which are listed as follows:

1. To extend the database with consistently surveyed estuaries in Malaysia to test and expand the theory.
2. To reorganize and homogenize the existing datasets from the literature and include new data from the surveys into a well-organized database. In the database, the estuaries are classified based on the reliability of the observations, geometry and type of mixing.
3. To Test the applicability of the existing one dimensional analytical salt intrusion model and its predictive methods for the Malaysian estuaries.
4. To improve and further simplify the predictive equations for the Van der Burgh and dispersion coefficient.
5. Finally, to develop methods to predict the bankfull discharge and estuary depth by relating the hydraulic geometry to the tidal dynamics.

It is worth to note that in establishing the predictive methods, we tried to make use of as much readily available or observable information as possible, which is particularly useful for ungauged estuaries.

#### 1.5. OUTLINES OF THE THESIS

This thesis is organized according to the objectives listed, providing background on the theory and survey methods. In this chapter, we briefly discussed the importance of estuaries mainly to mankind, and the problems faced by water managers and engineers in maintaining a healthy estuarine environment. The objectives of the study were summarized to provide some insight in the possible solutions proposed to solve the difficulties in estuary management. Short descriptions of the rest of the chapters in this thesis are as follows:

Chapter 2 introduces the theories applied in developing predictive methods. They are described according to the estuary classification, shape, tides, mixing processes, salinity, bankfull discharge and hydraulic geometry. The general equations adopted in the analyses processes of the studies are introduced.

Chapter 3 explains the processes involved in establishing the estuaries database. Here, we first illustrate the study area of the newly surveyed estuaries in Malaysia. Next, we explain the equipment and methods used in conducting the cross-sectional area, water level and salinity measurements. Subsequently, we discuss on the discharge data and

provide the links and references on where to obtain hydrological data either, from readily accessible databases or by request.

In Chapter 4 we test the existing 1-D analytical salt intrusion model and its predictive equations in the 7 newly surveyed Malaysian estuaries. The longitudinal salinity distributions are plotted against measured salinity curves by calibrating the Van der Brugh and dispersion coefficients. These calibrated variables are later compared to calculated values to validate the performance of the predictive equations. In the discussion section, we introduce an approach to adjust the underestimated discharge data, and how it affects the final results.

In Chapter 5 we revisited the existing predictive equations for the Van der Burgh coefficient  $K$  and dispersion coefficient  $D_0$ . Here, we attempt to improve and simplify the equations by taking into account only the easily measurable independent parameters. The new predictive methods are established on a selection of the most reliable measurements data for calibration. The less reliable data are merely used for verification.

In Chapter 6, we try to find a relation between the regime theory and tidal dynamics processes. We tested the applicability of hydraulic geometry in representing the hydraulic characteristics of an estuary (focusing mainly on the upstream part). Predictive methods are suggested to estimate the averaged estuary depth  $\bar{h}$ , estuarine flood number  $N_b$ , and bankfull discharge  $Q_b$ .

Chapter 7 summarizes the conclusions and the results obtained including the limitations of the developed predictive methods. Recommendations are given for future improvements and studies.



# 2

## **THEORY ON ESTUARY, TIDE, MIXING, SALINITY, BANKFULL DISCHARGE, AND HYDRAULIC GEOMETRY**

## 2.1. INTRODUCTION

THE definition of an estuary is subjective and closely depending on one's opinion [Dyer, 1997]. Over the 60 years, various definitions have been proposed by researchers including Cameron and Pritchard [1963], [Dalrymple et al., 1992], Dionne [1963], Perillo [1995], and others. In short, an estuary can be described as a transition medium between a sea and a river. It has a flat topography and is located most downstream where the river is connected to the ocean environment [Savenije, 2012]. Generally, an estuary consists of a single branch but in some coastal areas such as deltas, it is formed by a multi-network channel. Since an estuary receives water from both the sea and a river, it has characteristics of both storing and transporting water and sediment. Estuaries are naturally calm with little wave action compared to the open sea. However, floods can occur when high river discharge coincides with high tide especially during spring tide and the wet season.

Estuaries are affected by a combination of driving forces around its vicinity, including the tide, waves, river discharge, littoral sediment transport, and density difference between the saline and fresh water. These driving forces are key in determining estuary shape. Estuaries can be classified based on their shape, tidal influence, river influence, geology and salinity properties. Incorporating the different classification of estuary from various sources such as Pritchard [1952b, 1955], Cameron and Pritchard [1963], Pickard [1956, 1961], Fairbridge [1980], Perillo [1995], and Dyer [1997], Savenije [2005] summarized the overall classification as tabulated in Table 2.1.

Table 2.1: Summary of the estuary classification

Shape	Tidal wave	River influence	Geology	Salinity
Bay	Standing wave	No river discharge	-	Sea salinity
Ria	Mixed wave	Small river discharge	Drowned drainage system	High salinity; often hypersaline
Fjord	Mixed wave	Modest river discharge	Drowned glacier valley	Partially mixed to stratified
Funnel	Mixed wave; large tidal range	Seasonal discharge	Alluvial in coastal plain	Well mixed
Delta	Mixed wave; small tidal range	Seasonal discharge	Alluvial in coastal plain	Partially mixed
Prismatic channel	Progressive wave	Seasonal discharge	Man-made	Partially mixed to stratified

Fresh water discharge is one of the most important factors in determining the estuary type. However, this is the most difficult information to measure. Thus, by examining relationships between the measurable data, it would be an advantage to find some predictive measures to estimate parameters that are not directly obtainable.

## 2.2. SHAPE

The geometry of estuaries is generally found in two types: funnel and prismatic. For a tide dominated estuary the seaward geometry has a funnel shape, while a discharge

dominated estuary has nearly straight banks [Savenije, 2005, 2012]. A trumpet shape formation is caused by wave action near the mouth, and for this type of estuary the geometry is analysed in two sections: seaward and landward. In salt intrusion studies, tide dominated estuaries are more of interest as the minimum discharge during the dry season will exacerbate salt water intrusion. Figure 2.1 illustrates the examples of two types of geometry found in general. The estuary shown in Figure 2.1(a) is a single reach estuary that does not experience strong wave action. Figure 2.1(b) on the other hand is the estuary that is strongly affected by wave action near the mouth and is sectioned into two reaches at the inflection point,  $x_1$ .

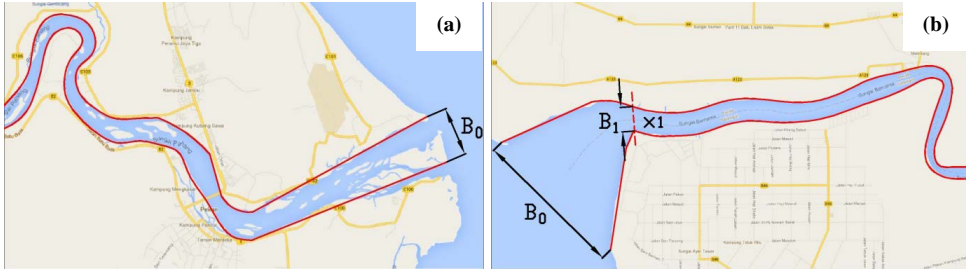


Figure 2.1: Geometry of estuaries in general: a) single reach channel; and b) trumpet or dual reach channel.

Studies to investigate the best representation of estuary shape in a mathematical way has been carried out since decades. As the estuary shape converges gradually towards inland, the relationship between the geometry and distance can no longer be presented in a simple linear function. In the earlier stage, the geometry is analysed with a trapezoidal mesh method. Later, the geometry, particularly the width is presented in exponential function [Friedrichs et al., 1998; Davies and Woodroffe, 2010]. Savenije [1989] suggested that the shape of an estuary generally can be expressed in an exponential function as:

$$A = A_0 e^{-\frac{x}{a}} \quad (2.1)$$

$$B = B_0 e^{-\frac{x}{b}} \quad (2.2)$$

$$h = h_0 e^{\frac{x(a-b)}{ab}} \quad (2.3)$$

where  $A$ ,  $B$  and  $h$  represent the tidally averaged cross-sectional area, width and depth at location  $x$ , while  $a$  and  $b$  are the cross-sectional and width convergence length. Estuaries that do not experience strong ocean waves near the mouth can generally be described by a single reach with only one convergence length, whereas those that experience strong waves near the mouth generally have two reaches with two convergence lengths; a short reach close to the sea with a short convergence length and a long one upstream with a longer convergence length. The geometry analyses proposed in Equations 2.1 to 2.3 have been widely used in many estuaries and the application has been proved to be valid [Nguyen and Savenije, 2006; Zhang et al., 2011; Gisen et al., 2014a].

It is important to note that the shape analysis is performed on tidally averaged geometry data. This implies that the estuary depth is obtained by compensating the measured data in reference to the average tidal level. In tidal dynamics and hydraulic geometry analyses, the second reach of the estuary is more crucial due to the absence of wave action and is most probably in morphological equilibrium. The shape analysis is important to provide boundary conditions for tidal dynamics, salinity and hydraulic geometry analyses.

### 2.3. TIDES

The dynamics of water is strongly interrelated to the geometry of the estuary. Wave action, tide, and fresh water discharge determine the shape of the mouth by forming sand bars, spits or barrier islands, and the funnelling of the estuary (deposition and erosion of sediment process). In return, the water level and velocity of the tide and river flow are strongly influenced by the shape of the estuary [Savenije, 2005, 2012]. In salt intrusion study, the condition of interest is when the river discharge is small and the system is tide dominated. The geometry of estuaries can also be classified according the tides condition as follows [Davies, 1964; Dyer, 1997]:

- Micro tidal estuary:  $H < 2\text{m}$ ; formation of sand bar and pit caused by sedimentation
- Meso tidal estuary:  $2\text{m} < H < 4\text{m}$ ; flood-ebb dominated estuaries
- Macro tidal estuary:  $H > 4\text{m}$ ; strong funnel shaped estuaries

Tides are commonly recognized in three types based on the tidal period: diurnal, mixed diurnal, and semi diurnal. A semi-diurnal tide has two nearly identical tidal cycles in a day (two high and two low water), whereas a diurnal tide has only one complete tidal cycle (one low and high water) [Pond and Pickard, 1983]. For the mixed diurnal, the difference of the tidal range between the two tidal cycles in a day is large and the effect of the smaller tidal range is almost insignificant compared to the larger ones [Gisen et al., 2014a]. Figure 2.2 display the water level oscillation during the tidal cycles in 24 hours for the different tides.

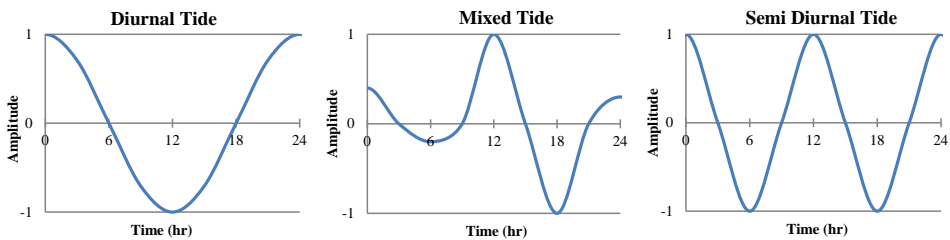


Figure 2.2: The tidal oscillation of the diurnal (left), mixed (middle) and semi diurnal (right) tides.

Other than knowing the tidal period, identifying the types of tidal wave in an estuary is also important. The type of tidal wave in an estuary is strongly influenced by the

geometry: semi-enclosed, prismatic or convergent. A fully standing wave only occurs in semi-enclosed body such as lagoon, where the wave can be entirely reflected when it hits the boundary of the closing structure. This type of tidal wave reaches its highest level when the velocity is zero (see Figure 2.3(a)). An example of standing wave in our regular life is when a person is playing on a swing. On the other hand, a progressive wave occurs only in a fully prismatic frictionless channel with infinite length. The velocity and water level amplitude are in phase as shown in Figure 2.3(b) [Dyer, 1997]. However, none of these apply in funnelled shape estuaries [Gisen and Savenije, 2014].

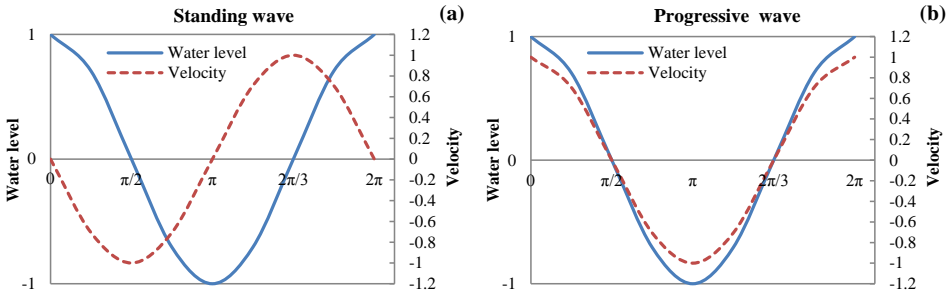


Figure 2.3: Types of tidal waves: a) purely standing wave; b) purely progressive wave.

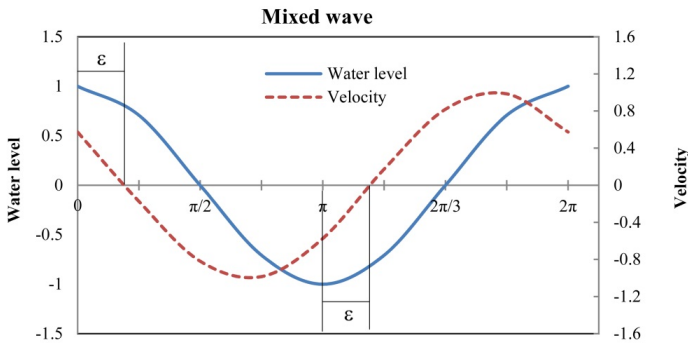


Figure 2.4: A mixed type tidal wave in converging estuary with the phase lag  $\epsilon$  between HW and HWS, as well as LW and LWS [Savenije, 2005, 2012].

In convergent estuaries, the water level always reaches the highest or lowest point before the tidal velocity becomes zero (or slack moment). The delay between the high water (HW) or low water (LW) and high water slack (HWS) or low water slack (LWS) is known as the phase lag  $\epsilon$ , which lies between 0 to  $\pi/2$ . Figure 2.4 illustrates the mixed type tidal wave which occurs in alluvial estuaries. Knowing the phase lag is crucial in tidal dynamics analysis to understand the tidal wave propagation. Furthermore, it is also an important parameter in predicting the average tidal depth in the case where minimal data are available.

## 2.4. MIXING

Substantial research has been done to determine the driving force of the mixing mechanism in an estuary which subsequently regulates the longitudinal salinity distribution. Mixing processes have been studied in several ways including turbulent mixing, transverse mixing, mixing due to gravitational circulation, density driven mixing, tidal driven mixing, wind driven mixing and residual circulation [Fischer, 1976]. Savenije [1993a] categorized mixing mechanisms into three types of dispersion: riverine hydraulics riverine dispersion due to the turbulence caused by the interaction between river flow and changes in geometry, where no tidal influence exists; tide driven dispersion caused by tidal circulation when interacted with geometry, channel roughness, wind effect, and tidal trapping; density driven mixing due to the different density of fluids in the estuary (sea and fresh water), causing gravitational circulation.

Smith [1980] in his work which was later confirmed by West and Broyd [1981] found that density driven dispersion is more likely to occur in wide and strongly convergent estuaries. West and Broyd [1981] claimed that tide driven dispersion occurs in prismatic channel with shallow depth and constant cross-section. This usually refers to the upstream part of the saline area in which the system is gradually dominated by the fresh water discharge. Savenije [1993a] found that both tide and density driven dispersion can occur simultaneously in an estuary. This is true for natural alluvial estuaries which generally have a wide and strong convergent geometry near the mouth, and switch to a less convergent shape upstream as illustrated in Figure 2.5. Near the mouth, where the density gradient is small, the mixing is primarily tide driven, whereas in the region with a strong salinity gradient, the density driven mixing is dominant.

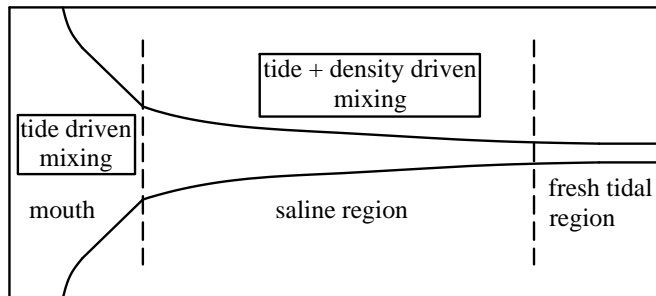


Figure 2.5: Illustration of the regions dominated by the tide and density driven dispersion.

Field observation and laboratory works have been carried out over several decades to find a reasonable description of mixing mechanisms. Making use of 5000 data of velocity and salinity from James River, Pritchard [1954] explained that the salt balance equation can be described by three terms: horizontal advective, vertical- diffusive transport and residual vertical velocity. Bowden and Gilligan [1971] who studied the Mersey Estuary obtained similar findings as Pritchard [1954] and they suggested that the longitudinal velocity can be categorized into net velocity of river flow, tidal variation of tidal cycle, irregularity of estuary shape in lateral direction, and vertical gravitational circulation. Their results showed that the vertical circulation is the main contribution of the net salt

transport at one of the central stations, which is about fifty percent of the total.

Three main laboratory observations were carried out to determine the mixing and dispersion in an estuary including the work by the US Army Corps of Engineers [Ippen and Harleman, 1961; Harleman and Ippen, 1967]– WES Flume, van Rees and Rigger [1969] – Delft Flume and Daniels [1974]. All the laboratory experiments were carried out using rectangular prismatic flumes with constant cross-section. The main difference between these experiments lies in the type of roughness applied to the system. The WES flume has vertical strips attached to the sides, Delft flume attached vertical strips to the bottom (standing upward), and Daniels used rocks to create roughness. Apart from that, the Delft flume had varying Chezy roughness, mean depth, and flume length, whereas Daniels [1974] had different width to depth ratio. Daniels [1974] obtained different results from the former two researchers in which he observed the occurrence of continuous stratification in eight experiments conducted. From the comparison, it can be concluded that the roughness plays an important role in mixing processes, which subsequently influences the dispersion distribution.

Analytical techniques have also been widely used to understand the physical processes of mixing as a cause for dispersion. Researchers who worked on analytical solutions to relate longitudinal mixing and dispersion with salinity distribution in estuary included Hansen and Rattray [1965], Fischer [1972], Thatcher [1972], Prandle [1981], Savenije [1993a], and Kuijper and van Rijn [2011]. Zimmerman [1976], de Swart et al. [1997], and Nguyen et al. [2008] developed analytical measures to investigate the important of tidal pumping in a strong ebb-flood channel with shallow depth and small islands within the main channel. Their models have been tested in the Dutch Wadden Sea, Eems Estuary and Western Scheldt Estuary, respectively.

## 2.5. RELATIONSHIP BETWEEN DISPERSION AND SALINITY DISTRIBUTION

Most researchers focused only on a specific type of mixing mechanism, and only after the 1980's, Prandle [1981], Savenije [1993a], Kuijper and van Rijn [2011] and [Gisen et al., 2014b] lumped the longitudinal mixing mechanism to develop a predictive model to compute the longitudinal distribution of salinity in an estuary. The one dimensional salt balance equation with the effective average tidal and cross-sectional area is written as:

$$A \frac{\partial s}{\partial t} + Q_f \frac{\partial s}{\partial x} - \frac{\partial}{\partial x} \left( AD \frac{\partial s}{\partial x} \right) = 0 \quad (2.4)$$

where  $s = s(x, t)$  is the salinity,  $Q_f$  and  $D$  represent the fresh water discharge and dispersion, respectively. Note that since the positive x-axis points upstream, that the fresh river discharge has a negative value. In steady state condition, the fresh water discharge remains unchanged over time and hence, the integration of Equation (2.4) yields:

$$Q_f (S - S_f) - AD \frac{\partial S}{\partial x} = 0 \quad (2.5)$$

where  $S(x)$  is the steady-state mean tidal salinity. At the upstream boundary of salt intrusion limit, the salinity  $S_f$  is near to fresh water discharge, and it is often close to zero.

From the integration of the salt balance equations, Prandle [1981] found and tested the followings relationship between dispersion and salinity and obtained reasonably successful results.

$$D = D_0 \quad (2.6)$$

$$D \propto \frac{\partial S}{\partial x} \quad (2.7)$$

$$D \propto \left( \frac{\partial S}{\partial x} \right)^k \quad (2.8)$$

Here,  $k$  has the value of 0, 1 and 2.  $D_0$  in Equation (2.6) refers to the dispersion at the estuary mouth. It is worth the attention that Equation (2.7) of Prandle is in agreement with the assumption made by Thatcher [1972] in his numerical one-dimensional model. The different number of  $k$  value represents the type of mixing mechanism of the dispersion:  $k = 0$  means the system is fully tide driven;  $k = 1$  indicates that it is fully density driven; and  $k = 2$  means there is also lateral stratification in density gradient. Savenije [1993a] reported that the result obtained by Prandle is contradicted by many other researchers. Prandle claimed that  $k$  value is much larger than unity in a channel or estuary that has constant cross-section, and  $k$  is zero in deep, wide and strong convergent estuaries. However, others claimed otherwise.

Savenije [1993a] took an effort to investigate and explain the disagreement in the work done by Prandle and others. In his study, he used the ratio of the dispersion and salinity instead of the salinity gradient as proposed by the earlier researchers, so that the relation becomes dimensionless as:

$$\frac{D}{D_0} = \left( \frac{S}{S_0} \right)^K \quad (2.9)$$

where  $S_0$  is the salinity at the mouth. Using data of 16 estuaries worldwide, and modification of the relation between the dispersion and salinity, Savenije found that at the mouth, the dominant mixing mechanism is contributed by the tide, whereas in the middle reach of the estuary the mixing is density-driven. In order to explain the changes of the mixing mechanism along the estuary, an example is given on the Scheldt Estuary as shown in Figure 2.6.

In this plot, it can be seen that the density-driven mixing has a much lower value near the mouth, and only starts to increase to a peak at the middle reach of the estuary. This finding also suggests that the assumption that the dispersion is lower near the mouth and increases upstream is incorrect, and should be the reverse. The basic concept of Savenije's method has later been verified by other researchers among others Nguyen and Savenije [2006], Kuijper and van Rijn [2011] and Nguyen et al. [2012].

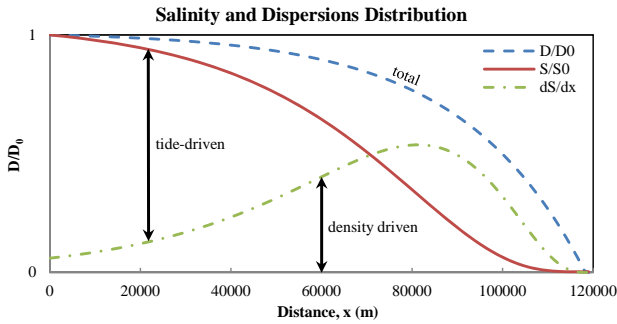


Figure 2.6: Total dispersion, tide-driven dispersion and density-driven dispersion in the Schelde estuary [Savenije, 1993a]

## 2.6. SALINITY DISTRIBUTION AND ONE DIMENSIONAL SALT INTRUSION MODEL

Depending on the hydrologic condition in the estuary region, the well mixed salinity distribution can be represented in four different curves as shown in Figure 2.7. A recession shape occurs in prismatic channels such as a navigation channel or an estuary that receives very high fresh water discharge. An estuary that has a trumpet shape (strongly converged mouth and then slightly converged upstream) usually has a bell shaped salinity curve. A dome shape curve commonly exists in a strongly funnelled channel. A humpback shape curve occurs in an hypersaline estuary [Pritchard, 1952a] where the evaporation exceeds rainfall and fresh water inflow [Savenije, 2005; Dyer, 1997]. These types of salt intrusion curves are illustrated in Figure 2.7.

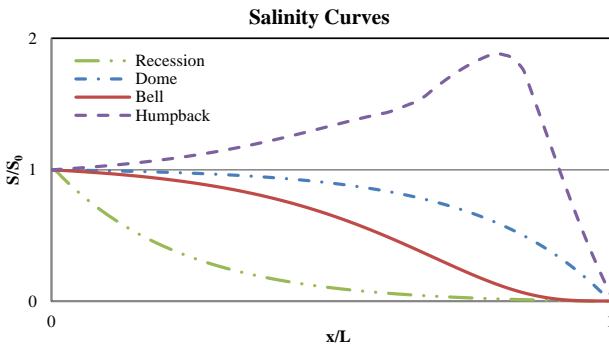


Figure 2.7: Types of well mixed salt intrusion curves.

The analytical one-dimensional salinity model developed by Savenije [1993c, 2005, 2012], presented below, is used to simulate the salinity profile in the estuaries studied. In a steady state situation, the partial temporal derivation in the salt balance equation is zero. Considering a constant fresh water discharge and tidally averaged cross-sectional

area, the salt balance equation can be written as:

$$S_i - S_f = -\frac{A}{|Q_f|} D_i \frac{dS_i}{dx} \quad (2.10)$$

where  $S_i = S_i(x)$  and  $D_i = D_i(x)$  are the salinity and dispersion at high water slack (HWS), tidal average (TA) or low water slack (LWS) condition. Since discharge has a negative value, the absolute value of  $|Q_f|$  is taken in Equation (2.10). It is worth noting that the changes in the cross-sectional area for different tidal conditions are compensated in the variation of the dispersion coefficient  $D_i$ . Making use of the Van der Burgh equation in combination with the salt balance equation, Savenije [2005, 2012] described the relation between dispersion and salinity to be:

$$\frac{dD_i}{dx} = -K \frac{|Q_f|}{A} \quad (2.11)$$

in which  $K$  is defined as the Van der Burgh coefficient (shape factor). Substituting Equation (2.10) into (2.11), the differential equation for the longitudinal salinity distribution is expressed as:

$$\frac{dS_i}{S_i - S_f} = \frac{1}{K} \frac{dD_i}{D_i} \quad (2.12)$$

Integrating Equation (2.12) and removing the subscript  $i$  (representation of HWS, TA, and LWS conditions) leads to:

$$\frac{S - S_f}{S_0 - S_f} = \left( \frac{D}{D_0} \right)^{1/K} \quad (2.13)$$

In Section 2.2, it is shown that the geometry parameters vary exponentially over the distance upstream. Substituting the exponential relation into the integration of Equation (2.11) gives:

$$\frac{D}{D_0} = 1 - \beta \left[ \exp\left(\frac{x}{a}\right) - 1 \right] \quad (2.14)$$

$$\text{where: } \beta = \frac{Ka|Q_f|}{D_0A_0} \quad (2.15)$$

Here  $\beta$  is the dispersion reduction rate. At the salt intrusion limit (upstream) where only fresh water discharge exist, the salinity is very small, and the dispersion coefficient becomes zero. This means that the distance  $x$  is equal to the salt intrusion length  $L$ . Hence, the intrusion length is expressed by:

$$L = a \ln\left(\frac{1}{\beta} + 1\right) \quad (2.16)$$

Equation (2.13) to (2.16) are the general equations used to compute the longitudinal salinity distribution based on Savenije [2005, 2012]'s one dimensional analytical solution.

Determining the salt intrusion length is crucial for estuary or delta water resources management, as most of the fresh water supplies in the area originate from pumping or extracting water from the estuary river. In case where pumping stations have to be built within the salt intrusion prone area, the extraction frequency can be precisely arranged by knowing the intrusion length at different period of tidal oscillation (spring and neap tide), HWS and LWS, and the amount of upstream fresh water discharge drained into the system. However, it is also important to notice that water extractions will subsequently induce further salt water intrusion. This makes the salt intrusion model an important instrument for water resources planning.

## 2.7. BANKFULL DISCHARGE

Since bankfull discharge is the key variable in downstream hydraulic geometry studies in rivers, it is worth to know the definition of bankfull discharge. From engineering perspective, bankfull stage is important for aquatic habitat design, channel restoration design and other river engineering works [Singh, 2003]. Several studies have been done since the 1970s to determine guidelines for the definition of bankfull flow and the streamflow recurrence interval that is able to define bankfull discharge. Dunne and Leopold [1978] claimed that a bankfull stage is defined as the effective discharge level that is able to provide the most optimal condition for channel self-maintenance by governing its sediment transport, bars forming or reforming actions, formation of bends and meanders, and other dynamic processes that leads to the average morphologic characteristics of the channel. Savenije [2003] stated that it is the discharge whereby the accumulated bed sediment is spilled over the banks, forming natural levees and maintaining stable cross-sections. During field observation, the ability to observe the boundary of the bankfull stage is quite a challenge as this is subjective. However, Dunne and Leopold [1978] proposed guidelines to identify bankfull marks based on their field experience. The guidelines include the followings:

- i geometry deviation from vertical bank to flat topography;
- ii changes in side slope from steep to gentle;
- iii changes in types of vegetation;
- iv changes in types of deposited sediment material;
- v boundary of the existence (above bankfull stage) and non-existence (below bankfull stage) of fine debris such as corns, needles, leaves and seeds);
- vi changes in the roughness and smoothness between cobbles and rocks.

For performing the frequency analysis in determining the appropriate bankfull discharge recurrence interval, Williams [1978] suggested that the datasets used should not vary in the amount of years selected to avoid large variability in the results. Nevertheless, it can be concluded from previous research by Williams [1978], Dury [1976], Castro and Jackson [2001], Savenije [2003] and among others that the recurrence interval of bankfull discharge is approximately 1.5 to 2 years of maximum annual flow. Castro and

Jackson [2001] also suggested that the variation in bankfull discharge recurrence interval (regional) depended on several factors such as climate, vegetation, and annual average precipitation.

2

## 2.8. HYDRAULIC GEOMETRY

Regime theory aims to explain relationships between channel characteristics and hydraulic drivers. Channel characteristics involve two sets of parameters including geometric (width, depth and cross-section) and hydraulic (velocity, friction and channel slope) variables. In general, hydraulic geometry studies are categorized into two types: at-a-station and downstream variation. At-a-station hydraulic geometry mainly focuses on the geometric changes in a particular channel cross-section due to a variable discharge over a period of time. The downstream hydraulic geometry considers the variation in the channel form for the entire stream, given a certain discharge frequency generally referred to as bankfull discharge [Lee and Julien, 2006]. Hydraulic geometry is of importance in river engineering because it reflects self-organization of a channel to adjust its cross-section, velocity, and channel slope to the river regime [Lacey, 1930; Singh, 2003].

Over the last century, substantial research has been done on the relations for hydraulic geometry. This work was pioneered by Lindley [1919] in the Indus River Basin. However, it was purely empirical and not well established until it was strengthened by Lacey [1930], who used a large amount of data from the design of irrigation canals in Pakistan. Lacey also formulated the equations for the regime concept empirically, which subsequently were modified by various researchers until today (e.g. Chong [1970]; Leopold and Maddock [1953]; Singh [2003]). Leopold and Maddock [1953] confirmed Lacey's regime theory and expressed the relation between channel geometry (width, depth and velocity) and discharge as power functions. Since then, regime theory has been widely used in river engineering projects to determine the effective dimensions of a channel for transporting a desired amount of discharge and sediment.

The general forms of the power functions are:

$$h_f = cQ_f^y \tag{2.17}$$

$$B_f = dQ_f^z \tag{2.18}$$

$$U_f = mQ_f^n \tag{2.19}$$

where  $h_f$ ,  $B_f$  and  $U_f$  are the depth, width, and flow velocity of a channel, respectively.  $Q_f$  represents the fresh water discharge in the channel. The symbols  $c$ ,  $d$  and  $m$  are the coefficients, while  $y$ ,  $z$  and  $n$  are the exponent of each power function. Since,

$$Q_f = B_f \cdot h_f \cdot U_f \tag{2.20}$$

it follows that the product of the coefficients must be equals to 1, the same applies to the sum of the exponents as below:

$$c \times d \times m = 1 \quad (2.21)$$

$$y + z + n = 1 \quad (2.22)$$

The exponent  $y$ ,  $z$  and  $n$  commonly have a value of approximately 1/3, 1/2 and 1/6. There are conditions that a channel has to fulfil for the application of the regime theory to be valid. According to most literature, the stream must be in stable condition where it has adjusted its dimensions so as to be able to transport or spill its sediment without introducing significant scouring or deposition. Yu and Wolman [1987] claimed that the flow should be uniform along the channel.

## 2.9. CONCLUSION

The above contains the general information on the theories applied in this entire study. Some of the information may not directly related to one another such as the hydraulic geometry theory and salinity model, but the new understanding obtained from the hydraulic geometry theory is useful especially in developing the predictive measures for the salinity distribution analysis. Furthermore, information on the shape and tide are adopted in all the analyses performed.



# 3

## ESTABLISHING DATABASE: SURVEY AND DATA

### 3.1. INTRODUCTION

THE data required for applying the salt intrusion model and to develop the predictive measures have been collected on-site, obtained from local authorities in Malaysia, browsed from literature and reports, and downloaded from online databases. Newly measured data were collected for seven estuaries in Malaysia (see Figure 3.1) during several field surveys. Field measurements were conducted during the dry season at Kurau, Perak, Bernam, Selangor, Linggi, Muar and Endau estuaries, with the assistance of the Institute of Coastal and Offshore Engineering, Universiti Teknologi Malaysia (UTM). The measurements were carried out at spring tide from February to March 2013 and mid-June to early August 2012. The data measured during the field work were: the salinity along the estuary; the variation of the water level; and the cross-sectional areas along the salt intrusion length.

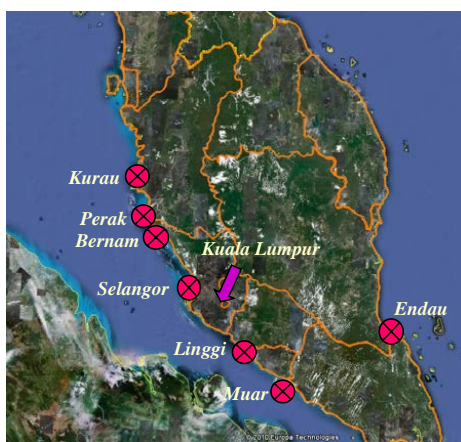


Figure 3.1: Locations of seven newly studied estuaries in the Peninsula Malaysia.

Figure 3.2 displays some of the equipment required for conducting the salinity, tidal dynamics and morphological survey. A portable notebook was used for setting up the divers (conductivity and pressure recorders) on-site. The pre-setup is an important process to make sure the divers are activated properly. If the diver setup is mistakenly initiated, the data recorded for the entire measurements period is unusable. The Diver Office software is complimentary and downloadable from Schlumberger Water Services website. Two Global Positioning Systems (GPS) were used to record the locations of every measurement. This is essential for identifying the positions where divers were installed (in case they are lost), and also for post-processing of salinity and cross-section data. Average water depths were captured using the Plastimo Echotest II handheld depth sounder due to the simplicity of handling.

For the salinity measurements, an YSI EcoSense EC300 Conductivity Meter attached with 10 m cable was employed. This instrument is able to measure water temperature, conductivity, turbidity and salinity simultaneously. It is worth to note that the conductivity and temperature have to be calibrated before use. For highest efficiency, it is encour-



Figure 3.2: Equipment used in conducting filed survey (from top left: netbook, GPS, handheld depth sounder, diver, conductivity meter, and Van Veen Grab)

aged to perform the calibration at least once a year. Sediment samples were collected for each estuaries during the moment of slack (flow velocity = 0) so that the Van Veen Grab could penetrate into the water as vertical as possible. Sampling locations are preferably positioned at a few kilometres upstream from the salinity limit.

Although the equipment shown in Figure 3.2 seems simple, they are adequate to carry out various measurements in cost effective ways. Additionally, sufficient amount of data could be collected within a week, particularly salinity measurement which could be completed in one single day.

## 3.2. SURVEY

### 3.2.1. PRELIMINARY OBSERVATIONS

Before any detailed survey began, preliminary observations were carried out to examine the proper and possible location to install the water level gauging tools. During observations, informal interviews were made with the local people living near the studied area to gain better understanding of the surrounding for safety purposes. Figure 3.3 shows some photos taken during the preliminary observations. Knowing the river conditions and having ideas on the locations of interest beforehand helped the surveyors in making a comprehensive planning to minimize errors and unwanted difficulties during the survey. Moreover, talking to the local people and authority allowed the surveyors to be aware of any possible danger (e.g. the existence of crocodiles in the river) and subsequently adopt the necessary precautions.

### 3.2.2. WATER LEVEL MEASUREMENT

Water level gauges were installed in several locations along the estuary before cross-section and salinity measurements were carried out. In this research, three to five CTD and TD-Divers (pressure recorders used to measure water level) were tied to jetties or tree trunks along the distance until the estimated limit of salt intrusion. A CTD-Diver



Figure 3.3: Photos of the preliminary observations before detailed survey were conducted.

3

has a corrosion proof housing and is able to record conductivity which makes it suitable to be installed at the mouth where salinity levels are the highest. Divers were installed during low water to make sure they were submerged for the whole period even during lowest tide. PVC (Polyvinyl chloride) pipes with holes and fishing ropes were used to hold the divers in place with durable connection to prevent the PVC pipes from being washed away by strong tide. All divers were previously set and initiated to record water level data for every minute. The recording time may be set in different intervals depending on the total period required for the survey. Figure 3.4 displays the detailed sketch of the diver installation.

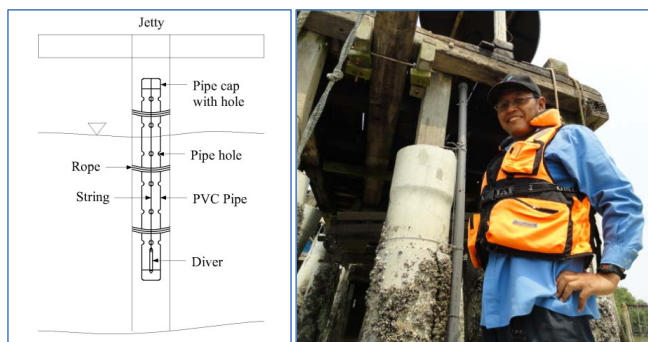


Figure 3.4: CTD diver used to measure the water level and sketch of the installation.

### 3.2.3. CROSS-SECTION MEASUREMENT

Cross-sectional profiles of the estuaries were surveyed by boat with a hand-held sonar system and GPS, after the divers were installed (see Figure 3.5). The cross-sectional areas were determined in relation to the observed mean tidal level and not in relation to some surveying datum or temporary benchmark, which were not available. At least 20 cross-sections were recorded for each estuary, from the mouth until a few kilometres beyond the final stop of the salinity measurements. The distance between each cross-section was taken at approximately 2 km interval. Channel depths were captured for a random interval while the boat was moving slowly from one bank to another, and the position of each measurement point was recorded with GPS. The date and times of measurements were noted precisely in order to correct the observed depth in accordance to the water level recorded by the divers. For the best results, it is recommended to carry out the

measurement near high tide.

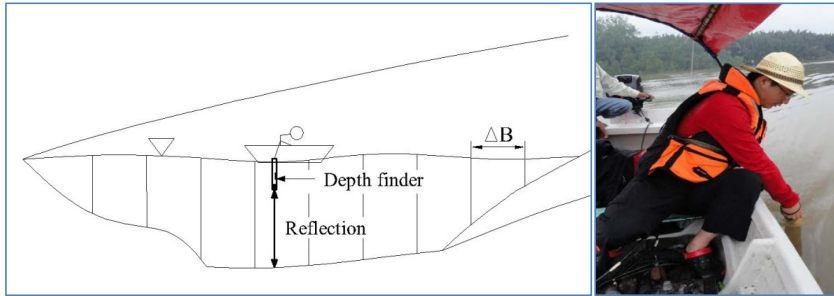


Figure 3.5: Hand-held depth sonar system with method of capturing cross-section measurement.

The geometry analysis was carried out based on Savenije [1986]’s theory for alluvial estuaries, where the change in the geometry of estuary varies exponentially over the distance as shown in Equations (2.1) to (2.3). The sketch of the geometry analyses in the general form are shown in Figure 3.6, and the geometry characteristics of all estuaries considered in this study are listed in Table 3.1.

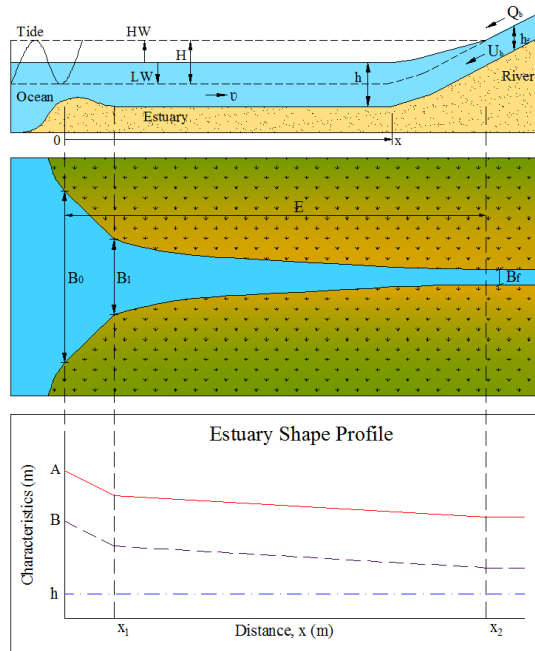


Figure 3.6: Illustration of the longitudinal section, top view and the geometry analysis of an estuary.

Table 3.1: Summary of the geometry analysis for all the estuaries considered in this study.

Estuary	$A_0$ ( $m^2$ )	$A_1$ ( $m^2$ )	$a_1$ (km)	$a_2$ (km)	$B_0$ (m)	$B_1$ (m)	$B_r$ (m)	$b_1$ (km)	$b_2$ (km)	$h_0$ (m)	$h_1$ (m)	$\bar{h}_1$ (m)	$x_1$ (m)
Kurau	1800	660	3.6	46	1400	130	20	1.5	28	1.3	5.2	6.2	3600
Perak	20500	9210	5.0	37	9100	2070	130	2.7	21	2.3	4.5	6.3	4000
Bernam	15800	4460	3.4	25	5600	1270	45	2.9	17	2.8	3.5	5.3	4300
Selangor	2200	1000	3.5	13	1100	270	35	2.0	13	2.0	3.6	3.7	2800
Muar	3300	1580	5.3	100	1800	280	55	2.1	31	1.8	5.6	8.2	3900
Endau	6600	2000	4.0	44	5200	310	72	1.7	44	1.3	6.5	6.5	4800
Rompin	1800	840	25.0	110	450	140	50	16.0	110	4.0	6.1	6.1	19000
Ulu Sedili Besar	1700	670	4.6	38	800	140	35	2.5	49	2.1	4.7	4.1	4300
Maputo	47500	4700	2.2	16	11700	1150	100	2.2	16	4.1	4.1	4.1	5100
Thames	67500	10900	17.0	23	9000	780	50	12.7	40	7.5	13.9	8.2	31000
Corantijn	69000	26800	19.0	64	30000	5000	400	10.0	48	2.3	5.4	6.7	18000
Sinnamary	3300	1120	2.5	39	2300	470	95	1.7	12	1.4	2.4	3.9	2700
MaeKlong	6500	1100	1.8	150	1400	240	150	1.8	150	4.6	4.6	4.6	3200
Lalang	2880	2880	167.0	167	360	360	130	94.0	94	8.0	8.0	10.3	0
Limpopo	1700	1140	50.4	115	550	180	90	18.0	115	3.1	6.3	6.3	20000
Tha Chin	20000	1440	1.9	87	3600	260	45	1.9	87	5.6	5.6	5.6	5000
ChaoPhya	4600	3100	30.0	130	860	470	200	20.0	130	5.4	6.5	6.5	12000
Edisto	14000	5150	2.0	15	3400	1250	60	2.0	15	4.1	4.1	4.1	2000
Elbe_Flanders	82000	27300	30.0	70	19000	3040	350	18.0	80	4.3	9.0	8.5	33000
Elbe_Kuijper	46000	46000	66.0	66	4500	4500	350	66.0	66	10.2	10.2	10.2	0
Elbe_Savenije	43000	43000	66.0	66	20000	2880	350	16.0	50	2.2	9.3	11.7	0
Pangani	9300	860	1.3	15	2900	270	35	1.3	15	3.2	3.2	3.2	3100
Rembau Linggi	5100	1500	0.4	8	1100	320	25	0.4	13	4.6	4.6	3.2	500
Landak	2000	2000	60.0	60	230	230	100	60.0	60	8.7	8.7	8.7	0
Delaware	255000	255000	41.0	41	37655	37655	120	42.0	42	6.8	6.8	6.4	0
Westerschelde	150000	150000	27.0	27	16000	16000	50	27.0	27	9.4	9.4	9.4	0
Pungue	14500	14500	18.5	19	5200	5200	50	18.5	19	2.8	2.8	2.8	0
Incomati	7900	1070	7.5	40	3950	380	22	6.4	40	2.0	2.8	2.8	15000
Solo	2070	2070	226.0	226	225	225	95	226.0	226	9.2	9.2	9.2	0
Eems	120000	120000	19.0	19	31623	31623	55	19.0	19	3.8	3.8	3.8	0
Tejo	100000	100000	13.0	13	20000	20000	180	13.0	13	5.0	5.0	5.0	0
Gambia	100000	35700	32.0	96	14000	3700	110	25.0	100	7.4	9.5	8.8	33000

### 3.2.4. SALINITY MEASUREMENT

Salinity measurements were carried out during High Water Slack (HWS-when the flow changes direction after high water) and Low Water Slack (LWS-when flow changes direction after low water) by a moving boat technique, moving with the speed of the tidal wave at HWS and LWS (see Savenije [2005, 2012]). The maximum and minimum salinity curves at HWS and LWS were thus observed, representing the envelopes of the salinity variation during a tidal cycle. A conductivity meter attached to a 10m cable was used to measure the salinity at every meter over the vertical during moments of slack. It is worth to note that a modest weight needs to be attached on the cable to enable the probe to penetrate into the water. Without the weight, the probe would tend to float on the water surface and make the measurement from the bottom not possible. A detailed sketch of the salinity measurement is presented in Figure 3.7. The measurements started from the mouth moving upstream, keeping pace with the tidal wave until the salinity level reached 0.1 ppt. Figure 3.8 shows photos of the slack moment when the tidal velocity is zero. This is also when the salinity level is at maximum.

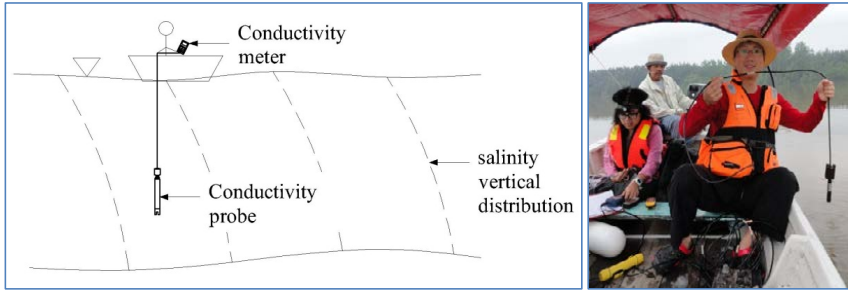


Figure 3.7: A portable conductivity meter used to measure the salinity level along the estuary with moving boat technique.



Figure 3.8: Slack moment when the flow is stagnant (velocity = 0)

### 3.3. DISCHARGE DATA

Information on streamflow is crucial in this research, as salt intrusion is strongly dependent on the balance between the tides and fresh water discharge draining into the estuary. Tidal information can be easily obtained from various tide prediction sources online, but not discharge information. Fresh water discharge is nearly unmeasurable in the tidal region, and the nearest streamflow stations available are often located further away from the tidal limit. Furthermore, to measure the discharge just outside the tidal region is time and energy consuming. As an alternative, discharge data was requested and obtained from existing open sources online databases and from the Department of Irrigation and Drainage, Malaysia (DID) – the authority in charge of the river networks in Malaysia. Since the discharge data are only collected from the nearest gauging stations, they do not cover the total discharge drained from the entire basins into the estuaries system. Nevertheless, this is considered sufficient for the initial analysis process.

For the salt intrusion study and the development of the predictive dispersion equation, daily discharge data for the particular date of each salinity measurement is required. This is due to the sensitivity of the salt intrusion length to the variation in fresh water discharge. Moreover, the variation in discharge also affects the type of mixing which subsequently influences the dispersion in estuary. Estimating daily discharge at the tidal limit is complicated because more factors have to be taken into account such as time-lag for the runoff to flow from the upstream to downstream region. Without

comprehensive surveying data to perform rainfall runoff and hydrological model, it is difficult to compute the discharge accurately.

In order to compensate for this problem, the discharge data adopted in this study is based on mean monthly streamflow data and yearly maximum discharge frequency. Figure 3.9 shows the maximum, mean and minimum monthly discharge distribution for the time period available of the Malaysian estuaries. From this figure, we can easily identify the duration of the dry and wet seasons. With this information, the best period of when to carry out the salt intrusion survey is acknowledged. In Chapter 6, bankfull discharge is used for the development of the depth and discharge predictive equations. In the process of determining the bankfull discharge recurrence interval, annually maximum frequency analysis was performed using Gumbel distribution. Discharge data of 23 available gauging stations were analysed for the Malaysian estuaries. Figures 3.10(a) to (i) display the frequency analysis for 7 newly and two reported surveyed estuaries in Malaysia (only 9 main stations were shown).

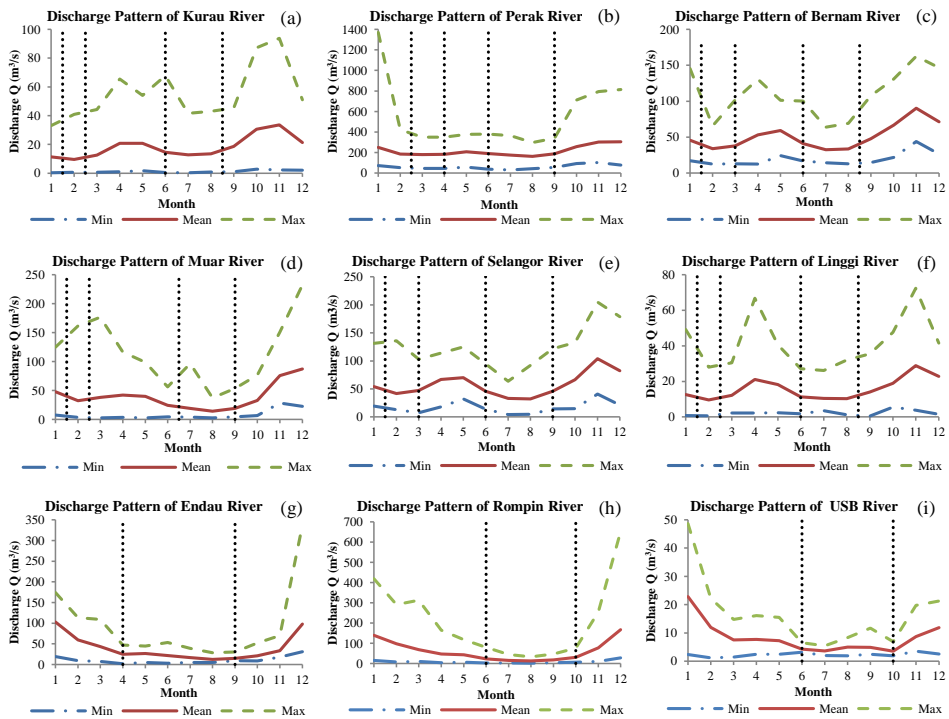


Figure 3.9: Long-term monthly discharge distribution of seven newly and two reported surveyed estuaries in Malaysia: a) Kurau River (1961-2012); b) Perak River (1961-2012); c) Bernam River (1961-2012); d) Selangor River (1961-2012); e) Linggi River (1961-2010); f) Muar River (1976-2012); g) Endau River (2000-2012); h) Rompin River (1983-2012); and i) Ulu Sedili Besar River (2006-2012).

Figure 3.11 displays the long-term yearly discharge distribution of the Malaysian estuaries. As can be seen in the plots, the data available for Endau and Ulu Sedili Besar river basin is only about 6 and 12 years, respectively. This indicates that the information

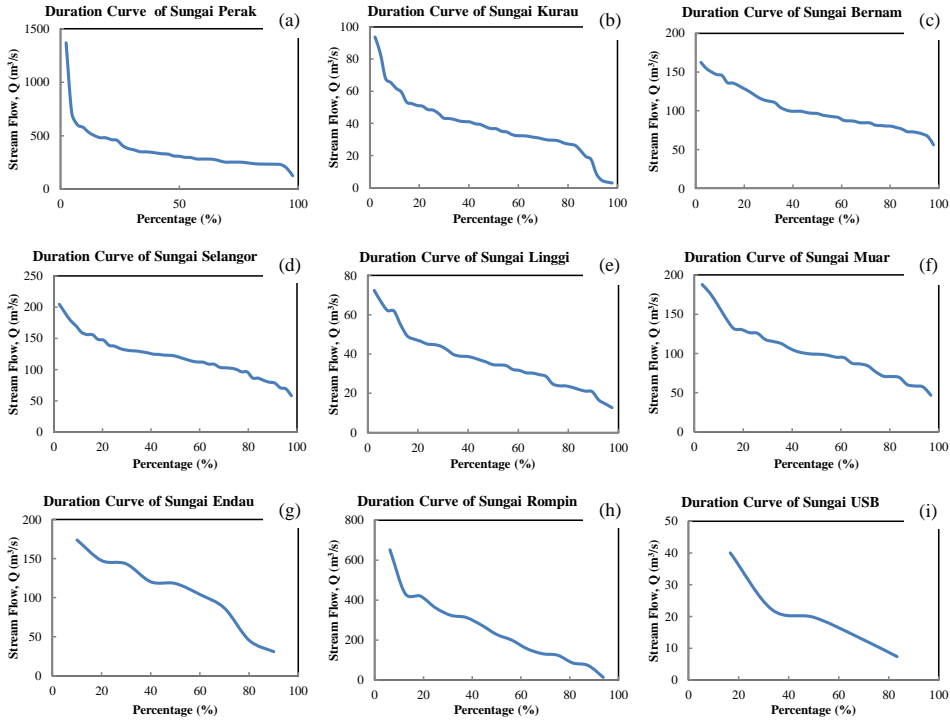


Figure 3.10: Durations curve of seven newly and two reported surveyed estuaries in Malaysia computed using Gumbel distribution: a) Kurau Estuary; b) Perak Estuary; c) Bernam Estuary; d) Selangor Estuary; e) Linggi Estuary; f) Muar Estuary; g) Endau Estuary; h) Rompin Estuary; and i) Ulu Sedili Besar Estuary.

gained from this data may be limited. However, this does not mean they are unusable. Hence, in this study some adjustments have been made to the total discharge information to reduce the underestimation of the streamflow in the estuary.

### 3.4. SOURCES OF DATABASE

Substantial amount of data on estuary shape, salinity, and tidal dynamics were collected from various sources including on-site survey, literature, official reports, and accessible online databases. A total of 30 estuary geometries with 95 salinity measurements worldwide were compiled and re-analysed. However, not all the datasets were used in all the analyses performed in this research. Selection of datasets was done based on the completeness of the data for required boundary condition parameters in each analysis. The only analysis which utilized the entire datasets is the development of the predictive equations for dispersion at tidal average condition.

The purpose of developing predictive methods in this research is to enable the estimation of important parameters such as discharge and dispersion in estuary with minimal data available. The advantage of the advancement in Information Technology (IT)

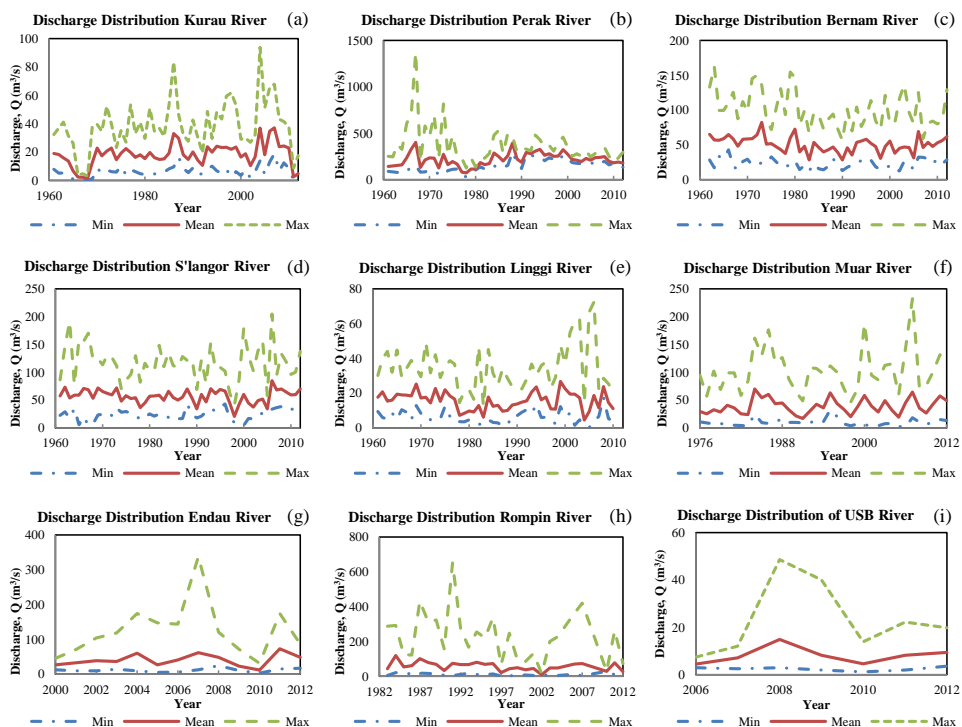


Figure 3.11: Long-term yearly discharge distribution of seven newly and two reported surveyed estuaries in Malaysia: a) Kurau River (1961-2012); b) Perak River (1961-2012); c) Bernam River (1961-2012); d) Selangor River (1961-2012); e) Linggi River (1961-2010); f) Muar River (1976-2012); g) Endau River (2000-2012); h) Rompin River (1983-2012); and i) Ulu Sedili Besar River (2006-2012).

nowadays is that data and information can be easily accessed and utilized. In developed countries such as United Kingdom, Netherlands, Germany and United States, hydrological data has been made free to download. As for most countries, hydrological data is still considered confidential for national security reasons. However, some are still accessible through official application processes.

Regardless of countries, cross-section data are the most difficult to obtain. They have to be requested directly from the authority, surveying company, other researchers or self-conduct field survey. Fortunately, with the free application of Google Earth and Bing Map, the plan view image can be used to estimate the top width for the entire river network of an estuary. As for the topography information, digital elevation model (DEM) can be downloaded without charges from United State Geological Survey (USGS) database. The best resolution of DEM available these days is  $30\text{ m} \times 30\text{ m}$  grid pixels. Tables 3.2 lists the types of data used in this research that are collected from various sources. Although it seems that lots of data are available online, information for important parameters such as average water depth and discharge in estuary are still not conveniently accessible. Hence, it would be a great advantage to develop several approaches

Table 3.2: Types of data collected from various accessible databases and their links of references.

Data	Source
Discharge	1, 4, 5, 10
Water Level	1, 2, 4, 5, 6, 10, 11
Tide	3, 8, 9, 10
Salinity	10, 11
Geometry	7, 10, 11
Topography	4, 7

No	Source	Reference
1	Department of Drainage and Irrigation Malaysia (DID)	<a href="http://h2o.water.gov.my/v2/index.cfm">http://h2o.water.gov.my/v2/index.cfm</a>
2	National Hydraulic Research Institute of Malaysia (NAHRIM)	<a href="http://www.nahrim.gov.my/index.php/en">http://www.nahrim.gov.my/index.php/en</a>
3	Department of Survey and Mapping Malaysia (JUPEM)	<a href="https://www.jupem.gov.my/index.php?action=main">https://www.jupem.gov.my/index.php?action=main</a>
4	United State Geological Survey (USGS)	<a href="http://www.usgs.gov/">http://www.usgs.gov/</a>
5	Centre for Ecology & Hydrology UK (CEH)	<a href="http://www.ceh.ac.uk/index.html">http://www.ceh.ac.uk/index.html</a>
6	Wasser- und Schifffahrtsverwaltung des Bundes - Germany	<a href="http://www.wsv.de/">http://www.wsv.de/</a> <a href="http://www.portal-tideelbe.de/">http://www.portal-tideelbe.de/</a>
7	Google Earth/Map	<a href="https://www.google.com/maps/preview">https://www.google.com/maps/preview</a> For Google Earth, download free software online
8	United Kingdom Hydrographic Office (UKHO)	<a href="http://www.ukho.gov.uk/easytide/">http://www.ukho.gov.uk/easytide/</a>
9	Worldwide Online Tides and Currents Predictions	<a href="http://tides.mobilegeographics.com/">http://tides.mobilegeographics.com/</a> <a href="http://www.tides4fishing.com/">http://www.tides4fishing.com/</a> <a href="http://www.tide-forecast.com/">http://www.tide-forecast.com/</a>
10	Literature, official reports and old database	Mainly Savenije, Toffolon, Cai, Gisen <a href="http://salinityandtides.com">http://salinityandtides.com</a> <a href="http://www.ing.unitn.it/~toffolon/dbest">http://www.ing.unitn.it/~toffolon/dbest</a>
11	Self-conduct survey	Gisen

that can be applied to estimate these parameters with minimal data available.

### 3.5. CONCLUSION

Field surveys are important particularly for verification purposes. Measurements must be carried out with good planning to avoid large measurement errors, waste of time, money and energy. Data is essential in almost every study and without it, research works can be impossible to continue. However, collecting data through field work often requires substantial amounts of funds and are time consuming. Fortunately, with the advancement in information technology, we nowadays are able to obtain data by downloading it through some official database. Some of the data are accessible without charge. Nevertheless, downloadable data are sometimes not enough or have low accuracy. Hence in this study, we aimed to find some approach to improve the data obtained and develop predictive measures with minimal data requirement.



# 4

## TESTING A 1-D ANALYTICAL SALT INTRUSION MODEL AND ITS PREDICTIVE EQUATIONS IN MALAYSIAN ESTUARIES

*Little is known about the salt intrusion behaviour in Malaysian estuaries. Study on salt intrusion generally requires large amounts of data especially if 2-D or 3-D numerical models are used. In poor data environments, 1-D analytical models are more appropriate. A fully analytical 1-D salt intrusion model which is simple to implement and requiring minimal data, was tested in six previously un-surveyed Malaysian estuaries (Kurau, Perak, Bernam, Selangor, Muar and Endau). The data required for this method can be collected during a single day of observations. Site measurements were conducted in these estuaries during the dry season (June-August 2012 and February-March 2013) near spring tide. Data on cross-sections (by echo-sounding), water levels (by pressure loggers) and salinity (by moving boat) were collected as input to the 1-D salt intrusion model. This chapter demonstrates a good fit between the simulated and observed salinity distribution for all six estuaries. Additionally, the two calibration parameters (the Van der Burgh's coefficient and the boundary condition for the dispersion) were compared with the existing predictive equations. Since gauging stations were only present in some nested catchments in the drainage basins, the river discharge had to be up-scaled to represent the total discharge*

---

This chapter is based on:

Gisen, J. I. A., H. H. G. Savenije, R. C. Nijzink, and A. K. Abd. Wahab (2014), Testing a 1-D Analytical Salt Intrusion Model and its Predictive Equations in Malaysian Estuaries., Hydrological Sciences Journal, (accepted).

contribution of the catchments. Subsequently, the correspondence between the calibration coefficients and the predictive equations was good, particularly in view of the uncertainty in the river discharge data used. This confirms that the predictive salt intrusion model is valid for the cases studied in Malaysia. The model provides a reliable predictive instrument which the water authority of Malaysia can use for making decisions on water abstractions or dredging.

#### 4.1. INTRODUCTION

GENERALLY, salt intrusion offers a threat to people living in or near estuaries. According to statistics provided by the Malaysian Ministry of Science, Technology and Environment in 2000, over 60% of Malaysia's population (concentrated in most of the major cities) lives within or near an estuarine environment [Ong et al., 1991]. Salt water intrusion deteriorates water supply quality and makes it unusable for daily consumption or agricultural activities. Besides that, change in the intrusion may disturb the balance in the estuarine ecosystem, which may cause the mangroves to grow slower or even die, reduce variety of aquatic life, or destroy the habitat of fireflies [van Breemen, 2008]. According to Van Breemen, the fireflies population in Malaysian estuaries is going towards extinction, one of the factors being salt intrusion. Changes in salinity levels may retard the growth of the berembang trees (*sonneratia caseolaris*), which serve as the natural breeding and displaying grounds for fireflies. Hence, a successful and effective management is required to preserve the sustainability of the resources in the estuarine ecosystem [Ibrahim et al., 1996].

Previous research indicated that the salinity, the mixing mechanism in estuaries, and the salt water intrusion length (total distance salt water travels into the river system) are strongly dependent on estuary shape, tidal behaviour, and the amount of fresh water discharge from the river [Ippen and Harleman, 1961; Dronkers, 1982; Savenije, 1986, 1993c; Shaha and Cho, 2009]. For example, water extraction and fresh water retention for aquaculture, in conjunction with sea level rise and reduced rainfall induced by climate change, will cause salinity to intrude further upstream. Several studies on salt intrusion have been carried out in South East Asia's estuaries including the Mekong Estuary, the Chao Phya Estuary, and the Red River Delta. Most of the earlier studies on Malaysian estuaries merely focused on how sedimentation (deposition of soil and sand into the river) affected the topography and vice versa. Only few have investigated the consequence of these changes in the context of salt intrusion [Ibrahim et al., 1996].

There are several one-dimensional analytical (e.g., Kuyper and van Rijn [2011]) and two or three-dimensional numerical models available today (e.g., MIKE 21, DELFT 3D, SWIM, and HYDRUS) which can be used to analyse salt intrusion in estuaries. In this present research, the analytical salt intrusion model developed by Savenije [1986, 1993b, 2005, 2012] is used because it is simple and requires a minimum amount of data. Being fully analytical, an additional advantage is that it provides a comprehensive understanding of the entire salt intrusion process. Moreover, the reliability of this salt intrusion model has been extensively tested in a wide number of estuaries around the world, including the Maputo and Incomati [Savenije, 1986], the Gambia [Savenije, 1988; Risley et al., 1993; Irvine et al., 2007], the Chao Phya [Savenije, 1989], the Yangtze [Zhang et al., 2011], the Red River Delta [Nguyen et al., 2012] and the Mekong [Nguyen and Savenije,

2006]. Nguyen and Savenije [2006] showed that this salt intrusion model can be utilized not only in a single river channel estuary but also in multiple branch delta estuaries. Nevertheless, the model also has some limitations. Savenije [2012] stated that the predictive equations of the model are still subject to improvement, and work best in natural alluvial estuaries. The predictive equations were derived on the basis of a variety of data from literature and field measurements that were not always consistent or that had incomplete information.

The aims are to test the effectiveness of the existing salt intrusion model at six previously un-surveyed estuaries in Malaysia and to discover if any modification is required. In order to successfully perform the analysis using the analytical model, real time data is required. Hence, on-site data collections of the topography and salinity concentration in the estuaries were carried out during the dry season near spring tide in the period June to August 2012 and February to March 2013. Shape (geometry) and salinity analysis were performed on each of the estuaries. The calibrated dimensionless parameters were subsequently compared to the predictive equations, to test their applicability in Malaysia estuaries. Finally, adjustments were made to cater for the ungauged parts of the catchments draining on the estuaries.

## 4.2. STUDY AREAS

In this study, six previously un-surveyed estuaries in Malaysia were selected: the Kurau, the Perak, the Bernam, the Selangor, the Muar and the Endau. Moreover, the runoff of the catchments draining on these estuaries is insufficiently known. Only some nested catchments within the drainage basins are gauged, but large parts are not. All these estuaries except the Endau are located on the west coast of Peninsular Malaysia, and along the Malacca Strait where the mouth faces the east coast of Sumatra, Indonesia (Figure 4.1). The Endau Estuary is located at the east coast of the peninsular facing the open South China Sea. The rivers draining on these estuaries are between 90 to 400 kilometres long, with a catchment area of 2000 to 14000 square kilometres as tabulated in Table 4.1.

Table 4.1: General information of the surveyed estuaries (Source: Economic Planning Unit Malaysia [1982].)

No	Estuaries	Coastline	State	River Length (km)	Catchment Area (km <sup>2</sup> )
1	Kurau	west	Perak	100	3255
2	Perak	west	Perak	400	14000
3	Bernam	west	Selangor	200	3335
4	Selangor	west	Selangor	120	1960
5	Muar	west	Johore	230	6160
6	Endau	east	Johore	95	4740

Most of the studied estuaries are natural with little human interference except for the Muar. The Kurau is surrounded by paddy field while agriculture is the main economic activity. Medium scale commercial fishing and aquaculture farming can also be found in this estuary. The Perak and Bernam estuaries are situated next to each other separated by a small village town named Bagan Datoh. Both catchments are covered with oil palm

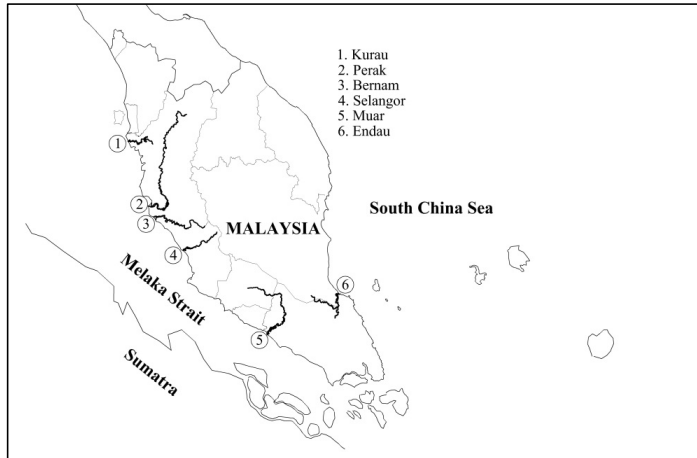


Figure 4.1: Overview of the river estuaries studied (not to scale): rivers are highlighted in darker lines.

plantations which is also the main economic activity. In the Bernam Estuary, the wide river mouth provides a good environment for medium scale commercial fishing. The Selangor estuary is a natural park which is famous for watching fireflies [van Breemen, 2008]. Moreover, it is also well-known for its large-scale commercial fishing activity. As for the Muar estuary, the densely populated Muar town is situated on the banks of the river mouth. This estuary is relatively deep due to dredging and sand mining. Some areas surrounding the Endau estuary are covered by paddy field while the majority has remained untouched and covered with forest reserves. There is a famous Endau-Rompin National Park situated at about 100 km upstream from the river mouth. The Endau River serves as the border between Pahang and Johore states. Figures 4.2(a) to (f) present an aerial view of all the estuaries. In Figure 4.2(d), there are three fresh water inlets situated at 3 km, 11 km and 15 km along the Selangor river estuary. These inlets drain water into the river during heavy rain to prevent the land from flooding.

All estuaries on the west coast experience a dominant semi-diurnal tide with a 12.4 hour tidal cycle. The pattern of the tidal oscillation remains the same throughout the year. The Endau estuary, which is situated on the east coast, has a mixed-diurnal and semi-diurnal tide. The difference between the two tidal behaviours can be seen in Figure 4.3(a) and (b). At spring tide, the tidal amplitude of the Kurau, Perak, Bernam, Selangor, Muar and Endau estuaries ranges from 2 to 4 meters, while at neap tide it varies from 0.2 to 1 meter. Every year from June to September, the west coast estuaries are slightly affected by the Southwest Monsoon from the Indian Ocean. The impact is small because the coastline is protected by Sumatra Island, and as a result, the salinity in Malacca Strait is lower as the fresh water discharge from the rivers draining towards the straits has diluted the salt water. From February to March, the west coast estuaries are not affected by the Northeast Monsoon, but the Endau estuary is considerably affected.

Besides the tide, salt intrusion mainly depends on the amount of fresh water drained into the estuary. Generally, the dry season in Malaysia lasts from May to August, and the



Figure 4.2: Aerial view of the estuaries from Google Earth (not to scale): a) Kurau Estuary; b) Perak Estuary with sand bar; c) Bernam Estuary; d) Selangor Estuary with three drainage sluices; e) Muar Estuary; f) Endau Estuary with one estuary tributary marked in dotted line.

wet season is from September to April [van Breemen, 2008]. Nevertheless, in the west coast of the Peninsula, there is a short dry period which takes place in February. An accurate estimation of the fresh water discharge in the tidal region is difficult to obtain. Large parts of the catchments are ungauged and most of the stream flow stations are located about 100 km or further from the estuary mouth. Based on the nearest stream flow stations available, the monthly averaged discharges for each of the river estuaries during dry and wet seasons are as displayed in Table 4.2.

All estuaries have a clear trumpet shape. The wide mouth of the estuaries is wave dominated, whereas the gradually converging estuary channel emerges from the balance between tide and river discharge. In term of salinity mixing mechanism, Ibrahim et al. [1996] mentioned that the estuaries on the centre west coast of Peninsular Malaysia are of the partially-mixed type. However, site observations showed that four of the estuaries (Kurau, Bernam, Muar and Endau) were well-mixed, while the other two estuaries (Selangor and Perak) were partially-mixed (meaning that there is a gradual increase of

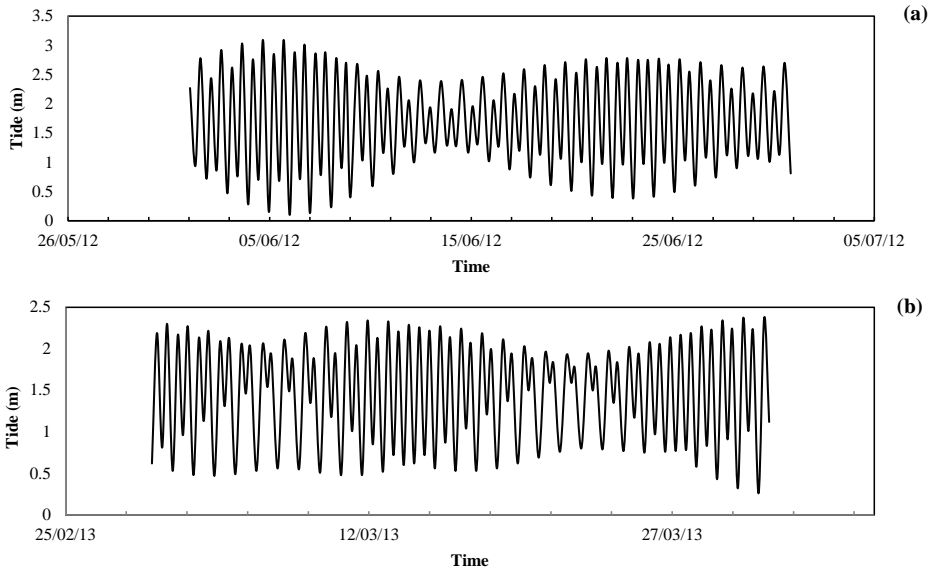


Figure 4.3: (a) Tidal oscillations in Bagan Datoh station (used for Bernam Estuary) showing a dominant semi-diurnal tide; (b) Tidal oscillations in Tanjong Sedili Kecil station (used for Endau Estuary) showing a mixed-tide tidal.

Table 4.2: Tidal range and average discharge information of the surveyed estuaries.

Estuary	Tidal Range [Spring] (m)	Tidal Range [Neap] (m)	Average Discharge [Wet] (m <sup>3</sup> /s)	Average Discharge [Dry] (m <sup>3</sup> /s)
Kurau	2.5	0.5	20	15
Perak	3	0.6	280	190
Bernam	3	0.6	90	30
Selangor	4	1.0	100	30
Muar	2	0.2	170	30
Endau	2	0.2	50	20

salinity over the depth). The partially-mixed form results from a relatively large river discharge compared to tidal flows.

### 4.3. BACKGROUND THEORIES

Savenije [1986, 2005, 2012]’s salt intrusion model involves two components: the shape and the longitudinal salinity distribution of an estuary. In shape analysis, the geometry of an alluvial estuary can be presented by exponential functions. According to Nguyen and Savenije [2006], Zhang et al. [2011] and Nguyen et al. [2012], this shape model can also be applied in multi-channel and multi-reach estuaries. Estuaries that do not expe-

rience strong ocean waves near the mouth can generally be described by a single reach with only one convergence length, whereas those that experience strong waves near the mouth generally have two reaches with two convergence lengths; a short reach close to the sea with a short convergence length and a long one upstream with a longer convergence length. The equations for the shape analysis are written as:

$$A = A_0 e^{-\frac{x}{a_1}} \quad \text{for } 0 < x \leq x_1 \quad (4.1)$$

$$A = A_1 e^{-\frac{x-x_1}{a_2}} \quad \text{for } x > x_1 \quad (4.2)$$

$$B = B_0 e^{-\frac{x}{b_1}} \quad \text{for } 0 < x \leq x_1 \quad (4.3)$$

$$B = B_1 e^{-\frac{x-x_1}{b_2}} \quad \text{for } x > x_1 \quad (4.4)$$

$$h = h_0 e^{\frac{x(a_1-b_1)}{a_1 b_1}} \quad \text{for } 0 < x \leq x_1 \quad (4.5)$$

$$h = h_1 e^{\frac{(x-x_1)(a_2-b_2)}{a_2 b_2}} \quad \text{for } x > x_1 \quad (4.6)$$

where  $A$ ,  $B$  and  $h$  represent the cross-sectional area, width and average depth at distance  $x$ ,  $A_0$ ,  $B_0$  and  $h_0$  are the cross-sectional area, width and average depth at the estuary mouth,  $a$  and  $b$  are the cross-sectional and width convergence length. The longitudinal distance,  $x_1$  is the inflection point where the wave dominated region ends and where there is a change in the convergence length. At this point, the cross-sectional area, width and average depth become  $A_1$ ,  $B_1$  and  $h_1$ . At this point, the convergence lengths switch from  $a_1$  to  $a_2$  and from  $b_1$  to  $b_2$ . The average depth is obtained by dividing the cross-sectional area by the width. Savenije [2005] mentioned that in ideal alluvial estuaries, the convergence length  $a_{1,2}$  and  $b_{1,2}$  are approximately equal (near constant depth).

In this study, the salinity distribution is simulated at TA condition and later converted to HWS situation for the comparison with the existing predictive equation of dispersion. Substituting the shape analysis of Equations (4.1) to (4.6) with the salt balance, using van der Burgh [1972]'s theory for longitudinal dispersion, the salinity distribution along the estuary (from the mouth to where the water becomes totally fresh) for a steady state condition [Savenije, 2005, 2012] is given by:

$$\frac{S^{TA} - S_f^{TA}}{S_0^{TA} - S_f^{TA}} = \left( \frac{D^{TA}}{D_0^{TA}} \right)^{\frac{1}{k}} \quad \text{for } 0 < x \leq x_1 \quad (4.7)$$

$$\frac{S^{TA} - S_f^{TA}}{S_1^{TA} - S_f^{TA}} = \left( \frac{D^{TA}}{D_1^{TA}} \right)^{\frac{1}{k}} \quad \text{for } x > x_1 \quad (4.8)$$

The symbols  $S^{TA}$  and  $D^{TA}$  are the salinity and dispersion as a function of the distance, while  $S_0^{TA}$  and  $D_0^{TA}$  represent the salinity and dispersion at the estuary mouth. At the inflection point, the dispersion and salinity are represented by the symbol  $D_1^{TA}$  and  $S_1^{TA}$ . The fresh water salinity is expressed by the symbol  $S_f^{TA}$ , which is normally close to zero. Considering the exponentially varying geometry, the equations for the dispersion are expressed as:

$$\frac{D^{TA}}{D_0^{TA}} = 1 - \beta_0^{TA} \left( \exp\left(\frac{x}{a_1}\right) - 1 \right) \quad \text{for } 0 < x \leq x_1 \quad (4.9)$$

$$\frac{D^{TA}}{D_1^{TA}} = 1 - \beta_1^{TA} \left( \exp\left(\frac{x-x_1}{a_2}\right) - 1 \right) \quad \text{for } x > x_1 \quad (4.10)$$

with:

$$\beta_0^{TA} = \frac{K a_1}{\alpha_0^{TA} A_0} \quad \text{for } 0 < x \leq x_1 \quad (4.11)$$

$$\beta_1^{TA} = \frac{K a_2}{\alpha_1^{TA} A_1} \quad \text{for } x > x_1 \quad (4.12)$$

and:

$$\alpha_0^{TA} = \frac{D_0^{TA}}{|Q_f|} \quad \text{for } 0 < x \leq x_1 \quad (4.13)$$

$$\alpha_1^{TA} = \frac{D_1^{TA}}{|Q_f|} \quad \text{for } x > x_1 \quad (4.14)$$

$Q_f$  is the fresh water discharge and  $K$  is the Van der Burgh coefficient, which ranges between 0 and 1 [Savenije, 2005].  $D_0$  and  $D_1$  represent the dispersion coefficient, while  $\beta_0$  and  $\beta_1$  are the dispersion reduction rate at the estuary mouth and at the inflection point, respectively. Due to the difficulty to obtain discharge and dispersion estimates, the dispersion and discharge are conveniently combined in the mixing number  $\alpha_0$  and  $\alpha_1$  to facilitate calibration.

Following from Equations (4.9) to (4.14), the salt intrusion length  $L$  can be computed for  $D = 0$  by the following equations:

$$L^{TA} = a_1 \ln \left( \frac{1}{\beta_0^{TA}} + 1 \right) \quad \text{for } 0 < x \leq x_1 \quad (4.15)$$

$$L^{TA} = x_1 + a_2 \ln \left( \frac{1}{\beta_1^{TA}} + 1 \right) \quad \text{for } x > x_1 \quad (4.16)$$

Since the final objective in salt intrusion analysis is to obtain the maximum distance the salt water penetrates into the estuary system, Savenije [2005, 2012] proposed that the salt intrusion length at HWS can be obtained by shifting the salinity curve at TA condition in landward for half of the tidal excursion  $E$ . In order to make this translation shift possible, the  $S^{TA}$  needs to be computed by Equations (4.7) and (4.8) until  $x = -E/2$  as shown below:

$$S^{HWS}(x) = S^{TA} \left( x - \frac{E}{2} \right) \quad (4.17)$$

Subsequently, the salt intrusion length equation becomes:

$$L^{HWS} = a_1 \ln \left( \frac{1}{\beta_0^{HWS}} + 1 \right) \quad (4.18)$$

For LWS situation, the dispersion and salinity curve is moved by half of the tidal excursion seaward as shown below:

$$S^{LWS}(x) = S^{TA} \left( x + \frac{E}{2} \right) \quad (4.19)$$

Illustration of the shifting method taking the salinity profile of the Kurau Estuary as an example, is displayed in Figure 4.4 for better understanding.

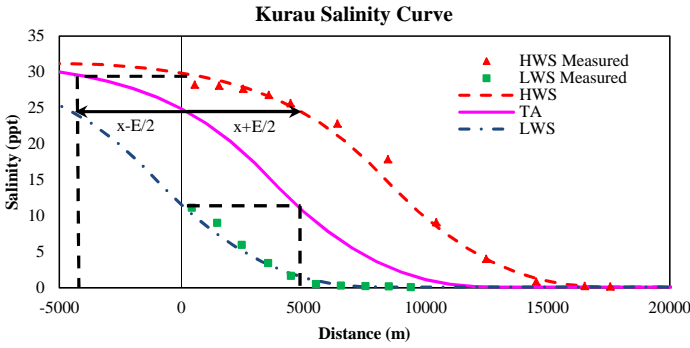


Figure 4.4: Illustration on how the shift from TA to HWS and LWS is done.

Since the  $D_0$  and  $K$  are two calibration parameters in the salt intrusion model, it can only be predictive if separate equations for  $K$  and  $D_0$  are available. Predictive equations were presented by Savenije [1993c], and later improved by Nguyen and Savenije [2006] with a larger datasets. The empirical predictive equations are expressed as:

$$\frac{D_0^{HWS}}{v_0 E_0} = 1400 \frac{\bar{h}}{a} \sqrt{N_R} \quad (4.20)$$

$$K = 0.2 \times 10^{-3} \left( \frac{E_0}{H_0} \right)^{0.65} \left( \frac{E_0}{C^2} \right)^{0.39} (1 - \delta_H b_2)^{-2.0} \left( \frac{b_2}{a_2} \right)^{0.85} \left( \frac{E_0 a_2}{A'} \right)^{0.14} \quad (4.21)$$

$$\text{with: } N_R = \frac{\Delta \rho}{\rho} \frac{g h Q_f T}{A_0 E_0 v_0^2} \quad (4.22)$$

$$\text{and: } E_0 = \frac{v_0 T}{\pi} \quad (4.23)$$

where  $D_0^{HWS}$  is the dispersion coefficient at estuary mouth during HWS,  $\bar{h}$  is the average depth,  $H_0$  is the tidal range at the mouth,  $C$  is the Chezy roughness,  $\delta$  is the damping rate, and  $A'$  is the cross-sectional area. The estuarine Richardson number  $N_R$  is defined

in Equation (4.22), where  $\rho$  is the water density,  $\Delta\rho$  is the density difference over the intrusion length,  $g$  is the gravitational force,  $T$  is the tidal period, and  $v_0$  and  $E_0$  are the velocity amplitude and tidal excursion at the mouth.

In this chapter, we have tested the applicability of these predictive equations in a range of very different previously un-surveyed estuaries, of which the characteristics are presented in the next section. In order to utilize the predictive equations for the dispersion, the fresh water discharge into the estuary on the day of measurement has to be known. Unfortunately, it is difficult to determine the discharge in the tidal region accurately, and the measurement is often time and energy consuming. As an alternative, discharge data was requested and obtained from the Department of Irrigation and Drainage, Malaysia (DID) – the authority in charge of the river networks in Malaysia. However, not the entire drainage basins of the estuaries are gauged with only partial coverage by gauges, the effect of which will be dealt with in Section 4.5.

#### 4.4. RESULTS AND ANALYSES

Essentially, the topography and salinity analysis carried out in this study is based on the tidal average (TA) condition. However, the existing predictive equation for the dispersion  $D_0$  was developed for high water slack (HWS) condition. In order to compare and verify the calibrated  $D_0$  with the predicted value, we calibrated the dispersion for both situations. All the results from the calibration were then applied into Equations (4.7) to (4.19) to compute the longitudinal salinity distribution in an estuary for three tidal conditions: High Water Slack (HWS), Tidal Average (TA), and Low Water Slack (LWS).

##### 4.4.1. GEOMETRY OF THE ESTUARIES

The geometry analyses were performed by utilizing Equations (4.1) to (4.6), for the estuaries in Malaysia including 7 newly surveyed [Gisen et al., 2014a] and 2 retrieved from literature [SMHB et al., 2000], and the results prove that the shape of the estuaries indeed follows an exponential function. All the estuaries studied appear to consist of two width and cross-sectional convergence lengths:  $a_1$ ,  $a_2$ ,  $b_1$  and  $b_2$ . Figures 4.5(a) to (i) indicate that for every estuary studied, the convergence length is shorter near the mouth (which is a wave dominated region) compared to the section after the inflection point, which is tide dominated. The summary of the geometry characteristics for the estuaries considered in this chapter are listed in Table 4.3. For the Linggi, Rompin and Ulu Sedili Besar Estuary, the geometry information is used in the study discussed in Chapter 5 and 6.

Since this study mainly focused on the upstream part of the estuary, the tidal dynamics processes in the wave dominated area (sharp trumpet shape) were neglected. Hence, all the analyses carried out began from the inflection points  $x_1$  towards the upstream region of inflection point  $x_2$  (see Figure 3.6). From this point onwards, the variation of the river width is so small that it can be considered nearly constant. In alluvial estuaries, the average tidal depth is often close to constant, although some estuaries may have slightly increasing or decreasing depth as shown in Figure 4.5. It is hypothesized by Cai et al. [2014a] that the mean depth is due to the residual slope introduced by the river discharge, which becomes more important as we move further upstream.

All the estuaries except the Selangor present different values of cross-sectional and

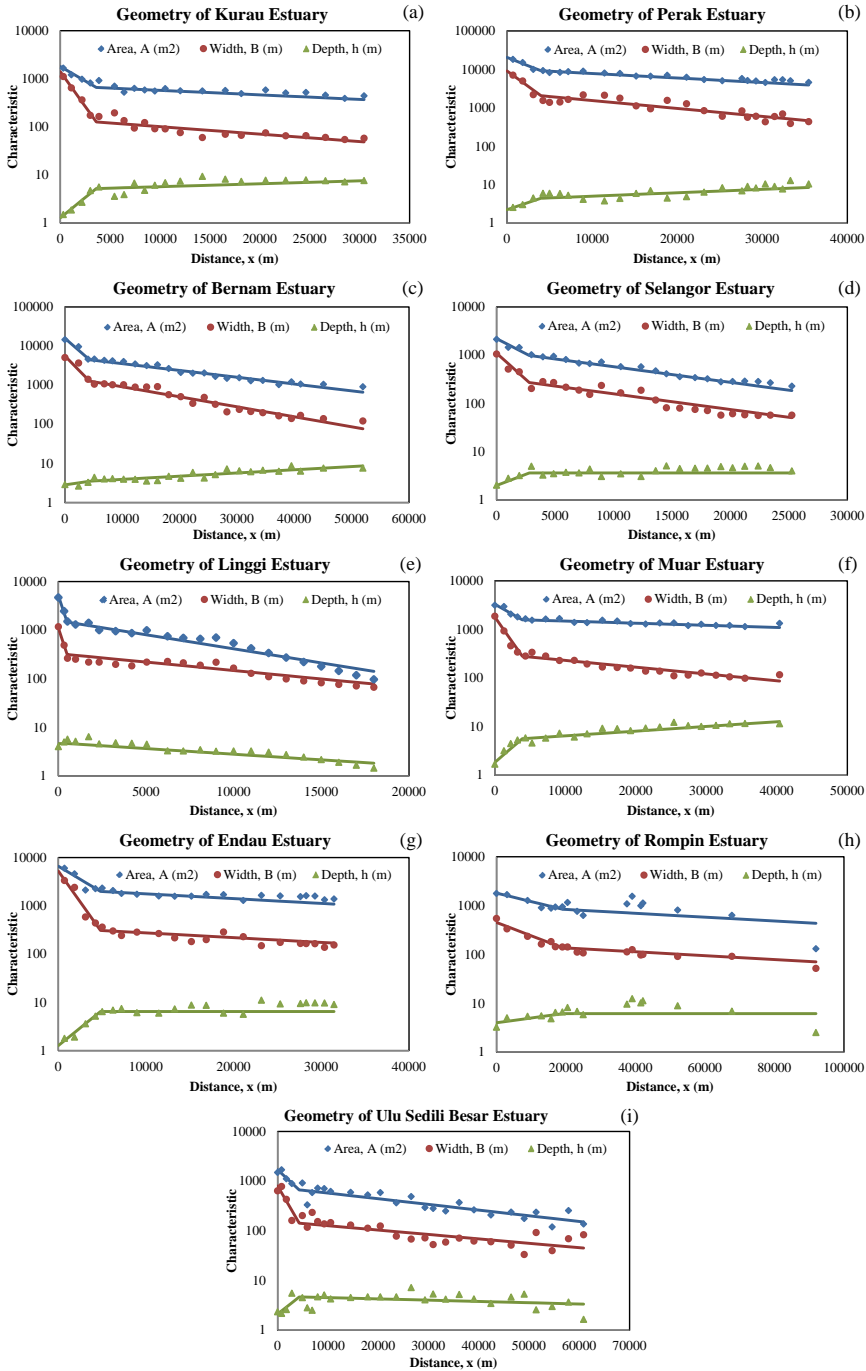


Figure 4.5: Results from the geometry analysis for 9 estuaries in Malaysia including 7 newly surveyed (Gisen, Savenije et al. 2014) and 2 from literature: a) Kurau; b) Perak; c) Linggi; d) Bernam; e) Selangor; f) Muar; g) Endau; h) Rompin; and i) Ulu Sedili Besar, displaying the cross-sectional area (m<sup>2</sup>), width (m) and depth (m).

Table 4.3: The geometry and tidal characteristics of the estuaries showing the cross-sectional area  $A$ , channel width  $B$ , cross-sectional area convergence length  $a$ , width convergence length  $b$ , averaged depth  $\bar{h}$ , and tidal range  $H_0$ . For  $A$  and  $B$ , the subscripts 0 and 1 are referring to the location at the mouth and inflection point, whereas for  $a$  and  $b$ , they are represented by the subscripts 1 and 2, respectively.

Estuary	$A_0$ ( $m^2$ )	$A_1$ ( $m^2$ )	$a_1$ (km)	$a_2$ (km)	$B_0$ (m)	$B_1$ (m)	$b_1$ (km)	$b_2$ (km)	$\bar{h}$ (m)	$H_0$ (m)
Kurau	1800	660	3.6	46	1400	130	1.5	28	5.3	2.0
Perak	20500	9210	5.0	37	9100	2070	2.7	21	5.8	2.5
Bernam	15800	4460	3.4	25	5600	1270	2.9	17	5.0	2.9
Selangor	2200	1000	3.5	13	1100	270	2.0	13	3.5	4.0
Muar	3300	1580	5.3	100	1800	280	2.1	31	7.4	2.0
Endau	6600	2000	4.0	44	5200	310	1.7	44	5.7	1.9

width convergence length, which indicate a gradually depth increase in upstream direction. On the other hand, the Selangor plot showed the convergence length  $a$  and  $b$  to be almost equal, with an almost constant depth. The Muar river estuary is the deepest among the three, which may be partly caused by dredging since sand barges carry tonnes of mined sand to the sea. It is worth noting that the observed depth listed in Table 4.3 represents the average depth of the entire estuary.

#### 4.4.2. SALINITY ANALYSIS

The observed vertical salinities obtained at HWS for all six estuaries are presented in Figures 4.6(a) to (f). From these figures, it can be summarized that the mixing mechanism in the studied areas consists of two types: well-mixed and partially mixed. The vertical salinity distribution patterns along the reach indicate that the estuaries that are located on the west-north and east coast have a partially mixed behaviour, while those at the centre-west coast are well-mixed. For the Selangor estuary, the deviating reading at 12 km from the mouth is caused by the discharge of a drainage outlet due to heavy local rain. The findings on the vertical salinity distribution in these surveys show a disagreement with the statement by Ibrahim et al. [1996] who claimed that the estuaries on the centre west-coast of Peninsular Malaysia are partially-mixed type (of course this depends on the river discharge at the time of observation).

On the basis of the geometry data, the longitudinal salinity distributions along the river estuaries were calculated using Equations (4.7) and (4.8). All analyses were performed based on both HWS and TA conditions, on the basis of which the dispersion for both situations are calculated using Equations (4.9) to (4.14). The Van der Burgh coefficient  $K$  and dispersion  $D_0$  were calibrated so as to obtain the best fit between the simulated salinity variations and the observed salinity data. Considering the fact that the velocity amplitude was not measured during the survey, the tidal excursion  $E$  was obtained also from calibration and is considered constant along the channel. Due to the difficulty in measuring discharge within the tidal region,  $D_0$  was calibrated in terms of the mixing number  $\alpha_0$ . In applying the analytical model to observation, the parameters  $K$ ,  $E$  and  $\alpha_0$  are used as calibration coefficients. Results of the salinity analysis are plotted in Figures 4.7(a) to (f). On the whole, it can be said that the analytical salt intrusion model performs well in representing the salinity distribution in all six estuaries despite

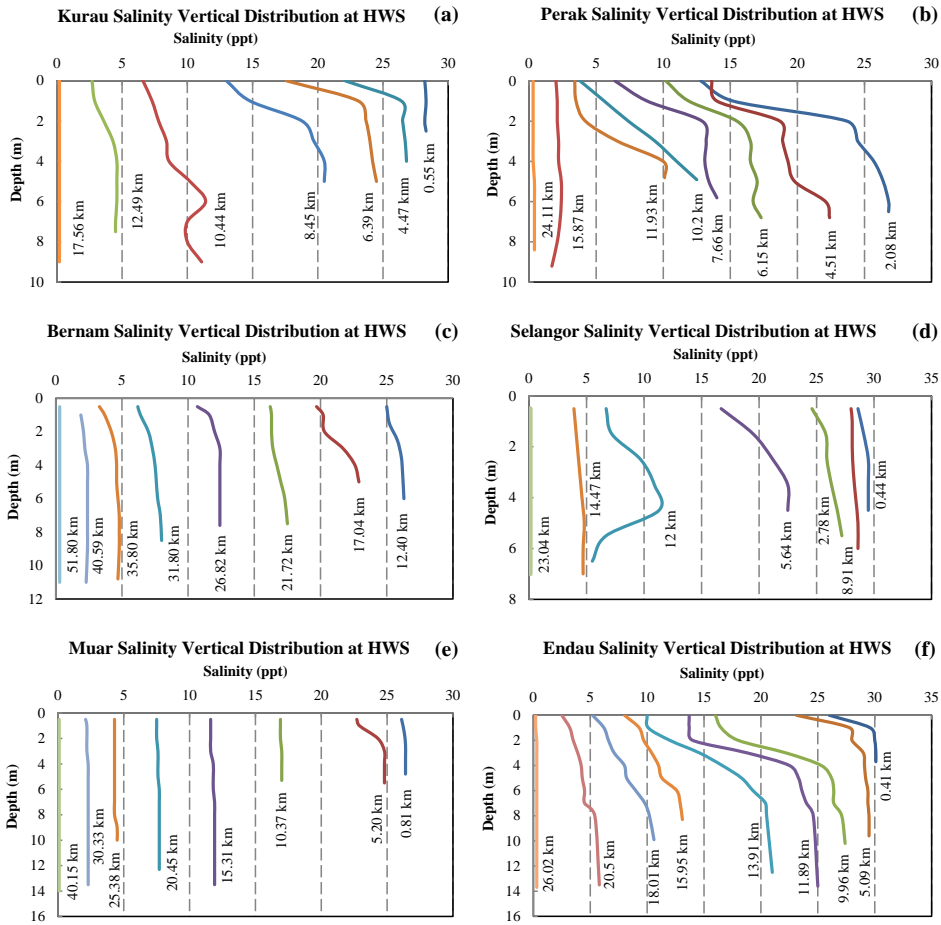


Figure 4.6: Measured vertical salinity distribution of the estuaries: a) Kurau (surveyed on 28th February 2013); b) Perak (surveyed on 14th March 2013); c) Bernam (surveyed on 21st June 2012); d) Selangor (surveyed on 24th July 2012); e) Muar (surveyed on 3rd August 2012); and f) Endau (surveyed on 28th March 2013), showing the salinity distribution at HWS (High Water Slack).

a few outliers which can be explained.

Some of the deviations (ppt) in the Bernam and Perak plots may have been caused by timing errors. Data may have been collected slightly earlier or later than HWS (leading to lower values) or LWS (leading to higher values). This was one of the first surveys and the team still had to become experienced in timing the measurements at HWS and LWS. Other deviations can be explained by the physical layout of the estuaries. In Figure 4.7(b), the first measurement point at the mouth of Perak estuary during LWS is much lower compared to the simulated curve. It is believed that this is caused by the sandbar in the middle of the mouth as shown in Figure 4.2(b). The existence of the sandbar is linked to dominant ebb and flood channels, which results in lateral variability of the

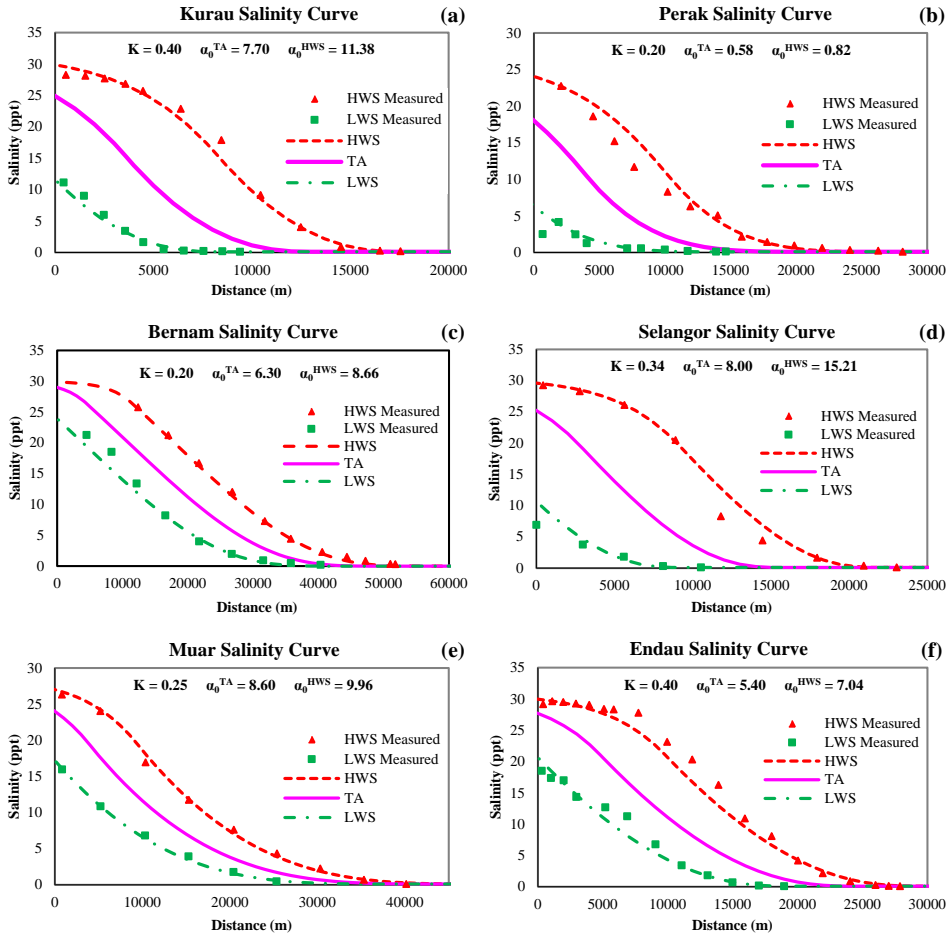


Figure 4.7: Measured and simulated longitudinal salinity profile of the estuaries: a) Kurau (surveyed on 28th February 2013); b) Perak (surveyed on 14th March 2013); c) Bernam (surveyed on 21st June 2012); d) Selangor (surveyed on 24th July 2012); e) Muar (surveyed on 3rd August 2012); and f) Endau (surveyed on 28th March 2013), showing the salinity distribution at HWS (High Water Slack), TA (Tidal Average) and LWS (Low Water Slack), as well as the calibrated values of the Van der Burgh coefficient  $K$  and mixing number  $\alpha_0$ .

salinity over the width.

For the Selangor plot, the lower values at HWS and LWS are due to the fresh water drainage through sluices shown in Figure 4.2(d): It was raining heavily on the day the survey was carried out, and hence drainage water was discharged into the river. This explains why the observed salinity concentrations are lower compared to the simulated values between 11 km to 15 km from the mouth. In the Endau plot, it can be seen that there is a deviation from the model with higher values in the middle reach. This pattern is present in both HWS and LWS. This is probably caused by the tributary at about 8 km from the mouth as displayed in Figure 4.2(f). This tributary drains less river discharge

than the Endau River, which causes the water in the tributary to be more saline than in the main estuary. During the tidal cycle, the more saline water that flows in and out of the tributary creates a higher salinity concentration near the confluence region, which propagates upstream. Of all the estuaries studied, the measurements in the Kurau provide the best correspondence with the simulated results.

It is also noticeable that the maximum salinity concentration at the mouth varies between estuaries. The Kurau, Bernam, Selangor and Endau Estuary show HWS salinity levels of 30 ppt, whereas the Perak and Muar have only 24 ppt and 27 ppt, respectively. The lower value of the Perak is probably caused by the sand bar extending into the sea. The lower value in the Muar Estuary is probably caused by the fresh water discharge from the rivers of Sumatra which affect the salinity near the estuary mouth (the estuary is situated nearest to Sumatra Island).

Figure 4.7(a) to (f) also show the total salt intrusion length for each of the estuaries. According to the plots, the salt water intrudes furthest in the Bernam Estuary, followed by the Muar, Endau, Perak, Selangor, and is shortest in the Kurau Estuary.

#### 4.4.3. COMPARISON WITH THE PREDICTIVE EQUATIONS

The salt intrusion model was verified by comparing the calibrated  $K$  and  $D_0$  values at HWS with the results obtained from the predictive Equations (4.20) to (4.23). The comparison performed in this study is based on HWS because the data of Savenije [2012] to which the newly surveyed estuaries are compared were calibrated at HWS. The discharge data,  $Q_f$  used to compute  $D_0$  is obtained from the nearest streamflow station from the estuary mouth. This implies that we neglected any inflow from the tributaries between the mouth and the station.

Table 4.4: Salinity distribution data showing the salinity at the mouth,  $S_0$ , Van der Burgh's coefficient,  $K$ , fresh water discharge  $Q_f$ , tidal excursion  $E$ , dispersion coefficient at High Water Slack,  $D_0^{HWS}$ , mixing number at High Water Slack  $\alpha_0^{HWS}$  and salt intrusion length at High Water Slack,  $L^{HWS}$ .

Estuary	$S_0^{HWS}$ (ppt)	$Q_f$ ( $m^3/s$ )	$E$ (km)	$K$ calib.	$K$ pred.	$D_0^{HWS}$ calib. ( $m^2/s$ )	$D_0^{HWS}$ pred. ( $m^2/s$ )	$\alpha_0^{HWS}$ calib. ( $m^{-1}$ )	$\alpha_0^{HWS}$ pred. ( $m^{-1}$ )	$L^{HWS}$ meas. (km)	$L^{HWS}$ pred. (km)
Kurau	30	28	9.4	0.40	0.35	319	466	11.38	16.63	18	28
Perak	24	132	12.5	0.20	0.23	108	421	0.82	3.19	29	59
Bernam	30	23	14.0	0.20	0.25	199	283	8.66	12.33	58	62
Selangor	30	39	12.7	0.34	0.35	593	1046	15.21	26.83	22	28
Muar	27	11	11	0.25	0.23	110	159	9.96	14.42	51	73
Endau	30	6	10	0.40	0.39	42	129	7.04	21.51	29	60

Figure 4.8(a) demonstrates that the computed Van der Burgh's coefficient  $K$  from the predictive equation presents a very good correlation with the calibrated values, where all the data points are distributed near the perfect agreement line. However, Savenije [2012] concluded that the accuracy of the predictive equation for  $K$  is still weak if compared to the calibrated result from measurement, and has to be cautiously applied. Using the predictive equation for  $K$  and  $D_0^{HWS}$ , the model appears to overestimate the values for the Dispersion  $D_0^{HWS}$ , mixing number  $\alpha_0^{HWS}$  and salt intrusion length,  $L^{HWS}$  compared

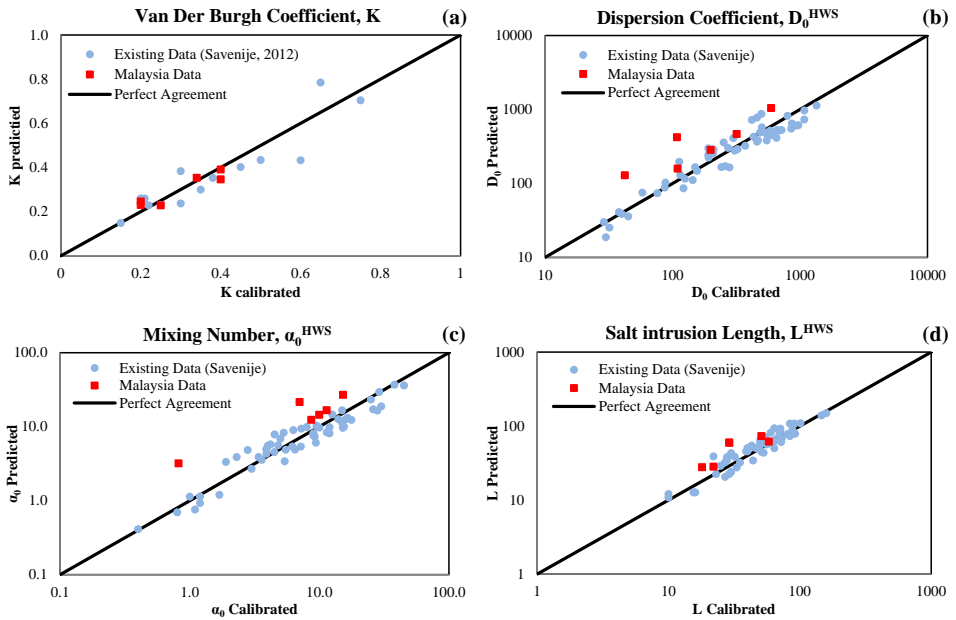


Figure 4.8: Comparison between predicted and calibrated results for: a) Van der Burgh's coefficient  $K$ ; b) dispersion coefficient at High Water Slack  $D_0^{HWS}$ ; c) mixing number at High Water Slack  $\alpha_0^{HWS}$ ; d) salt intrusion length at High Water Slack  $L^{HWS}$ . Square markers are the newly surveyed estuaries, round markers are the estuaries reported in Savenije (2012).

to the calibrated ones as shown in Figures 4.8(b) to (d). This is likely due to the underestimation of the fresh water discharge, since it does not account for the intermediate catchments. The most significant deviation is in the Perak Estuary. It is known that the nearest available streamflow station is 187 km upstream, and there are several tributaries downstream draining on the estuary. The confluences with the tributaries (Bidor, Kinta and Terus River) are situated at approximately 65 km to 75 km from the estuary mouth. Since the discharge from these estuaries is not taken into account, it is reasonable that the calculated salt intrusion length has a higher value than the observed, as the discharge used is too low. Values of the parameters from both approaches are summarized in Table 4.4.

#### 4.4.4. MODELS PERFORMANCE

The performance of the models in simulating and predicting the salt intrusion in estuaries was done by evaluating the correlation between the computed and predicted results to the measured data. In this study, the degree of accuracy for the models was defined with two model accuracy statistics: Root-Mean-Squared error (RMS) and Nash-Sutcliffe efficiency (NS). The equations used to perform the statistical analysis are as shown below:

$$E_{RMS} = \sqrt{\frac{1}{n} \sum_{i=1}^n (P_i - O_i)^2} \quad (4.24)$$

$$E_{NS} = 1 - \frac{\sum_{i=1}^n (P_i - O_i)^2}{\sum_{i=1}^n (O_i - \bar{O}_i)^2} \quad (4.25)$$

where  $P_i$  is the calculated or predicted value at certain point or estuaries,  $O_i$  is the observed value from measurement, and  $\bar{O}_i$  is the average of the observed values. Table 4.5 displays the outcome from the model accuracy analysis for the salinity models of each estuary and the predictive models.

Table 4.5: Results of the model performance in term of Root-Mean-Squared error (MS) and Nash-Sutcliffe efficiency (NS).

<b>Salinity Model Fitting</b>		
<b>Estuary</b>	<b>RMS</b>	<b>NS</b>
Kurau	0.96ppt	0.99
Perak	1.35ppt	0.95
Bernam	0.89ppt	0.99
Selangor	1.71ppt	0.98
Muar	0.42ppt	1.00
Endau	1.46ppt	0.98
<b>Predictive Models</b>		
Van der Burgh's $K$	0.03	0.92
Dispersion $D_0$	258 m <sup>2</sup> /s	-1.04
Mixing Number $\alpha_0$	6 m <sup>-1</sup>	-0.80
Intrusion Length $L^{HWS}$	18 km	-0.21

It is clearly shown in the results that the analytical salt intrusion model has a very good fit for all the estuaries. The RMS error obtained for each estuary is about 1.2 ppt which is acceptable. The fit of the simulated result with the measurement data is best represented by the NS coefficient where all the values are near to unity. This means that the analytical salt model is very reliable and efficient in simulating the salinity level in the Malaysian estuaries. Nevertheless, the predictive model for the Van der Burgh coefficient presents a satisfactory result with RMS error of 0.03 and a very high NS efficiency of 0.92. On the other hand, the performance of the predictive model for the dispersion coefficient is not very satisfying. The RMS errors are relatively large with the value of 258 m<sup>2</sup>s<sup>-1</sup>, 6 m<sup>-1</sup>, and 18 km for the dispersion, mixing number and salt intrusion length, respectively. It is also similar for the NS efficiency, the results show negative efficiency which means that the calibrated or observed mean gives better prediction than the model.

Although the predictive equations do not perform very well in this study, this appears to be largely due to the uncertainty in the discharge data (underestimated because large parts of the drainage basin are not included in the discharge data used) which can also be observed in Figures 4.9 to 4.11. A measure to reduce this uncertainty is presented in the next section.

## 4.5. CORRECTING FOR THE UNGAUGED WATERSHEDS

### 4.5.1. ADJUSTMENT OF THE RIVER DISCHARGE

The fresh water discharge uncertainty is considerable in this study due to the unavailability of streamflow data within the tidal region. Due to the influence of the tide, the fresh water discharge becomes very difficult to measure. The best location to collect discharge data is at the point where the tidal influence ends. However, setting up a gauging station at the tidal limit may be inconvenient and costly. Moreover, some estuaries have tributaries that contribute large amount of fresh water discharge within the tidal region which are also not easy to define. In order to tackle the problem, the streamflow data used were collected from the nearest upstream station. However, the gauging stations are often located far from the tidal region, not catering for intermediate catchments. Due to this reason, several adjustments have to be made on the discharge data including:

1. Streamflow data taken from the upstream gauging stations do not represent the total fresh water flows into the estuaries.
2. Daily discharge fluctuates too much. Therefore average monthly data have been used in reference to the month in which the survey was carried out for each estuary.
3. In order to avoid overestimation of the freshwater discharge, only the sloped areas from the catchments are considered since they generate most of the runoff. The topography maps are shown in Figure 4.9. The information for Linggi, Rompin and Ulu Sedili Besar is used in Chapter 5 and 6.
4. The total fresh water discharge into the estuary has been obtained by extrapolating the total sloped area, using the empirical power function established from the plot of the monthly averaged streamflow against the sloped area of each gauging station, as presented in Figure 4.10. The information for Linggi, Rompin and Ulu Sedili Besar is used in Chapter 5 and 6.

We also tested the correlation between the river discharge with the total catchment area, but this resulted in lower correlation. It is important to note that this method is valid only in the region where the climate and topography characteristics are homogeneous for the entire area. Figures 4.9(a) to (i) display the gauged and ungauged areas for each estuary. As can be seen, most discharge stations only cover a small portion of the entire river basins, while there are also tributaries downstream. In this chapter, the discussion includes only six estuaries (Kurau, Perak, Bernam, Selangor, Muar and Endau), while for the Linggi, Rompin and Ulu Sedili Besar, the information is used in Chapter 5.

Besides the area, one of the more important factors contributing to higher discharge is the topography. Mountainous and hilly catchments such as the Kurau and Perak Estuary are expected to carry larger flow than the flat lands (e.g., Muar and Endau). Using this information, simple power laws as shown in Figures 4.10(a) to (g) were used to relate the observed discharge to the drainage area. These relationships were used to compute the discharges for the entire drainage area of the estuaries. The adjusted discharges obtained from the power relation were subsequently used in the predictive equation for

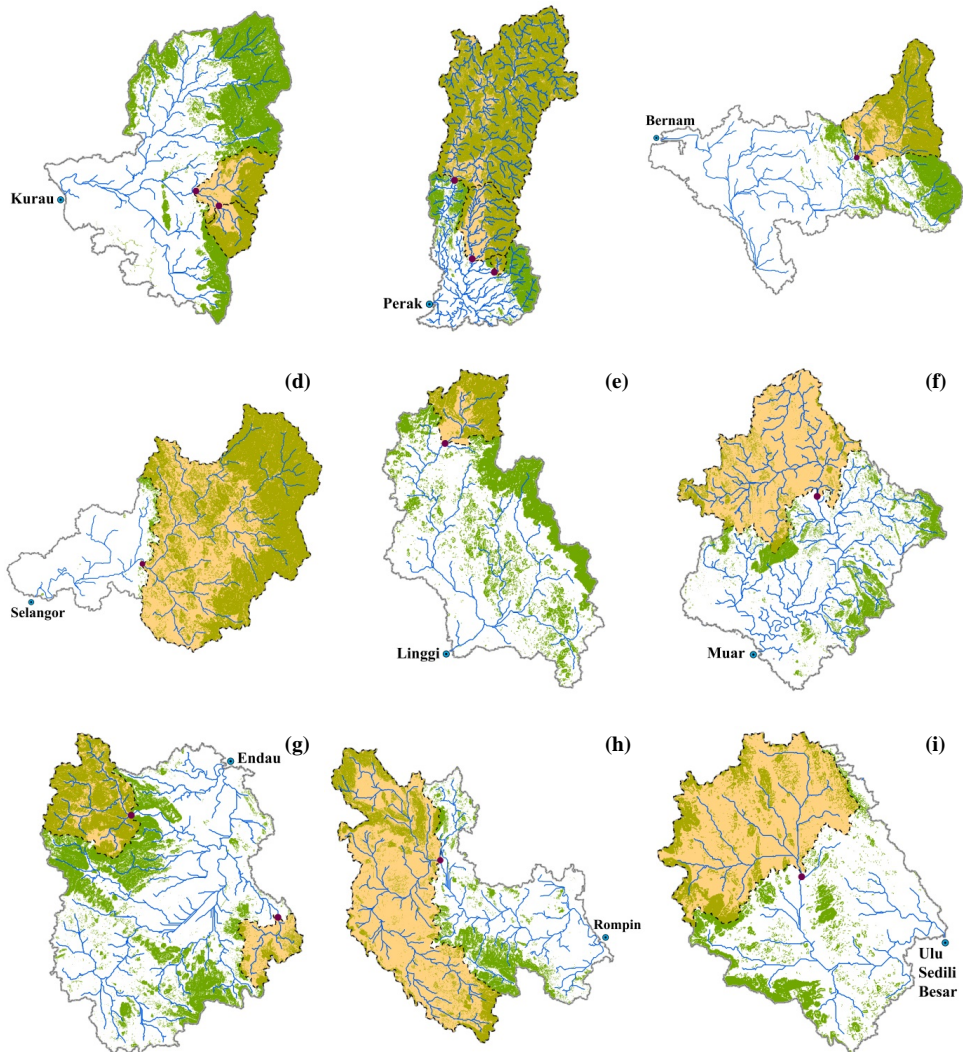


**Fig. 4.9** Map of the gauged and ungauged watersheds of each estuary showing the sloped area in green (not to scale): a) Kurau; b) Perak; c) Bernam; d) Selangor; e) Linggi; f) Muar; g) Endau; h) Rompin; i) Ulu Sedili Besar Estuary, with the gauged area highlighted in yellow.

Figure 4.9: Map of the gauged and ungauged watersheds of: a) Kurau; b) Perak; c) Bernam; d) Selangor; e) Linggi; f) Muar; g) Endau; h) Rompin; and i) Ulu Sedili Besar Estuary, showing the sloped area in green and the gauged area highlighted in yellow (not to scale).

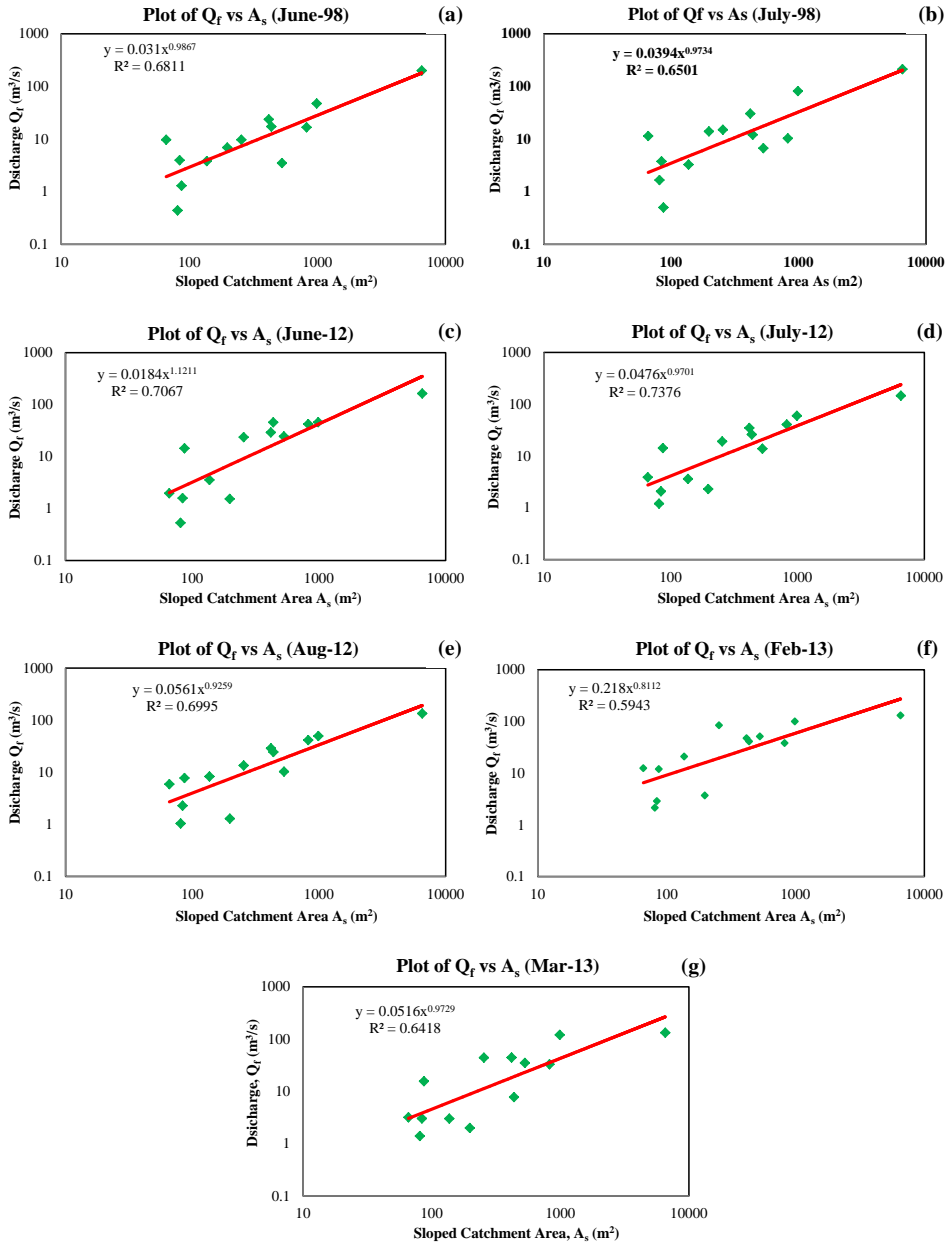


Figure 4.10: Power relation between the river discharge and the drainage area during the month of each salinity measurement: a) June 1998; b) July 1998; c) June 2012; d) July 2012; and e) August 2012; f) February 2013; g) March 2013.  $A_s$  is the sloped part of the catchment.

the dispersion to examine how this affects the predicted result. The distributions of the newly calculated parameters in this study are displayed in Figures 4.11(a) to (c). Table 4.6 lists the adjusted discharge and predictions, compared to the original ones.

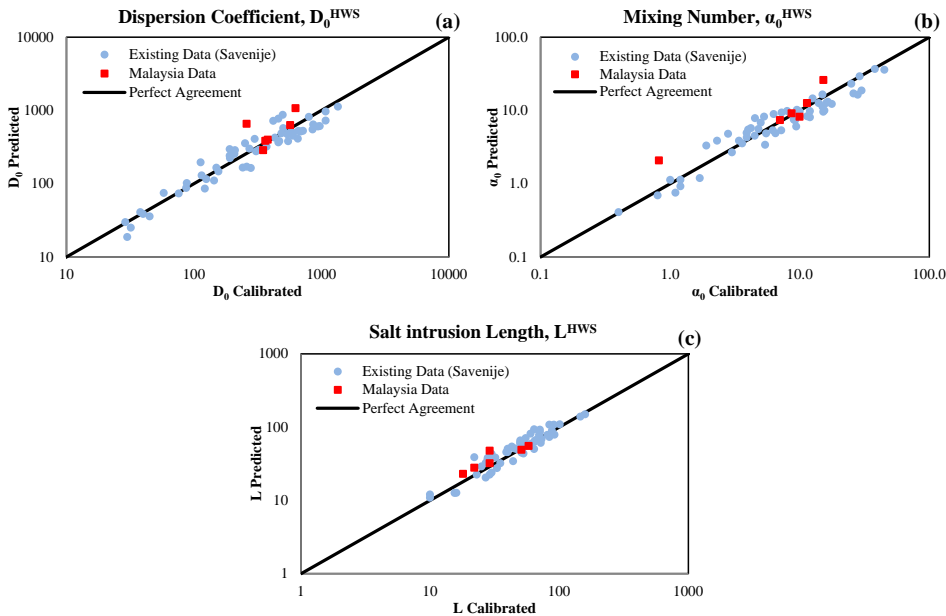


Figure 4.11: Comparison between the new predicted and calibrated results for: a) dispersion coefficient at High Water Slack  $D_0^{HWS}$ ; b) mixing number at High Water Slack  $\alpha_0^{HWS}$ ; c) salt intrusion length at High Water Slack  $L^{HWS}$ . Square markers are the newly surveyed estuaries, round markers are the estuaries reported in Savenije (2012).

The results in particular the maximum salt intrusion lengths, show clear improvement due to the adjusted discharge values. Since the adjusted fresh water discharge has merely been computed based on the area of the drainage basins, this method tends to over-estimate the discharge from flat lands areas such as in the case for the Muar. Contrarily, the method still underestimated the amount of discharge for the mountainous and hilly estuaries especially the Perak. This is reasonable because the Perak Estuary lies in the wettest region in Malaysia. Thus, to balance the intrusion length, larger discharge is required. Furthermore, It also appears that this method have underestimate the discharge draining into the Kurau Estuary, and overestimate the one for Bernam Estuary. This is because the Kurau and Bernam discharge calculation were based on the discharge observed only in a small part of the catchments.

#### 4.5.2. UNCERTAINTY OF THE PREDICTIVE MODELS

Besides the uncertainty from the discharge data, there are also uncertainties in the Van der Burgh  $K$  and dispersion  $D_0^{HWS}$  predictive models. As the models are developed empirically based on an amount of datasets from literature, the reliability of some datasets

Table 4.6: Comparison of the predicted parameters with original data for fresh water discharge  $Q_f$ , and improved discharge  $Q_{Nf}$  – dispersion coefficient at High Water Slack,  $D_0^{HWS}$ , mixing number at High Water Slack  $\alpha_0^{HWS}$  and salt intrusion length at High Water Slack,  $L^{HWS}$ .

Estuary	$Q_f$ ( $m^3/s$ )	$Q_{Nf}$ ( $m^3/s$ )	$D_0^{HWS}$ calib. ( $m^2/s$ )	$D_{N0}^{HWS}$ calib. ( $m^2/s$ )	$D_0^{HWS}$ pred. ( $m^2/s$ )	$D_{N0}^{HWS}$ pred. ( $m^2/s$ )	$\alpha_0^{HWS}$ calib. ( $m^{-1}$ )	$\alpha_0^{HWS}$ pred. ( $m^{-1}$ )	$\alpha_{N0}^{HWS}$ pred. ( $m^{-1}$ )	$L^{HWS}$ meas. (km)	$L^{HWS}$ pred. (km)	$L_N^{HWS}$ pred. (km)
Kurau	28	50	319	569	466	631	11.38	16.63	12.63	18	32	23
Perak	132	316	108	259	421	657	0.82	3.19	2.08	29	59	48
Bernam	23	42	199	364	283	385	8.66	12.33	9.16	58	62	55
Selangor	39	41	593	627	1046	1076	15.21	26.82	26.09	22	28	28
Muar	11	35	110	349	159	288	9.96	14.42	8.20	51	73	49
Endau	6	54	42	380	129	400	7.04	21.51	7.41	29	60	32

are questionable. Moreover, the weighted convergence length obtained via iteration process in the predictive dispersion equation maybe uncertain as the convergence length at the seaward part of the estuary is much shorter than the one at the landward part. Thus, this may influence the efficiency of the results.

Nevertheless, the overall performance of the predictive model for dispersion improves with the adjusted discharge values. The Root-Mean Squared error and Nash-Sutcliffe efficiency for each parameter are shown in Table 4.7. Although the new predicted values represent better results, the errors are still large with low Nash-Sutcliffe efficiency. Hence, it is recommended to shift the predictive measures from HWS to TA condition as it is believed the model is more stable in TA situation.

Table 4.7: Results of the model performance in term of the Root Mean-Squared error (RMS) and Nash-Sutcliffe efficiency (NS) with adjusted discharge values.

Predictive Models		
Parameter	RMS	NS
Dispersion $D_0$	248 $m^2/s$	-2.66
Mixing Number $\alpha_0$	5 $m^{-1}$	-0.08
Intrusion Length $L^{HWS}$	8 km	0.67

### 4.6. CONCLUSIONS

This study has verified that the one-dimensional analytical salt intrusion model is a valid tool to analyse the salt intrusion condition in six previously not surveyed estuaries in Malaysia. This model was used for the first time in Malaysian estuaries and the results are promising. Results from the shape analysis have proved that the geometry of an estuary can be well expressed by branched exponential functions. An excellent fit between the measured and calculated salinity using the model indicates that all six estuaries can be well described by the analytical model. Good correlation between the computed and calibrated Van der Burgh's coefficient  $K$  shows that the predictive model for  $K$  is reasonably efficient to be used in these estuaries. Nevertheless, the over-estimated results for the dispersion  $D_0$ , mixing number  $\alpha_0$  and salt intrusion length  $L$  suggest that the

observed river discharge is probably too low in relation to the actual discharge. This is mainly due to an underestimation of the drainage into the estuaries.

The streamflow stations available are located too far upstream from the salt intrusion region and they only cover a part of the total drainage basin. By a rather rough area-wise compensation of the river discharge, a much better performance of the predictive equations was obtained. In order to provide a more reliable estimate of the discharge into the estuaries, it is recommended to set up a hydrological model for the intermediate catchments making use of the hydrological performance of the nested catchments within these basins (e.g. using the rational method).

Though no significant environmental problems were found in these estuaries, this study still provides useful information on their current condition. Moreover, the information obtained is also important in making engineering decisions. The model shows that human interference such as dredging and fresh water extraction will increase the salt intrusion length. By utilizing the predictive equations, we can estimate the minimum amount of river discharge needed, and maximum depth allowed for dredging to prevent salt water to intrude further into the concerned area. Thus, this simple and effective approach presented in this study can describe the current state of salt intrusion in Malaysian estuaries, and be used for future development. This also suggests that the Malaysian water authority should consider regulating both water extraction and dredging to avoid severe salt intrusion problems.



# 5

## NEW PREDICTIVE VAN DER BURGH AND DISPERSION EQUATIONS AND METHODS FOR THEIR DETERMINATION

*For one-dimensional salt intrusion models to be predictive, we need predictive equations to link model parameters to observable hydraulic and geometric variables. The one dimensional model of Savenije [1993c] made use of predictive equation for the Van der Burgh coefficient  $K$  and the dispersion at the seaward boundary  $D_0$ . Here we have improved these equations by using an expanded database, including new previously un-surveyed estuaries. Furthermore, we derived a revised predictive equation for the dispersion at tidal average (TA) condition and with the boundary situated at the well identifiable inflection point where the estuary changes from wave-dominated to tide-dominated geometry. We used 89 salinity profiles in 30 estuaries (including 7 recently studied estuaries in Malaysia), and empirically derived a range of equations using various combinations of dimensionless parameters. We split our data in two separated datasets: 1) with more reliable data for calibration; and 2) with less reliable data for validation. The dimensionless parameters that gave the best performance depended on the geometry, tidal strength, friction and the Richardson Number. The limitation of the equations is that the friction is generally unknown. In order to overcome this problem, a coupling has been made with the*

---

This chapter is based on:

Gisen, J. I. A., H. H. G. Savenije, and R. C. Nijzink, New predictive Van der Burgh and dispersion equations and methods for their determination., Hydrol. Earth Syst. Sc., (submitted).

*analytical hydraulic model of Cai et al. [2012], which makes use of observed tidal damping and by which the friction can be determined.*

## 5.1. INTRODUCTION

PREDICTIVE methods to determine salinity profiles in estuaries can be very useful to water resources managers, particularly when applied to ungauged estuaries where only a minimal amount of data is available. Before any decision is made on collecting detailed field observations, it is useful to obtain a first estimate of the strength and range of the salt intrusion in the area of interest. Such estimate can be made if there are predictive equations available to compute the longitudinal salinity profile along the estuary. With reliable predictive equations, water managers are able to estimate how far salt water intrudes into the river system under different circumstances, and more importantly, how interventions may change this situation.

The one-dimensional salt intrusion model of Savenije [1993c] makes use of the Van der Burgh and dispersion equation to represent the longitudinal variation of the salinity. The Van der Burgh and dispersion coefficient at the ocean boundary are obtained by calibration of the simulated salinity curve to observations. Savenije [1993c] established a predictive equation for each of these parameters, so that the longitudinal salinity distribution could be estimated when data were lacking or to monitor the impact of interventions, such as dredging or fresh water withdrawal. The predictive equations have subsequently been modified and tested by several researchers including Savenije [2005], Nguyen and Savenije [2006], Kuijper and van Rijn [2011], and Shaha and Cho [2009].

In this chapter, we shall revisit the predictive equations in the light of new insights on how friction and estuary shape affect tidal mixing, makes use of new observation in 7 previously ungauged estuaries in Malaysia that were sampled through a consistent approach. As a result, we present the fully revised and more accurate predictive equations for the Van der Burgh coefficient and for the boundary value of the dispersion at a well identifiable location, based on tidal average (TA) condition.

## 5.2. EXISTING PREDICTIVE EQUATIONS

### 5.2.1. VAN DER BURGH'S COEFFICIENT

Van der Burgh's coefficient  $K$  is also known as the "shape factor" of the salinity curve [Savenije, 1993a]. Based on salinity measurements of 15 estuaries, Savenije found that  $K$  is strongly related to the geometry (the convergence length  $a$  or  $b$  and the width  $B$ ) and its influence is more significant at the tail of the salinity curve (upstream). Moreover, Savenije [1986, 1989] observed that every estuary had its own characteristic value of  $K$ , ranging from zero to one. Assuming that the Van der Burgh coefficient is not time-dependent, Savenije [1993c] established an empirical predictive equation for  $K$  as:

$$K = 0.16 \times 10^{-6} \frac{h_0^{0.69} g^{1.12} T^{2.24}}{H_0^{0.59} b^{1.10} B_0^{0.13}} \quad (5.1)$$

where  $h_0$ ,  $H_0$ , and  $B_0$  are the depth, tidal range and width at the estuary mouth, respectively. The symbol  $T$  represents the tidal period, while  $b$  is the width convergence length, and  $g$  is the gravity acceleration.

More than 10 years later, Savenije [2005] modified the predictive equation involving more parameters:

$$K = 0.2 \times 10^{-3} \left( \frac{E}{H} \right)^{0.65} \left( \frac{E}{C^2} \right)^{0.39} (1 - \delta_H b)^{-2.0} \left( \frac{b}{a} \right)^{0.85} \left( \frac{Ea}{A'} \right)^{0.14} \quad (5.2)$$

The symbols  $E$ ,  $H$ , and  $A'$  refer to the tidal excursion, tidal range, and a boundary value for the cross-sectional area, respectively. This relation had a correlation of 0.96 and seemed very promising. However, as can be seen from the equation, the Chezy roughness  $C$  and damping  $\delta_H$  had to be computed from tidal dynamics analysis.

### 5.2.2. DISPERSION COEFFICIENT

Dispersion is not a physical parameter; it is rather the product of averaging, representing the mixing of saline and fresh water in an estuary as a result of residual circulation induced by density gradients (gravitational circulation) and tidal movement. In salt intrusion modelling, the definition of dispersion is often unclear as it is scale dependent and not directly measurable. The role of dispersion is only meaningful if it is related to the appropriate temporal and spatial scale of mixing, which here we identify as the tidal period (time scale), tidal excursion (longitudinal mixing length), estuary width (lateral mixing length) and depth (vertical mixing length). A physically based description of the dispersion would allow the analytical solution of the salt intrusion profile.

Dispersion due to gravitational circulation has been studied since 1957, as summarized by Fischer [1976]. This type of dispersion is also known as density driven dispersion between the two main sources: sea water and fresh river water. Schultz and Simmons [1957] were some of the first to relate buoyancy to mixing in estuaries, whereby they introduced the ratio between fresh water discharge and tidal volume to represent the degree of stratification. This ratio is also known as the Canter-Cremers number  $N$  as defined by Harleman and Abraham [1966]. The buoyancy effect or stratification in an estuary can also be represented by the Estuarine Richardson Number  $N_r$  which is the ratio of potential energy of the buoyant fresh water to the kinetic energy of the tide:

$$N_r = \frac{\Delta\rho}{\rho} \frac{gh}{v^2} \frac{Q_f T}{AE} \quad (5.3)$$

where  $\rho$  is the water density,  $\Delta\rho$  is the density difference over the salt intrusion length, and  $v$  is tidal velocity amplitude. The difference between  $N$  and  $N_r$  lies in the densimetric Froude number  $F_d$  which is expressed as:

$$F_d = \frac{\rho}{\Delta\rho} \cdot \frac{v^2}{gh} \quad (5.4)$$

Since then, researchers have tried to look for a relation between dispersion and estuarine numbers. Laboratory results of WES flume, Delft flume and Daniels [1974] indicated an agreement with the result of Fischer [1972] in computing the salt intrusion length, using shear velocity instead of mean velocity in the Estuarine Richardson number. Subsequently, the relationship between the dispersion and modified  $N_r$  also gave

good correlation for all the other cases (mostly flume experiments). Thatcher [1972] suggested that the longitudinal dispersion is proportional to the salinity gradient and included this in his one dimensional analytical salt intrusion model, which later was used by Fischer [1972] to model the vertical salinity and velocity distribution. A disadvantage of all these methods was that they did not account for convergence (implicitly assuming an infinitely large convergence length) and that the tidal excursion, as the most important mixing length scale, was missing in the derivations.

Deriving the dimensionless dispersion coefficient from scaling the steady state salt balance equation, Savenije [2005] developed the following empirical predictive relation for the longitudinal dispersion at the estuary mouth for HWS:

$$D_0^{HWS} = 1400 \frac{\bar{h}}{a} \sqrt{N_r} (vE) \quad (5.5)$$

The estuary shape was represented by the ratio of the averaged depth  $\bar{h}$  to the convergence length  $a$ , while the dispersion was made dimensionless by the tidal velocity amplitude and tidal excursion which was not considered in any of the earlier studies. The applicability of these predictive equations has been widely tested in many estuaries including multi-channel estuaries.

Kuijper and van Rijn [2011] later modified the predictive equation including the dimensionless friction ( $C^2/g$ ). The equation was divided into two depending on the types of channel – prismatic and convergent:

Convergent channel:

$$D_0 = l_1 \sqrt{\pi} \left( \frac{\sqrt{\Delta\rho g h_0 / \rho}}{v} \right)^{p1} \left( \frac{C^2}{g} \right)^{p2} \left( \frac{|U_f|}{v} \right)^{p3} \frac{E}{a} v h_0 \quad (5.6)$$

Prismatic channel:

$$D_0 = l_2 \sqrt{\pi} \left( \frac{\sqrt{\Delta\rho g h_0 / \rho}}{v} \right)^{p1} \left( \frac{C^2}{g} \right)^{p2} \left( \frac{|U_f|}{v} \right)^{p3} v h_0 \quad (5.7)$$

where  $u$  is the fresh water velocity. These equations can be used to calculate dispersion locally at any location. However, the weakness is that it is no longer predictive as calibration is required to determine the  $p$  values to fit the measurement data.  $l_1$  and  $l_2$  are the coefficients for the convergent and prismatic channel, respectively.

### 5.2.3. SALT INTRUSION LENGTH

Several researchers have tried to develop a general relation for the salt intrusion length. The development of such predictive equations was done empirically based on a reasonable amount of data. A pioneer effort was made by van der Burgh [1972], making use of prototype information from the Dutch and German estuaries. His equation for the salt intrusion length as summarized by Savenije [1992, 1993c, 2005] is as follows:

$$L^{TA} = 26\pi \frac{h_0}{K} F^{-1.0} N^{-0.5} \quad (5.8)$$

$$\text{with: } F = \frac{v}{\sqrt{gh_0}} \quad (5.9)$$

$$\text{and: } N = \frac{|Q_f|T}{P_t} = \frac{A|U_f|T}{AvT} \cdot \pi = \frac{|U_f|}{v} \cdot \pi \quad (5.10)$$

In this equation,  $L^{TA}$  is the salt intrusion length at TA situation,  $F$  is the Froude number, and  $P_t$  is the tidal flood volume.

A year later, Rigter [1973] established another empirical equation for the salt intrusion length at LWS using experimental data of Delft Hydraulic Laboratory and the WES flume.

$$L^{LWS} = 1.5\pi \frac{h_0}{f_D} (F_d^{-1} N^{-1} - 1.7) \quad (5.11)$$

It is important to note that Van der Burgh's coefficient  $K$  is replaced by the Darcy-Weisbach's roughness  $f_D = 8g/C^2$  and  $F$  is represented by the densimetric Froude number  $F_d$ . Fischer [1974] re-conducted the empirical analysis using the same batch of data from Rigter [1973] and came out with a slightly different result.

$$L^{LWS} = 17.7 \frac{h_0}{f_D^{0.625}} F_d^{-0.75} N^{-0.25} \quad (5.12)$$

Here, it can be seen that despite using the same parameters, the powers of  $f_D$ ,  $F_d$  and  $N$  are different.

About 20 years later, Van Os and Abraham [1990] established a similar equation as Rigter [1973] with a slightly different coefficient:

$$L^{LWS} = 4.4 \frac{h_0}{f_D} (F_d^{-1} N^{-1}) \quad (5.13)$$

All these methods were based on flume data with prismatic geometry. Savenije [1993c, 2005, 2012] who explicitly accounted for channel convergence and the tidal excursion, developed a predictive equation for the salt intrusion length at HWS. The reasoning was that the maximum salt intrusion length occurs during HWS, which is most important for water resources management. Based on Equation (5.5), the equation reads:

$$L^{HWS} = a \ln \left( 1400 \frac{\bar{h} E_0 v_0}{K a^2 u_0} N_r^{0.5} + 1 \right) \quad (5.14)$$

where  $v_0$  is the tidal velocity amplitude at the mouth. It is worth noting that Savenije follows Van der Burgh's equation, with an additional shape indicator referring to the area convergence length  $a$ .

Most of the empirical equations discussed above are based on LWS except for Van der Burgh's and Savenije's methods which are based on TA and HWS, respectively. However, they can easily be brought in agreement with each other by adding  $E/2$  or  $E$  to  $L^{HWS}$ , respectively. Here, we aim to develop a universal predictive equation for estimating the Van der Burgh and dispersion coefficient for TA condition, which can be applied in the salt intrusion model to predict the salinity profile for any estuary worldwide under different tidal and flood conditions.

### 5.3. METHODS

In this chapter, the main focus is on the mixing mechanisms which lead to longitudinal dispersion in estuaries: the tide and density driven dispersion. Key parameters are developed based on measurable parameters of geometry, tidal hydraulics and fresh water discharge. In total 89 measurements data of 30 estuaries worldwide have been used to develop the predictive equations. Measurements in 7 newly surveyed estuaries were collected from 2011 to 2013 in Malaysia, whereas the remaining were compiled by revisiting existing data available in the database of Savenije [2005] and from professional reports. The locations of the estuaries studied are displayed in Figure 5.1.

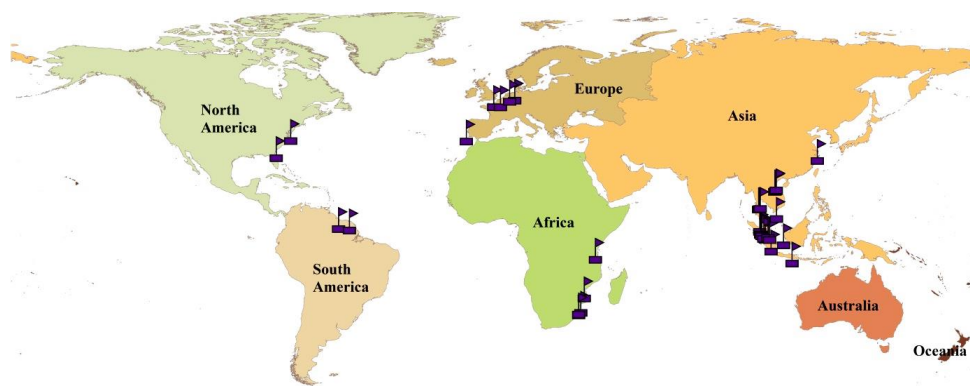


Figure 5.1: Global map showing the locations of the estuaries studied.

Adjustments have been made to the geometry (see Appendix A.1 for the plots of the geometry) and salinity analysis for some of the estuaries to ensure consistency in the input data used. The entire dataset was split into two: reliable and less reliable data. The reliable dataset have been used to develop the predictive equations, whereas the less reliable ones have been used for verification purposes. The study was performed based on Savenije [1993c, 2005, 2012]’s method for predicting  $K$  and  $D_0$  with some modifications. The modifications include:

- All geometry and tide information used refers to the well identifiable inflection point  $x_1$  as the boundary condition.
- Analyses were performed on TA condition instead of HWS, which is consistent with the geometry information.
- Estuary roughness and the ratio of estuary width to river width have been added in the predictive equations.
- The parameters chosen are mostly independent and easy to observe without the need for prior calibration.

Although the predictive equations are based on the tidal average (TA) situation, one can still compute the salinity distribution for both low water slack (LWS) and high water slack (HWS) by shifting the curve over  $E/2$  in seaward and landward direction.

### 5.3.1. SELECTING THE DIMENSIONLESS RATIOS

Revising the parameters selected by Savenije [1993c] and Savenije [2005], we found that the latter contained some parameters that required tidal dynamics analysis while one of the ratios was not dimensionless. The followings are the dimensionless ratios selected for the revised predictive equation for the Van der Burgh coefficient:

$$K = f \left( \frac{B_f}{B_1}, \frac{g}{C^2}, \frac{E_1}{H_1}, \frac{\bar{h}_1}{b_2}, \frac{\bar{h}_1}{H_1}, \frac{\lambda_1}{E_1} \right) \quad (5.15)$$

where  $B_f$  is the river regime width, and  $\lambda_1 = \sqrt{g\bar{h}_1/r_s}$  is the wave length at the inflection point with  $r_s$  being the storage width ratio (defined as the ratio between storage width and stream width). The symbols  $B_1$ ,  $E_1$ ,  $h_1$ ,  $H_1$  and  $b_2$  represent the estuary width, tidal excursion, averaged estuary depth, tidal range and width convergence length at the inflection point  $x_1$ . It is worth noting that the roughness  $C = K_m \bar{h}_1^{1/6}$  was obtained through calibration using the tidal dynamics solution of Cai et al. [2012] which makes use of observed tidal damping. In the above equation, it can be seen that all parameters used have been defined at the inflection point  $x_1$ . It is also important to note that the convergence length adopted is of the second reach not the first part of the estuary. Generally the tidal indicators  $E$  and  $H$ , are defined at the mouth. In order to obtain the tidal excursion and tidal damping at the inflection point, a projection can be made considering tidal damping as follows [Kuijper and van Rijn, 2011]:

$$H_1 = H_0 \cdot \exp(\delta_H x_1) \quad (5.16)$$

$$E_1 = E_0 \cdot \exp(\delta_H x_1) \quad (5.17)$$

where the damping factor  $\delta_H$  also follows from the tidal dynamics simulation of Cai et al. [2012]. The values of  $H_1$  and  $E_1$  used in the dimensionless ratios represent the condition of spring tide, where  $v$  is considered to be closed to 1 m/s [Bruun and Gerritsen, 1960; Pethick, 1984; Langbein, 1963]. This is to ensure that  $K$  is time-independent representing a general characteristic of an estuary. As a result,  $E$  essentially reflects the tidal period as described in Equation 5.18 (see also 5.1).

$$E = \frac{vT}{\pi} \quad (5.18)$$

For the dispersion coefficient, eight dimensionless ratios have been selected with 18 different types of equations including the one of Savenije [1993c, 2005] as benchmark. The dispersion coefficient is represented in dimensionless form as:

$$\frac{D_1}{v_1 E_1} = f \left( N_{r1}, \frac{h_1}{a_2}, \frac{g}{C^2}, \frac{H_1}{E_1}, \frac{h_1}{E_1}, \frac{\lambda_1}{E_1}, \frac{\lambda_1}{a_2}, \frac{B_1}{h_1} \right) \quad (5.19)$$

$$\text{with: } N_{r1} = \frac{\Delta\rho}{\rho} \frac{g h_1}{v_1^2} \frac{Q_f T}{A_1 E_1} \quad (5.20)$$

where  $N_{r1}$  is the Estuarine Richardson number with  $v_1$  being the tidal velocity amplitude, both at the inflection point. It is important to note that the values taken for  $E_1$

and  $H_1$  in the dispersion analysis are based on the real-time data captured during measurements and the depth is referring to the depth at the inflection point. In general, the density different between the saline and fresh water is taken as  $(25/35)S_0 \text{ kg/m}^3$  and the fresh water density as  $1000 \text{ kg/m}^3$ . The fresh water discharge data were adjusted for the 7 newly surveyed estuaries so that the runoff contribution downstream of the gauging station was also considered in the analysis. Stepwise multiple regression analysis has been used to identify the best combination of the dimensionless ratios in predicting  $K$  and  $D_1$ . The efficiency of the established equations was examined by comparing the correlation coefficient  $R^2$  and the standard error  $SE$ . The predicted results calculated by the most suitable equations were plotted against the calibrated values to evaluate their predictive performance.

### 5.3.2. SUBSTITUTION OF PREDICTIVE EQUATIONS IN THE SALT INTRUSION MODEL

Since the predictive dispersion is computed at the inflection point  $x_1$ , reverse calculation has to be done to obtain the dispersion at the mouth. This is necessary to enable the simulation of the longitudinal salinity distribution starting from the mouth to the salt intrusion limit. Inverse integration from  $x_1$  to  $x = 0$  of Equation (2.11) yields for the dispersion at the estuary mouth:

$$D_0^{TA} = D_1^{TA} \left\{ 1 + \beta_{rev}^{TA} \left[ 1 - \exp\left(-\frac{x_1}{a_1}\right) \right] \right\} \quad (5.21)$$

$$\text{with: } \beta_{rev}^{TA} = \frac{K a_1}{\alpha_1^{TA} A_1} \quad (5.22)$$

$$\text{and: } \alpha_1^{TA} = \frac{D_1^{TA}}{|Q_f|} \quad (5.23)$$

where  $\beta_{rev}$  is the reversed dispersion reduction rate, whereas  $A_1$ ,  $D_1$  and  $\alpha_1$  are the cross-sectional area, dispersion coefficient and mixing number at the inflection point, respectively. It is important to note that the convergence length  $a_1$  applied in Equations (5.21) and (5.22) is of the first section of the estuary. The relation between dispersion and salinity is then expressed by:

$$\frac{S^{TA} - S_f^{TA}}{S_1^{TA} - S_f^{TA}} = \left( \frac{D^{TA}}{D_1^{TA}} \right)^{\frac{1}{K}} \quad (5.24)$$

where  $S_1$  refers to the salinity at the inflection point.

Substituting the tidally average dispersion coefficient into the general form of the salt intrusion length of Savenije [1993c, 2005] yields:

$$L^{TA} = x_1 + a_2 \ln\left(\frac{1}{\beta_1^{TA}} + 1\right) \quad (5.25)$$

$$\text{with: } \beta_1^{TA} = \frac{K a_2}{\alpha_1^{TA} A_1} \quad (5.26)$$

Note that all parameters used in these equations refer to the inflection point. We obtain the salinity profile at HWS and LWS by moving the salinity curve over  $E/2$  in the upstream and downstream direction. Similarly, the maximum salt intrusion length can be obtained by shifting the intrusion length at TA in landward direction by half of the tidal excursion at the mouth as:

$$L^{HWS} = L^{TA} + \frac{E_0}{2} \quad (5.27)$$

and the LWS intrusion length by moving the tidal excursion seaward .

$$L^{LWS} = L^{TA} - \frac{E_0}{2} \quad (5.28)$$

### 5.3.3. DATA

Data were divided into two categories: reliable and less reliable. There are 47 measurements grouped under the reliable dataset, and 38 measurements under the less reliable dataset (see Appendix A.2 and A.3). This distinction was made based on the following criteria.

Criteria for classifying estuaries as reliable:

- The estuary is generally in steady state condition.
- The fresh water discharge is estimated, observed or measured correctly.
- The estuary is alluvial and undisturbed.
- Complete measurement data for tidal dynamics and salinity analysis are available.

Criteria for classifying estuaries as less reliable:

- The estuary is not in steady state particularly during low river discharge. This depends on the ratio of the time scale of system response to the time scale of discharge reduction (see Savenije [2012])(NSS).
- The estimation of the fresh water discharge is uncertain (UQ).
- The estuary may not be alluvial (e.g. dredged, modified or constricted by rocky banks)(NA).
- Information on tidal dynamics and salinity is lacking or unclear (IL).

The estuaries that fall under category NSS, UQ, NA, and IL are listed in Table 5.1. It is worth noting that only the reliable set is used in regression analysis. The less reliable ones are merely plotted for verification purpose.

## 5.4. RESULTS AND ANALYSIS

### 5.4.1. PREDICTIVE EQUATION FOR THE VAN DER BURGH COEFFICIENT $K$

Results from the stepwise multiple regression analyses show that the best combinations of the dimensionless ratios to represent the Van der Burgh predictive equation are:

$$K = 8.03 \times 10^{-6} \left(\frac{B_f}{B_1}\right)^{0.30} \left(\frac{g}{C^2}\right)^{0.09} \left(\frac{E_1}{H_1}\right)^{0.97} \left(\frac{\bar{h}_1}{b_2}\right)^{0.11} \left(\frac{H_1}{\bar{h}_1}\right)^{1.10} \left(\frac{\lambda_1}{E_1}\right)^{1.68} \quad (5.29)$$

or:

$$K = 8.03 \times 10^{-6} \cdot \pi^{0.71} \left( \frac{B_f^{0.30} g^{0.93} H_1^{0.13} T^{0.97}}{B_1^{0.30} C^{0.18} v_1^{0.71} b_2^{0.11} \bar{h}_1^{0.15} r_s^{0.84}} \right) \quad (5.30)$$

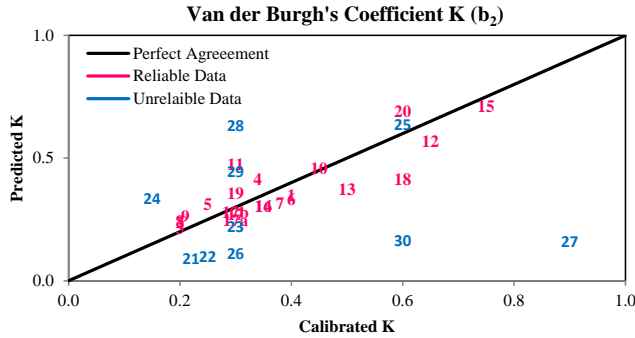


Figure 5.2: Performance of the predictive equation for the Van der Burgh coefficient against the calibrated values.

where Equation (5.30) is the simplified form. The correlation coefficient  $R^2$  and the standard error  $SE$  obtained for predictive  $K$  equation is 0.72 and 0.11, respectively. If we had used the cross-sectional area convergence  $a_2$  instead of  $b_2$ , then the correlation would be slightly poorer. Hence the width convergence is a better indicator, which is fortunate because it is easier to determine. From the equation, we can see that the parameters that have the most influence on the Van der Burgh coefficient is the tidal period, followed by the gravity acceleration, the storage width ratio and tidal velocity amplitude which have the power of 0.97, 0.93, 0.84 and 0.71, respectively. The importance of the friction appears to be minor, which is also fortunate as  $C$  is not directly observable. The estuary to river width ratio shows higher power than the convergence length, which indicates that the width is a better shape indicator. Finally, we should realize that  $0 \leq K \leq 1$  according to Savenije [1993a]. For prismatic channel where  $b_2$  becomes infinity,  $K$  approaches zero, implying constant dispersion.

Figure 5.2 shows the plot of the predicted  $K$  against the calibrated value. All the reliable data points appear to fall close to the perfect agreement line. About half the unreliable data points were outliers particularly the Gambia (30) and Tejo (27) Estuary which lie much further away from the perfect agreement line. This is not strange in the sense

Table 5.1: Data used to develop the predictive equation for the Van der Burgh coefficient  $K$ .

Reliable set for calibration															
No	Estuary	$A_1$ [10 <sup>3</sup> ] (m <sup>2</sup> )	$a_2$ (km)	$B_1$ (m)	$B_r$ (m)	$b_2$ (km)	$\bar{h}_1$ (m)	$x_1$ (km)	$H_0$ (m)	$E_0$ (km)	T (hr)	$K_m$	$\delta_H$ (10 <sup>-6</sup> m <sup>-1</sup> )	K Cal	K Pre
1	Kurau	0.7	46	130	20	28	6.2	3.6	2.3	14	12	30	-6.30	0.40	0.35
2	Perak	9.2	37	2070	130	21	6.3	4.0	2.8	14	12	65	3.00	0.20	0.24
3	Bernam	4.5	25	1270	45	17	5.3	4.3	2.9	14	12	70	1.70	0.20	0.22
4	Selangor	1.0	13	270	35	13	3.7	2.8	4.0	14	12	40	-3.70	0.34	0.42
5	Muar	1.6	100	280	55	31	8.2	3.9	2.0	14	12	45	-2.68	0.25	0.32
6	Endau	2.0	44	310	72	44	6.5	4.8	1.9	14	12	45	-1.30	0.40	0.33
7	Maputo	4.7	16	1150	100	16	4.1	5.1	3.3	14	12	58	2.00	0.38	0.32
8	Thames (New)	10.9	23	780	50	40	8.2	31.0	5.3	14	12	45	1.10	0.20	0.24
9	Corantijn	26.8	64	5000	400	48	6.7	18.0	3.1	14	12	40	-1.70	0.21	0.27
10	Sinnamary	1.1	39	470	95	12	3.9	2.7	3.3	14	12	40	-5.00	0.45	0.46
11	MaeKlong	1.1	150	240	150	150	4.6	3.2	3.6	14	12	40	-4.20	0.30	0.48
12	Lalang	2.9	167	360	130	94	10.3	0.0	2.6	28	24	84	-0.54	0.65	0.57
13	Limpopo	1.1	115	180	90	115	6.3	20.0	1.9	14	12	43	1.70	0.50	0.38
14	Tha Chin (New)	1.4	87	260	45	87	5.6	5.0	2.6	14	12	50	-5.50	0.35	0.31
15	ChaoPhya	3.1	130	470	200	130	6.5	12.0	3.4	28	24	65	-2.20	0.75	0.71
16	Edisto	5.2	15	1250	60	15	4.1	2.0	3.2	14	12	30	-8.80	0.35	0.31
17	Elbe_Flanders	27.3	70	3040	350	80	8.5	33.0	4.7	14	12	32	2.00	0.30	0.27
17a	Elbe_Kuijper	46.0	66	4500	350	66	10.2	0.0	4.7	14	12	32	2.00	0.30	0.25
17b	Elbe_Savenije	43.0	66	2880	350	50	11.7	0.0	4.6	14	12	32	2.00	0.30	0.28
18	Pangani	0.9	15	270	35	15	3.2	3.1	4.2	14	12	42	10.00	0.60	0.41
19	Rembau Linggi	1.5	8	320	25	13	3.2	0.5	2.0	14	12	30	-14.00	0.30	0.36
20	Landak	2.0	60	230	100	60	8.7	0.0	1.6	28	24	45	-6.70	0.60	0.69

Less reliable sets for verification															
No	Estuary	$A_1$ [10 <sup>3</sup> ] (m <sup>2</sup> )	$a_2$ (km)	$B_1$ (m)	$B_r$ (m)	$b_2$ (km)	$\bar{h}_1$ (m)	$x_1$ (km)	$H_0$ (m)	$E_0$ (km)	T (hr)	$K_m$	$\delta_H$ (10 <sup>-6</sup> m <sup>-1</sup> )	K Cal	K Pre
<sup>3,4</sup> 21	Delaware	255.0	41	37655	120	42	6.4	0.0	1.8	14	12	55	0.65	0.22	0.09
<sup>2,3</sup> 22	Westerschelde	150.0	27	16000	50	27	9.4	0.0	4.0	14	12	46	2.80	0.25	0.10
<sup>1,2,4</sup> 23	Pungue	14.5	19	5200	50	19	2.8	0.0	6.7	14	12	31	-8.50	0.30	0.22
<sup>2</sup> 24	Incomati	1.1	40	380	22	40	2.8	15.0	3.3	14	12	56	-19.90	0.15	0.34
<sup>2,4</sup> 25	Solo	2.1	226	225	95	226	9.2	0.0	1.8	28	24	31	3.00	0.60	0.64
<sup>2,4</sup> 26	Eems	120.0	19	31623	55	19	3.8	0.0	3.6	14	12	31	-0.70	0.30	0.11
<sup>2,3</sup> 27	Tejo	100.0	13	20000	180	13	5.0	0.0	3.6	14	12	56	2.20	0.90	0.16
<sup>2,4</sup> 28	Rompin	0.8	110	140	50	110	6.1	19.0	2.5	14	12	15	-33.40	0.30	0.64
<sup>2,4</sup> 29	Ulu Sedili Besar	0.7	38	140	35	49	4.1	4.3	2.5	14	12	30	-25.50	0.30	0.45
<sup>1,3</sup> 30	Gambia	35.7	96	3700	110	100	8.8	33.0	1.83	14	12	35	-1.00	0.60	0.16

Note: <sup>1</sup> Non-steady state (NSS); <sup>2</sup> Uncertain discharge (UQ); <sup>3</sup> Non-Alluvial (NA); <sup>4</sup> Information lacking (IL).

that the Tejo Estuary is not entirely alluvial, and its narrow and deep mouth caused by a rock outcrop formation turns it into a fjord type estuary. As for the Gambia, it is an unsteady state estuary. Nevertheless, for the rest of the outliers we believe that they would fit better if good data had been available. The results are summarized in Table 5.1.

**5.4.2. PREDICTIVE EQUATION FOR THE DISPERSION COEFFICIENT  $D$**

In this study, 18 combinations of the dimensionless ratios were established by multiple regression method of which the results are displayed in Table 5.2 and Figure 5.3. By observing the exponent, it can be seen that the power of the Estuarine Richardson number  $N_r$  varies little, indicating the clear correlation with  $N_r$  compared to the other parameters. The next parameter that has a high exponent is the dimensionless roughness, of which the inclusion improves the correlation. As for the rest of the dimensionless ratios, it appears that the contribution is minimal. Hence, the best equations chosen for further analysis are Equations (R2), (R4) and (R9).

Table 5.2: Equations obtained from multiple regressions analysis.

Equations for multiple regression analysis	
$\frac{D_1^{TA}}{v_1 E_1} = 2141 N_r^{0.84} \left( \frac{h_1}{a_2} \right)$ (R1)	$\frac{D_1^{TA}}{v_1 E_1} = 0.2942 N_r^{0.56} \left( \frac{a_2}{h_1} \right)^{0.04} \left( \frac{g}{C^2} \right)^{0.23}$ (R10)
$\frac{D_1^{TA}}{v_1 E_1} = 0.1167 N_r^{0.57}$ (R2)	$\frac{D_1^{TA}}{v_1 E_1} = 0.2347 N_r^{0.57} \left( \frac{g}{C^2} \right)^{0.23} \left( \frac{E_1}{H_1} \right)^{0.08}$ (R11)
$\frac{D_1^{TA}}{v_1 E_1} = 0.1515 N_r^{0.58} \left( \frac{h_1}{a_2} \right)^{0.03}$ (R3)	$\frac{D_1^{TA}}{v_1 E_1} = 0.4225 N_r^{0.57} \left( \frac{g}{C^2} \right)^{0.22} \left( \frac{a_2}{\lambda_1} \right)^{0.02}$ (R12)
$\frac{D_1^{TA}}{v_1 E_1} = 0.3958 N_r^{0.57} \left( \frac{g}{C^2} \right)^{0.21}$ (R4)	$\frac{D_1^{TA}}{v_1 E_1} = 0.3873 N_r^{0.57} \left( \frac{g}{C^2} \right)^{0.21} \left( \frac{\lambda_1}{E_1} \right)^{0.01}$ (R13)
$\frac{D_1^{TA}}{v_1 E_1} = 0.2812 N_r^{0.57} \left( \frac{H_1}{E_1} \right)^{0.10}$ (R5)	$\frac{D_1^{TA}}{v_1 E_1} = 49.83 \left( N_r \cdot \frac{g}{C^2} \cdot \frac{H_1}{E_1} \right)^{0.44}$ (R14)
$\frac{D_1^{TA}}{v_1 E_1} = 0.1344 N_r^{0.57} \left( \frac{h_1}{E_1} \right)^{0.02}$ (R6)	$\frac{D_1^{TA}}{v_1 E_1} = 0.2708 \left( N_r \cdot \frac{g}{C^2} \cdot \frac{\lambda_1}{E_1} \right)^{0.45}$ (R15)
$\frac{D_1^{TA}}{v_1 E_1} = 0.1243 N_r^{0.58} \left( \frac{E_1}{\lambda_1} \right)^{0.02}$ (R7)	$\frac{D_1^{TA}}{v_1 E_1} = 0.2338 N_r^{0.56} \left( \frac{a_2}{h_1} \right)^{0.03} \left( \frac{g}{C^2} \right)^{0.24} \left( \frac{E_1}{H_1} \right)^{0.05}$ (R16)
$\frac{D_1^{TA}}{v_1 E_1} = 0.1138 N_r^{0.58} \left( \frac{\lambda_1}{a_2} \right)^{0.02}$ (R8)	$\frac{D_1^{TA}}{v_1 E_1} = 0.0514 \left( \frac{g}{C^2} \right)^{0.29} \left( \frac{E_1}{H_1} \right)^{0.12}$ (R17)
$\frac{D_1^{TA}}{v_1 E_1} = 1.9474 \left( N_r \cdot \frac{g}{C^2} \right)^{0.51}$ (R9)	$\frac{D_1^{TA}}{v_1 E_1} = 0.5746 \left( \frac{g}{C^2} \right)^{0.31} \left( \frac{h_1}{B_1} \right)^{0.27}$ (R18)

Performance of the Predictive Equations

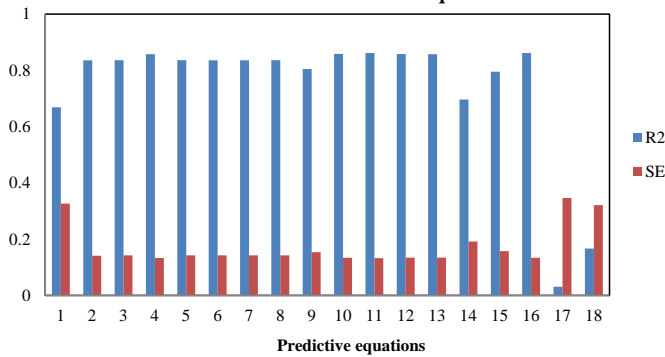


Figure 5.3: Chart showing the correlation coefficient  $R^2$  and standard error  $SE$  for each predictive equations.

It is interesting to note that the performance of the benchmark equation of Savenije [1993c, 2005] (Equation (R1)) is rather poor, with  $R^2$  and  $SE$  of 0.67 and 0.33. These significant differences may be caused by the homogenisation of the input information (e.g. geometry), and the use of selective data for calibration. With more or less equal performance, it is decided that the simplest equation with the best performance is the

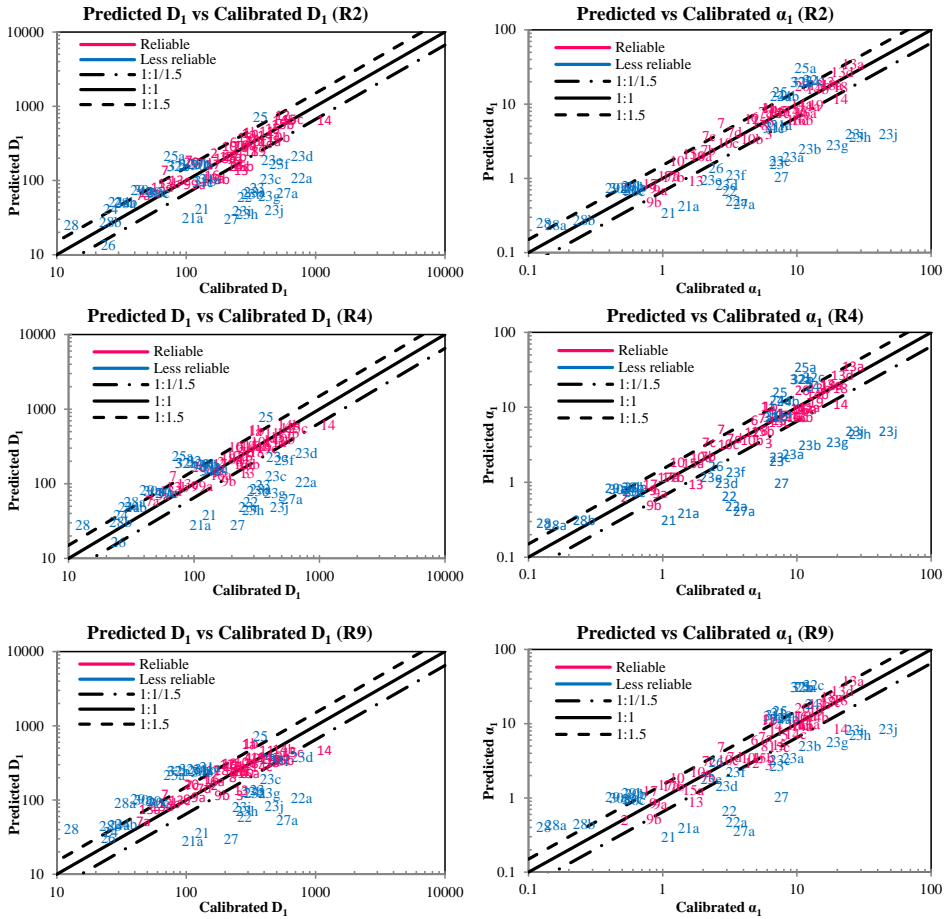


Figure 5.4: Performance of the predictive equations for the dispersion coefficient (left) and mixing number (right) against calibrated values.

most attractive one. Therefore, we conclude that Equation (R4) is the best to predict the tidal average dispersion coefficient at  $x_1$ . This is also theoretically the most attractive, since laboratory experiments have demonstrated that both  $N_r$  and the roughness are key parameters. Nevertheless, if the Chezy roughness is unknown, then Equation (R2) can be applied. Equations (R2), (R4) and (R9) have an  $R^2$  of 0.84, 0.86 and 0.80 with  $SE$  of 0.14, 0.13 and 0.15, respectively. We can also conclude that although estuary shape is the key in defining  $K$ , the dispersion boundary condition  $D_1$  appears to be determined by hydraulic parameters.

Figure 5.4 displays the plots of the predicted  $D_1$  and  $\alpha_1$  against the calibrated values for both the reliable and less reliable datasets using Equations (R2),(R4) and (R9). Here, it is shown that all the reliable data points fall nicely within the range of a factor 1.5. Some of the less reliable data points are also within or near the range except several

obvious outliers such as the Delaware, Schelde, Pungue, and Tejo. This is because the Pungue is often in an unsteady state condition, while the Schelde is dredged, and the Tejo and Delaware are not completely alluvial. In addition, the doubt on the accuracy of the discharge data is also one of the factors contributing to poor results. It can be seen that all the predictive equations selected have underestimated the values of the dispersion coefficient for the outlying data points, indicating a possible underestimation of the river discharge.

Comparing the outliers in both plots, it appears that the unreliable data are distributed closer to the reference lines if the dispersion is represented in term of the mixing number. This implies that the fresh water discharge is partly to blame for the discrepancy. The data used for the regression and results of the predicted dispersion are tabulated in Appendix A.2.

### 5.4.3. MODIFIED PREDICTIVE EQUATION FOR MAXIMUM SALT INTRUSION LENGTH $L^{HWS}$

Comparison between the predicted and calibrated salt intrusion length has been done for HWS condition instead of TA. This is because the salt intrudes furthest into the river system at HWS, and the maximum intrusion is the information water managers are most interested in. Substituting the predictive dispersion Equations (R2), (R4) and (R9) into the general form for salt intrusion length yields:

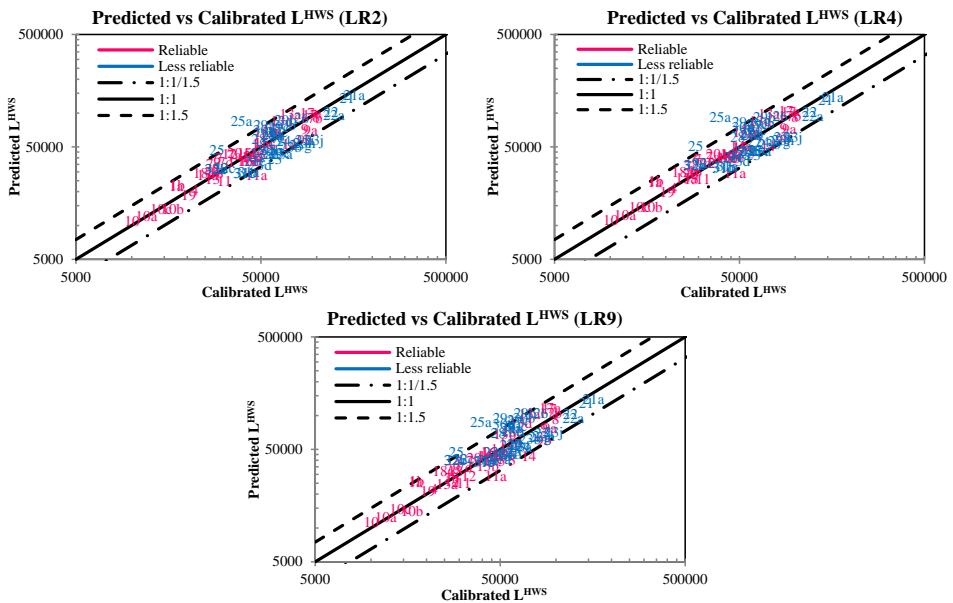


Figure 5.5: Comparison between the predicted and calibrated maximum salt intrusion  $L^{HWS}$  for Equations (LR2), (LR4) and (LR9).

$$L^{HWS} = x_1 + a_2 \ln \left( 0.1167 \frac{E_1 v_1}{K a_2 u_1} N_r^{0.57} + 1 \right) + \frac{E_0}{2} \quad (\text{LR2})$$

$$L^{HWS} = x_1 + a_2 \ln \left( 0.3958 \frac{E_1 v_1 g^{0.21}}{K a_2 u_1 C^{0.42}} N_r^{0.57} + 1 \right) + \frac{E_0}{2} \quad (\text{LR4})$$

$$L^{HWS} = x_1 + a_2 \ln \left( 1.9474 \frac{E_1 v_1 g^{0.51}}{K a_2 u_1 C^{1.02}} N_r^{0.51} + 1 \right) + \frac{E_0}{2} \quad (\text{LR9})$$

Figure 5.5 shows the performance of these equations in predicting the maximum salt intrusion length. In the plots using Equations (LR2), (LR4), and (LR9), all data points fall within the range of factor 1.5 except the Solo Estuary. The list of data and the results are summarized in Appendix A.3. It appears that the predictive equations overestimated the intrusion length in the Solo Estuary. This may be due to the nearly prismatic shape of the channel which has a very long convergence length of 226 km.

#### 5.4.4. LONGITUDINAL SALINITY PROFILES

The salinity curve can be computed by applying Equations (LR2), (LR4), and (LR9) with the different dispersions calculated by each of the predictive measure developed. Considering the substantial amount of salinity measurements available, only the salinity profiles of the 7 newly surveyed estuaries are discussed. The plots of all salinity profiles will be uploaded as electronic material at the website – <http://salinityandtides.com>. Figure 5.6 demonstrates the performance of the simulated longitudinal salinity distribution with and without calibration of  $K$  and  $D_1$ .

From the salinity curve comparison, it appears that all the predictive equations do not performed very well for Kurau and Bernam estuaries. This may be caused by the uncertainty in discharge data. The Kurau and Bernam discharge calculation were based on the discharge observed in a small part of the catchments of about 12% and 20% of the total area, respectively [Gisen et al., 2014a]. Thus, it is possible that we may have underestimate the discharge draining into the Kurau Estuary, and overestimate the one for Bernam Estuary. It is also interesting to note that Equation (LR9) works better in predicting the salinity distribution for some of the estuaries such as the Perak, Linggi and Endau estuary. As for most of the cases, Equation (LR4) appears to give the best fit. The difference in the performance of these equations suggests that there is a possibility that the equations are subject to improvement if more reliable measurements are available. Thus, it is appropriate to retain the three Equations (LR2), (LR4), and (LR9) for consideration.

## 5.5. DISCUSSION

Before Savenije [1993a]'s effort to develop predictive equations for the Van der Burgh and dispersion coefficient, these parameters could only be obtained by calibration. Without site measurements, it was impossible to make any estimate of the salinity distribution along an estuary. The predictive equations of Savenije [1993a, 2005] were able to estimate the value of  $K$  and  $D$  reasonably well in reference to the calibration data. However,

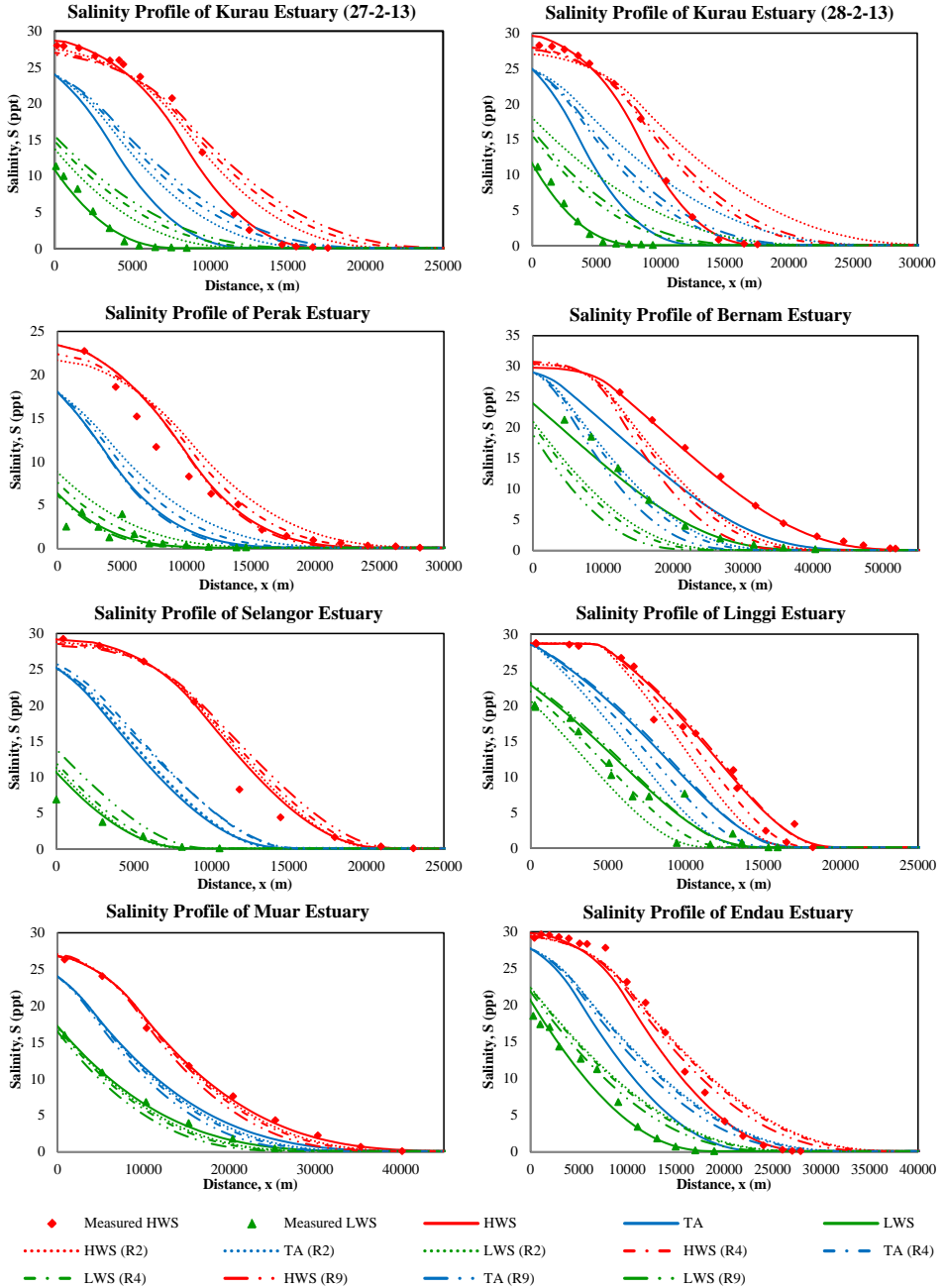


Figure 5.6: Calibrated (solid lines) and predicted (dashed lines) salinity curves compared to observations (symbols) for HWS, TA and LWS in the 7 newly surveyed Malaysian estuaries.

after re-evaluating and re-analysing the available data, we found that the equations do not work as well for all estuaries.

In this study, we have collected an additional 32 salinity profiles from 16 new estuaries for consideration in the analysis. Moreover, the measurements were split into two datasets to make sure that only the reliable data were used for establishing the revised equations. In previous work, the data were not split. The selection process is important so that the results are not influenced by incomplete or uncertain data. Re-examining the available measurements from the old database ensures that all data used are accessible and consistent. The new compilation also provides a section containing important information about each measurement (see electronic additional material – salinity worksheet at <http://salinityandtides.com>).

Another important modification in this work is the change in the selected boundary condition. In this research, we decided to process the cross-sectional data in reference to the tidal averaged situation (TA), whereas previous methods were based on HWS and LWS, which led to inconsistencies because the geometry during low and high water can be different from tidal average situation. Moreover, in this study we fixed the location of the downstream boundary at the inflection point  $x_1$  and not at the estuary mouth (adopted by all the earlier researchers). The reasons and advantages of moving the downstream boundary to the inflection point are:

- to eliminate the difficulty of determining the exact location of the estuary mouth.
- to reduce the effect from wind and waves.
- to eliminate the dilemma of which geometry parameters to use in the predictive equation.

In Savenije [1993a, 2005]'s and Kuijper and van Rijn [2011]'s predictive model, the cross-sectional area convergence length applied to calculate the salt intrusion length was the weighted value obtained from an iteration process. Hence, with the change of the downstream boundary to  $x_1$ , this process is no longer needed and the predictive measures are more consistent.

The new set of dimensionless ratios proposed in this study to establish the predictive equation for  $K$  contains mostly measurable independent parameters. The selection was made based on the existing equations, considering only the parameters that are easy to obtain. It is worth noting that the ratio  $(1 - \delta_H b)$  has been removed from the equation because the damping changes from spring to neap tide. Furthermore, it also decreases or decreases towards upstream and is highly influenced by fresh water discharge. The river to estuary width ratio has been added in the new equation as an additional geometry indicator besides the depth and convergence length. This ratio appeared to have great influence on  $K$ .

For the predictive dispersion equation, the ratio of the depth to the convergence length is no longer important, but the longitudinal length scale  $E$  and velocity amplitude  $v$  remain important in the scaling of  $D_1$ . The elimination of  $\bar{h}/a$  allows the new equation to be applied also in prismatic channels. In the old equation, when  $a_2$  approaching infinity, the calculation became invalid. Since Kuijper and van Rijn [2011] suggested that the friction parameter is related to the vertical mixing,  $g/C^2$  has been included in this

new equation and it indeed improved the correlation. Savenije [2005] did not consider roughness in his predictive equation for dispersion.

Although some improvements and simplicity have been introduced in this study, there are limitations in using the new equations. Until now, we have only taken into account single network estuaries. Furthermore, it has implicitly been assumed that no water is entering or leaving the tributaries in the estuary region. If these are large tributaries or large areas draining on the estuary, then these should be accounted for. From the plot of Van der Burg's coefficient, we found that the performance in predicting  $K$  is rather low. This indicates that the equation has to be used with caution. Another constraint in using the developed equations is the friction factor. The Chezy roughness is not directly measurable and can only be obtained by calibration using a tidal dynamics model. However, if this information is impossible to get, it can be neglected (the correlation only decrease to 0.70 for the predictive equation without roughness). If cross-sectional area information is lacking, then  $b_1$  can be used to replace  $a_1$ . For the depth estimates, one can made used of the method presented by Gisen and Savenije [2014] which links  $\bar{h}_1$  to the bankfull discharge.

## 5.6. CONCLUSION

Calibrating  $K$  and  $D_1$  is only possible if measurement of the salinity distribution is available. In a situation where data are limited, a predictive equation is required to estimate the desired variables. A good predictive equation should be simple (parameters can be easily measured) and efficient. The predictive equations established in this study consist of mostly measurable independent parameters. Options are suggested for the case in which data are very limited. The adjustment of the downstream boundary to the inflection point has clarified the selection of the right geometry parameters to be used and the position of the downstream boundary.

The analysis based on tidal average conditions enables the entire process to be carried out consistently, whereby model and data errors can be reduced. The obtained salt intrusion can easily be converted from TA to HWS by adding half of the tidal excursion. The performance of the predictive equation for  $K$  is rather good with a  $R^2$  value of 0.72. For the dispersion, the correlation of 0.86 seems very promising. All the reliable data points fall within a factor of 1.5 for both the predicted  $K$  and  $D_1$  results. Some less reliable ones are also within this range. This indicates that the predictive equations developed are appropriate to be applied in getting a first estimate of the  $K$  and  $D_1$ . Subsequently, the longitudinal salinity distribution in an estuary can be estimated.

Hence, these tools can be very helpful for water managers and engineering to make preliminary estimates on the salt intrusion in an estuary of interest and to analyse the impact of interventions. Finally, it is recommended to collect more reliable measurements to strengthen the development of the empirical relationships. New data are also required for validation purposes.

# 6

## ESTIMATING BANKFULL DISCHARGE AND DEPTH IN UNGAUGED ESTUARIES

*It is difficult to measure river discharge accurately in an estuary, and particularly in the region where the tidal flow dominates over the river discharge. River discharge is important for the morphology and hydrodynamics of estuaries as it influences the salt intrusion process, tidal dynamics, fresh water supply (water resources management) and the occurrence of floods. Here, we try to derive river regime characteristics from the seaward end: the estuary. It is found that there are empirical relationships that link the geometry of an estuary to its river regime, which can be used to estimate river discharge characteristics with the least of data available. The aims of this study are: 1) to derive empirical relations between geometrical characteristics of estuaries and the bankfull discharge; 2) to explore a physical explanation for this relation; and 3) to estimate the bankfull discharge in estuaries. The physical connection between an estuary and its river regime is found by combining estuary shape analysis, tidal dynamic analysis and Lacey's hydraulic geometry theory. The relationships found between the estuary depth, width and bankfull river discharge have been tested in 23 estuaries around the world (with 7 recently surveyed estuaries). From the analysis, it shows that the depth of an estuary is a function of the bankfull flood discharge to the power of 1/3, which is in agreement with Lacey's formula. This finding not only provides a method to estimate estuary depth, it also allows estimating flood discharge characteristics from readily available estuary shape indicators.*

---

This chapter is based on:

Gisen, J. I. A., and H. H. G. Savenije, Estimating bankfull discharge and depth in ungauged estuaries., Water Resources Research, (under review).

## 6.1. INTRODUCTION

ESTIMATING river discharge in the tidal region of estuaries accurately is difficult when the ratio of tidal flow to river discharge is large [Cai et al., 2014a]. As a result, gauging stations are generally situated well outside the tidal region. The river discharge is not only important for determining the salt intrusion, the potential for irrigation or for ecological reasons, it is also important for understanding the morphology of estuaries. Recently, a new technology for estimating river discharge has become available using Horizontal Acoustic Doppler Current Profiler (H-ADCP) (e.g. Bechle and Wu [2014]; Hoitink et al. [2009]; Sassi et al. [2011a]). However, this approach involves an extended period of repeated surveys which generally consumes considerable amount of time, energy and money. Moftakhari et al. [2013] introduced an analytical solution known as tidal discharge estimation (TDE) to hindcast river flow in San Francisco Bay, making use of time series analysis, but this requires extended periods of observation data.

6

Little research has been done on the relationship between estuary shape and hydrodynamics in alluvial estuaries and even less linking the shape to the hydrology of the drainage basin. Only in recent years, efforts have been taken by Sassi et al. [2012] to study the downstream hydraulic geometry in a tidally influenced estuary, incorporating a moving boat technique with mounted H-ADCP. Townend [2012] established an idealized 3D model to predict the geometry of a range of UK estuaries, using the hydraulic geometry theory. This study aims to develop empirical relations between estuary shape and river discharge which are particularly useful for ungauged estuaries, and to investigate the physical explanation involved. The study focuses on estuaries that are fully alluvial, with limited upstream regulation or dredging. Being alluvial implies that there is a substantial contribution of occasional sediment-laden river discharge [Savenije, 2005]. Examples of alluvial estuaries includes deltas and funnels shaped estuaries, but excludes tidal inlets, bays, rias, fjords, sounds and submerged river valleys. Data from literature, national authorities, and field survey have been collected to derive empirical relations between the geometry and bankfull river discharge. The main contribution of this research is the development of simple approaches to estimate estuary depth and bankfull discharge from minimum available data. Basic information such as topography and tide can be easily obtained through online open databases shared by various local authorities and researchers. Depth estimates can subsequently be made using analytical tidal dynamics equations, while bankfull discharge can be predicted from the river width. Finally, the Canter-Cremers flood number (the relation between the tidal and river flood volume) can be determined on the basis of estuary shape.

Making use of the relationships established in this study, one can make a preliminary estimate of the averaged depth and bankfull flood discharge in an alluvial estuary just by knowing the estuary width and tidal range. This can be a very useful tool for water managers and engineers to gain insight into the hydrologic and hydraulic condition of an ungauged estuary before detailed investigations are carried out.

## 6.2. BACKGROUND THEORIES

### 6.2.1. TIDAL DYNAMICS ANALYSIS

Tidal dynamics refers to the motion of the tide due to gravitational forces induced primarily by the movement of the sun, moon and earth. In estuaries, where both tides and streamflow exist, the hydrodynamics become complicated, as it has to take into account not only the tidal influence but also the effect of river discharge. When the tide propagates into an estuary from the open sea, the change in topography such as variation of depth and funnelling of banks, forces the tide to change its behaviour. Instead of moving in circular motion like in the open sea, the tidal wave moves exclusively in inland direction whereby the water moves periodically both in vertical (high and low water) and horizontally (ebb and flood) direction. The flood and ebb currents, in interactions with the fresh water discharge, determine the distance saline water penetrates into the estuary.

Many numerical tools including 1D, 2D and 3D models have been developed to analyse the hydrodynamics of estuaries. However, an analytical approach has the advantage that it provides direct insight into the processes and is relatively easy to use [Savenije et al., 2008]. Tidal dynamics in converging alluvial estuaries can be described analytically based on the equations for conservation of mass and momentum in a 1-D analytical approach to calculate tidal damping, wave celerity, tidal velocity amplitude, phase lag and average tidal depth [Cai and Savenije, 2013; Cai et al., 2012; Savenije et al., 2008]. In this study, the analytical model of [Savenije et al., 2008] is used because it provides explicit relationships for the parameters in question.

Since the seaward part of an estuary is wave-dominated, only the landward (tide-dominated) region will be considered in the hydrodynamics analysis. The geometry indicator used in this study is represented by either the cross-sectional or width convergence length. The governing dimensionless equations of Savenije et al. [2008] are presented in Table 6.1. Utilizing the width convergence length  $b_2$  in the phase lag equation gives Equations (6.1) and (6.5) for the general and ideal situations (damping  $\delta = 0$ ), where  $\varepsilon$  represents the phase lag between high water (HW) and high water slack (HWS) (or low water (LW) and low water slack (LWS)),  $\delta$  is the damping number,  $\lambda$  is the celerity number, and  $\gamma$  is the estuary shape number as defined in Equations (6.3), (6.8) and (6.9), respectively.

The estuary shape number represents the ratio between the classical wave celerity  $c_0$ , tidal frequency  $\omega$  and convergence length  $b_2$  [Savenije, 1992, 1993b]. The tidal period  $T$  varies among estuaries, with 12.4 hours for a semi-diurnal tide, and 24 hours for a diurnal tide [Pond and Pickard, 1983]. The phase lag is an important parameter in tidal dynamics as it determines the type of tidal wave, the occurrence of damping or amplification, and thus the wave celerity. For mixed-tidal wave condition, the phase lag ranges between 0 and  $\pi/2$  as displayed in Equation (6.11) [Dyer, 1997]. If the phase lag is near to zero (highest water level with zero velocity), the tidal wave behaves as a standing wave; if it is close to  $\pi/2$ , it behaves as a progressive wave. It should be observed that in convergent alluvial estuaries, purely standing or progressive waves do not occur and that the phase lag  $\varepsilon$  is bound by the condition  $0 < \varepsilon < \pi/2$  [Savenije, 2005].

The second dimensionless equation is the scaling equation (Equation (6.2)), where  $\mu$  is the velocity number derived from Equation (6.7),  $r_s$  is the storage width ratio of

Table 6.1: Dimensionless equations applied in the tidal dynamics analysis.

<b>Governing Equations</b>				
Variables	Phase lag $\tan(\epsilon)$	Scaling $\mu$	Damping $\delta$	Celerity $\lambda^2$
General condition	$\frac{\lambda}{\gamma - \delta}$ (6.1)	$\frac{\sin \epsilon}{\lambda} = \frac{\cos \epsilon}{\gamma - \delta}$ (6.2)	$\frac{\mu^2}{\mu^2 + 1} (\gamma - \chi \mu^2 \lambda^2)$ (6.3)	$1 - \delta (\gamma - \delta)$ (6.4)
Ideal estuary	$\frac{1}{\gamma}$ (6.5)	$\frac{1}{\sqrt{1 + \gamma^2}}$ (6.6)	0	1
<b>Symbols definition</b>				
Velocity number $\mu = \frac{1}{r_s} \cdot \frac{v \bar{h}}{\eta c_0}$	(6.7)	Celerity number $\lambda = \frac{c_0}{c_x}$	(6.8)	
Estuary shape number $\gamma = \frac{c_0}{\omega b_2}$	(6.9)	Friction number $\chi = r_s f \frac{c_0 \eta}{\omega \bar{h}^2}$	(6.10)	
Phase lag $\epsilon = \frac{\pi}{2} - (\phi_z - \phi_u)$	(6.11)	Friction factor $f = \frac{g \left[ 1 - (4\eta/3\bar{h})^2 \right]^{-1}}{K_m^2 \bar{h}^{-1/3}}$	(6.12)	
Tidal frequency $\omega = \frac{2\pi}{T}$	(6.13)	Wave celerity at the mouth $c_0 = \sqrt{\frac{g \bar{h}}{r_s}}$	(6.14)	

the total (regime) width  $B$  over the effective (storage) width  $B_e$  which has the value in the order of 1-2 [Cai and Savenije, 2013],  $v$  is the tidal velocity amplitude,  $\eta$  is the tidal amplitude (half of the tidal range  $H$ ), and  $\bar{h}$  is the average depth of an estuary. When the tidal velocity amplitude is known, the tidal excursion  $E$  can be computed as:

$$E = \frac{vT}{\pi} \quad (6.15)$$

Bruun and Gerritsen [1960], Pethick [1984] and Langbein [1963] observed that tidal inlets appear to have surprisingly uniform tidal velocity amplitude of  $1 \text{ ms}^{-1}$  during spring tide. This occurs in all alluvial estuaries regardless of the type of tide and location. Savenije [2005] observed that, as a consequence of the exponential shape, this also applies along the estuary axis, resulting in a constant tidal excursion.

In the tide-dominated area, the tidal damping can be expressed by a simple dimensionless linear equation [Savenije, 2001; Savenije et al., 2008] shown in Equation (6.3). It can be seen from the equation that the damping is dependent on the channel roughness, which in this paper is symbolized by the friction number  $\chi$  (see Equation (6.10)), where  $f$  is the friction factor, based on Manning's equation. As the tidal wave propagates inland in an estuary, the convergence in the geometry increases the wave energy per unit width which is simultaneously dissipated by friction. In an ideal estuary, where there is no damping or amplification, the amount of energy gained per unit width is equal to the energy dissipated through friction. If the convergence is stronger than the friction, the tidal wave is amplified. Conversely, damping occurs if the convergence is weaker than

the friction [Cai et al., 2012].

The analytical relation between celerity and tidal damping or amplification was developed by Savenije and Veling [2005], who incorporated tidal damping into the classical celerity equation. Expressing the celerity equation in dimensionless form yields Equation (6.4). In an ideal estuary, the wave celerity is the same as for a progressive wave. If the wave celerity is larger than  $c_0$ , the tide is amplified. Otherwise, it is damped. Estimation of the average tidal depth can be derived analytically from the scaling equation (Equation (6.2)) by rewriting the damping in the form of the tidal range damping rate  $\delta_H$  which gives:

$$\frac{\bar{h}}{b_2} = \frac{H}{E(1 - \delta_H b_2)} \cos(\epsilon) \quad (6.16)$$

$$\text{where: } \delta_H = \delta \frac{\omega}{c_0} \quad (6.17)$$

Depending on the amount of information available, this equation can be used with either the width convergence or cross-sectional area convergence length. In cases where cross sectional data are not available, the width convergence length can be used assuming that the depth is near constant. Details on the methods for each analysis will be described in the methods section.

### 6.2.2. HYDRAULIC GEOMETRY (REGIME THEORY)

Lacey [1930] is among the pioneer in discovering the theory of hydraulic geometry. He originally presented his regime theory in the form of wetted perimeter as:

$$P_b = 4.8Q_b^{0.5} \quad (6.18)$$

where  $P_b$  is the wetted perimeter and  $Q_b$  is the fresh water discharge [Cao and Knight, 2002; Savenije, 2003]. The subscript  $b$  represent the bankfull condition. Assuming that the channel width is much larger than the depth, Equation (6.18) can be written in term of channel width  $B_b$  as:

$$B_b = 4.8Q_b^{0.5} \quad (6.19)$$

More recently, Savenije [2003] elaborated Lacey's formula, making use of Lane [1955]'s stable channel theory to seek for a possible physical explanation of the regime theory. Incorporating the findings from Blench [1952], and Simon and Albertson [1963] who studied hydraulic geometry of different bed and bank materials, Savenije replaced the coefficient in Equation (6.19) with a sediment material coefficient known as  $k_s$ :

$$B_b = k_s Q_b^{0.5} \quad (6.20)$$

According to Simon and Albertson [1963], coefficient  $k_s$  has the values of 3.1 for coarse sand and 6.2 for sand. Combining Equations (2.17) and (2.18) with the coefficients  $y = 1/3$  and  $z = 1/2$  for bankfull condition, Cao and Knight [1996, 2002] presented a relationship between bankfull depth and width as:

$$h_b = \frac{1}{\psi} B_b^\theta \quad (6.21)$$

where  $\psi$  is a constant for the basic regime theory and  $\theta$  is the exponent of the river width with a value of 2/3. Besides, the bankfull depth is also suggested to be proportional to the bankfull discharge with a power  $\gamma = 1/3$  as:

$$h_b = cQ_b^\gamma \quad (6.22)$$

Hydraulic geometry theory is in general used to predict channel properties in a regime river network where there is no tidal effect. In tidally dominated areas such as deltas and estuaries, the converging channel geometry and fluctuating water level induced by the tidal cycle make the system more complex compared to a river regime. Despite this complexity, efforts have been made to discover and extend the applicability of the hydraulic geometry to the estuarine region. Sassi et al. [2012] developed a method to measure the tidal influenced on delta morphology for a case study of a multi-channel estuary in Indonesia: the Mahakam Delta, adopting a two-dimensional finite element model. Further work was carried out by Townend [2012] who predicted the geometry characteristics of a wide range of estuaries in United Kingdoms. He idealized the estuary in a three-dimensional form, described by the tidal prism and surface area of intertidal flats. The governing parameters were estimated by considering only the external estuarine properties such as mean sea level, tidal range, river discharge and sediment transport.

In this study, we make use of an exponential 1-D topography and analytical tidal dynamics model in combination with Lacey's hydraulic geometry theory to predict estuary depth and the bankfull discharge feeding the estuary. The proposed method is simple and applicable to a wide range of estuaries. Moreover, it can be used with minimum data available and is useful to obtain first order estimates in preparation of a more detailed field study.

### 6.3. METHODS

The targeted area of study is the region of transition between river and estuary where the tide dominates river discharge. In the region of interest, there is a gradual transition of a constant river width to an exponentially varying estuary width as tabulated in Table 6.2. Survey data from 23 estuaries around the world have been used to investigate the relationship between estuary geometry and fresh water discharge by incorporating the downstream hydraulic geometry theory. According to Lee and Julien [2006], downstream hydraulic geometry considers the variation in the channel form for the entire stream, given a certain discharge frequency, referred to as bankfull discharge. This seems appropriate as the data obtained in this study is limited. In order to make the theory hold, several criteria have to be met:

1. The estuary is fully alluvial, with minimal human interventions.
2. It is funnel shaped with a geometry that varies exponentially.
3. The estuary is long enough for the mixed tidal wave to occur.

4. The estuary has a nearly constant depth.
5. The tidal data collected refers to spring tidal condition.

Table 6.2: Summary of the geometry analysis for all the estuaries considered in this study.

No	Estuary	$A_0$ (m <sup>2</sup> )	$A_1$ (m <sup>2</sup> )	$B_0$ (m)	$B_1$ (m)	$a_1$ (km)	$a_2$ (km)	$b_1$ (km)	$b_2$ (km)	$\bar{h}_1$ (m)	$x_1$ (m)
1	Kurau	<sup>1</sup> 1800	660	1400	130	3.6	46	1.5	28	6.2	3600
2	Perak	<sup>1</sup> 20500	9210	9100	2070	5.0	37	2.7	21	6.3	4000
3	Bernam	<sup>1</sup> 15800	4460	5600	1270	3.4	25	2.9	17	5.3	4300
4	Selangor	<sup>1</sup> 2200	1000	1100	270	3.5	13.4	2	13.4	3.7	2800
5	Muar	<sup>1</sup> 3300	1580	1800	280	5.3	100	2.1	31	8.2	3900
6	Endau	<sup>1</sup> 6600	2000	5200	310	4.0	44	1.7	44	6.5	4800
7	Linggi	<sup>1</sup> 5100	1500	1100	320	0.4	7.5	0.4	12.5	3.2	500
8	Rompin	<sup>2</sup> 1800	840	450	140	25.0	110	16	110	6.1	19000
9	Ulu Sedili Besar	<sup>2</sup> 1700	670	800	140	4.6	38	2.5	49	4.1	4300
10	Maputo	<sup>3</sup> 47500	4700	11700	1150	2.2	16	2.2	16	4.1	5100
11	Corantijn	<sup>3</sup> 69000	26800	30000	5000	19	64	10	48	6.7	18000
12	Mea Klong	<sup>3</sup> 6500	1100	1400	240	1.8	150	1.8	150	4.6	3200
13	Lalang	<sup>3</sup> 2880	-	360	-	167.0	-	94	-	10.3	-
14	Limpopo	<sup>3</sup> 1700	1140	550	180	50.4	130	18	130	6.3	20000
15	Tha Chin	<sup>3</sup> 20000	1440	3600	260	1.9	87	1.9	87	5.6	5000
16	Chao Phya	<sup>3</sup> 4600	3100	860	470	30.0	130	20	130	6.5	12000
17	Delaware	<sup>3</sup> 255000	-	37655	-	41.0	-	42	-	6.4	-
18	Pungue	<sup>3</sup> 14500	-	5200	-	18.5	-	18.5	-	2.8	-
19	Incomati	<sup>3</sup> 7900	1070	3950	380	7.5	40	6.4	40	2.8	15000
20	Eems	<sup>3</sup> 120000	-	31623	-	19.0	-	19	-	3.8	-
21	Gambia	<sup>3</sup> 100000	35700	14000	3700	32.0	96	25	100	8.8	33000
22	Thames	<sup>3</sup> 67500	10900	9000	780	17.0	23	12.7	40	8.2	31000
23	Schelde	<sup>3</sup> 150000	-	16000	-	27.0	-	27	-	9.4	-

Source: <sup>1</sup> Surveyed by authors (2011-2013); <sup>2</sup> Malaysia National Water Resources Study (2000); <sup>3</sup> Savenije (2005, 2012).

The methodology described in this study involves five elements: estuary shape, upscaling of fresh water discharge, tidal dynamics, regime relations and estimation of the estuarine flood number.

### 6.3.1. ESTIMATING THE RUNOFF OF THE TOTAL DRAINAGE BASIN

It is important to note that the discharge data available for the Malaysian estuaries represent an underestimation of the total fresh water discharge into the estuary. This is because the nearest discharge stations are located well landward from the tidal region, which implies that the contributions from seaward tributaries are neglected. To account for this information gap, an upscaling approach has been adopted. Since we only use annually maximum discharge data for the frequency analysis, the time lag in the hydrograph can be neglected. The adjusted discharge has been estimated in proportion to the drainage area, considering two different landscape classes (see Figure 6.1): one considering only the sloped area; and the other based on the entire catchment area including flatland. The GIS topography maps of the 9 estuaries are displayed in Figure 6.2. These

maps were processed using a DEM at 90 m resolution, downloaded from the USGS website.

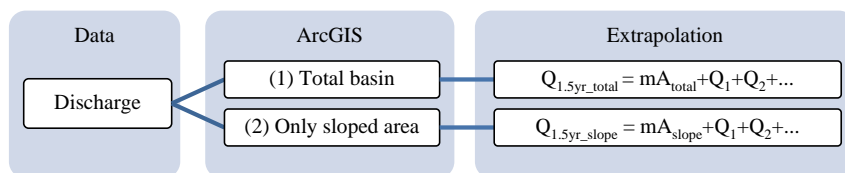


Figure 6.1: The methods tested to improved the underestimated value of the collected bankfull discharge.

In determining the upscaling equations, the catchments were grouped depending on the number of stations available. For catchments that had more than four discharge stations, such as the Perak and Endau, the regression was done using the data of the nested catchment only. For the others, the data were grouped so as to have enough data points for regression. Data were grouped by their location in the east (Endau, Rompin, and Ulu Sedili Besar) or west (Kurau, Perak, Bernam, Selangor, Muar, and Linggi) of the Malaysian Peninsula. Regressions for each group were performed using both upscaling methods, as shown in Figure 6.1.

Figure 6.3 shows the discharge-catchment relation as a power function. Such a relationship is only valid if the climate and the general topography in the study region are homogeneous. The upscaling results displayed are obtained using the second method that only uses the sloped part of the catchments, as it better accounted for landscape variability compared to the first method. This is because some catchments such as Selangor, Muar, Endau, and Ulu Sedili Besar, have more flatland areas in the seaward region which are expected not to contribute much to the bankfull discharge. By considering only the sloped area, overestimation of the bankfull discharge could be avoided.

Substantial amounts of data have been utilized in conducting this study. Some data are readily available from the literature, and some were collected via several field surveys. In most developed countries such as the United Kingdom, United State, Netherlands and Germany, hydrological data are shared openly with the public through their official governmental website without any charges. Topography (satellite data) and mapping information are also accessible with the aid of Google Earth and the United States Geological Survey (USGS) website. Details on the types of data collected from the literature, field surveys, Malaysian authorities, and free online applications are listed in Table 3.2.

### 6.3.2. ESTIMATING THE DEPTH FROM TIDAL HYDRAULICS

Information on the cross-sectional area and tidal depth can only be analysed and plotted if observations are available. However, there are still many estuaries around the globe of which the bathymetry has not been surveyed. Since the width can be observed by satellite, the most important unknown is the estuary depth. Depending on the amount of data available, the average depth has been calculated for three different conditions and compared to the observed depth obtained from field surveys. The three computed depths obtained from the tidal dynamics analysis include the hydraulic depth  $h_{hyd}$ , regime depth  $h_{reg}$ , and ideal depth  $h_{ideal}$ .

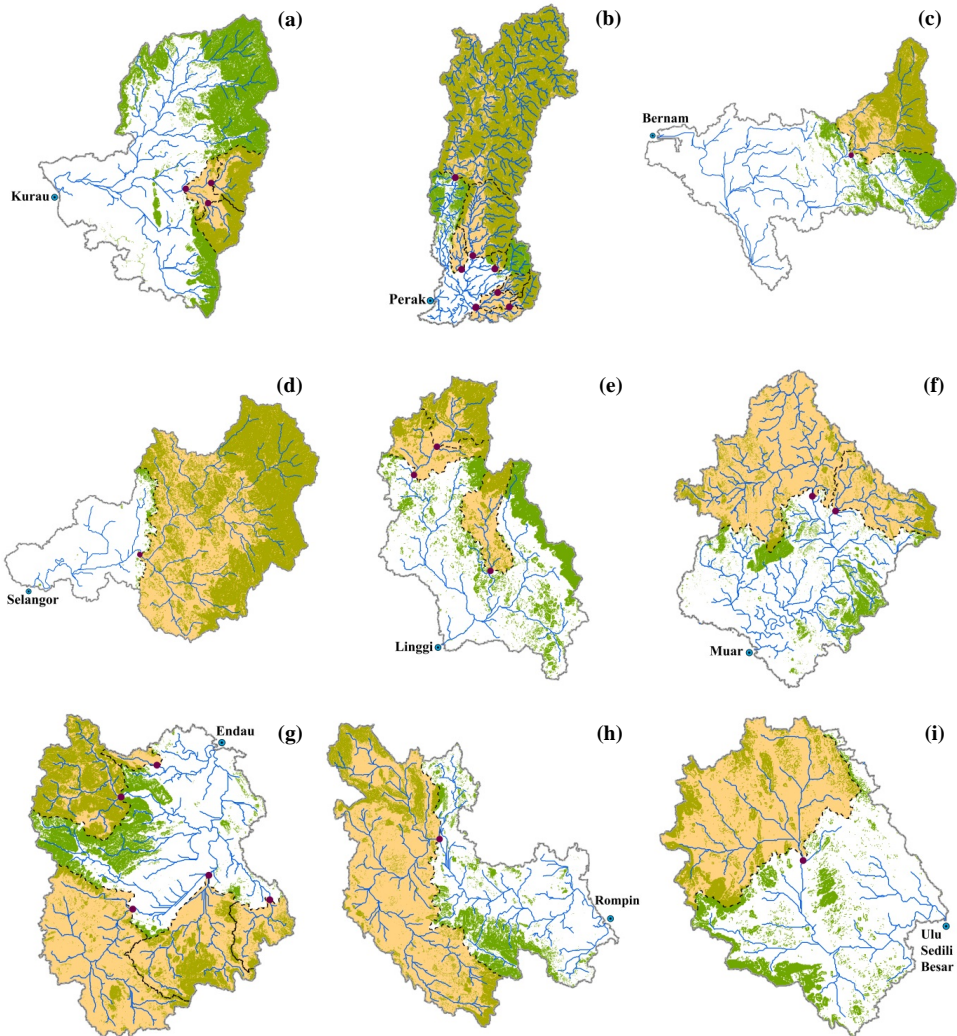


Figure 6.2: Topography maps of the 9 studied catchments in Malaysia: a) Kurau; b) Perak; c) Linggi; d) Bernam; e) Selangor; f) Muar; g) Endau; h) Rompin; and i) Ulu Sedili Besar, with green patches representing the sloped area in the gauged (in yellow) and ungauged are. Maps are not to scale.

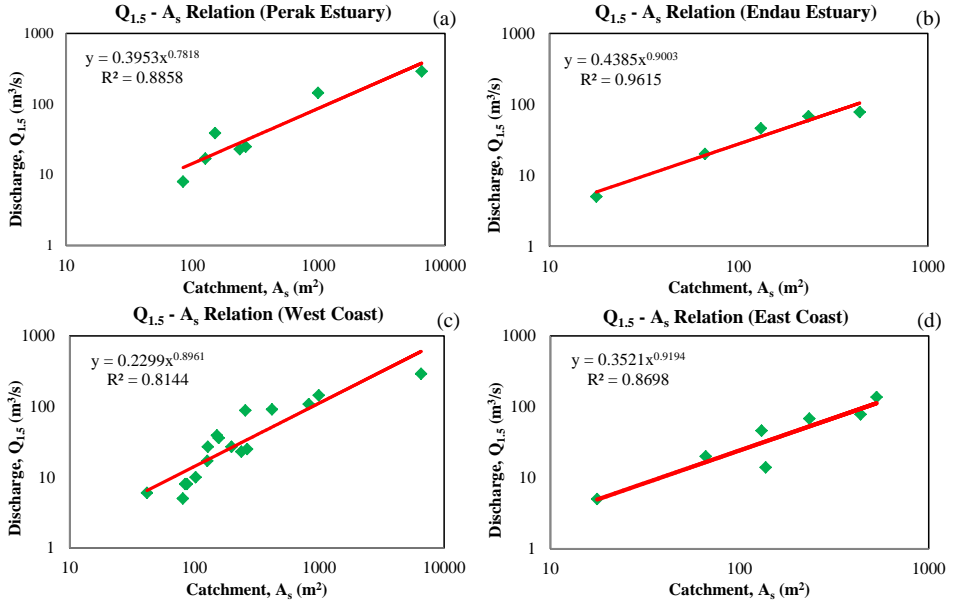


Figure 6.3: Regression between bankfull discharge and catchment area using data from available gauging stations, in which extrapolation is done based on region: a) Perak Estuary; b) Endau Estuary; c) West Coast Estuaries; and d) East Coast Estuaries.  $A_s$  ( $m^2$ ) is the sloped part of the catchments.

6

The formulas used to obtain the depth for different levels of data availability are based on Equations (6.23) to (6.26) in the order of decreasing available information:

- i Data on estuary width, water level, velocity and damping or amplification are available, but no cross-sectional data.

$$h_{hyd} = \frac{Hb_2}{(1 - \delta_H b_2)} \cdot \frac{\pi}{vT} \cdot \cos(\epsilon) \quad (6.23)$$

where  $\cos(\epsilon)$  can be estimated in dimensionless form as:

$$\cos(\epsilon) = \frac{\gamma - \delta}{\sqrt{\lambda^2 + (\gamma - \delta)^2}} \quad (6.24)$$

- ii Observed data of estuary width, water level and damping or amplification are available, with no tidal velocity information. Therefore, it is assumed that the tidal velocity amplitude corresponds with the “regime” value of  $1 \text{ ms}^{-1}$  at spring tide.

$$h_{reg} = \frac{Hb_2}{(1 - \delta_H b_2)} \cdot \frac{\pi}{T} \cdot \frac{\cos(\epsilon)}{(v = 1)} \quad (6.25)$$

- iii Only the estuary width is known with no hydraulic data available. The additional assumption made is that there is no significant tidal damping or amplification (ideal estuary where  $\delta_H = 0$ ), and the velocity amplitude  $v = 1 \text{ ms}^{-1}$  at spring tide.

$$h_{ideal} = \frac{Hb_2}{T} \pi \cdot \frac{\cos(\epsilon)}{(v = 1)} \quad (6.26)$$

In estuaries with an open landward boundary (so called estuaries of infinite length),  $\cos(\epsilon)$  is close to unity [Savenije et al., 2008]. Hence, by performing an iteration process (initially assuming  $\cos(\epsilon) = 1$ ), the values for  $\bar{h}$  and  $\cos(\epsilon)$  can be obtained. The value for the tidal range  $H$  is taken as the average spring tidal range over a few years period, which can be obtained from any online tidal prediction website. In this analysis, the geometry indicator is represented by the width convergence length  $b_2$ . Table 6.3 lists the summary of the input data for the tidal dynamics analysis to estimate the estuary depth. The observed averaged depth is taken as the initial depth in the iteration process.

Table 6.3: List of parameters used in the tidal dynamics analysis to predict the average depth for different data availability conditions.

No	River	$b_2$ (km)	$\bar{h}_1$ (m)	H (m)	v (m/s)	T (hr)	E (km)	$\delta_H$ ( $\text{m}^{-1}$ )
1	Kurau	28	6.2	2.30	0.66	12	9	-6.30
2	Perak	21	6.3	2.80	0.88	12	13	3.00
3	Bernam	17	5.3	2.90	0.98	12	14	1.70
4	Selangor	13.4	3.7	4.00	0.89	12	13	-3.70
5	Muar	31	8.2	2.00	0.77	12	11	-2.70
6	Endau	44	6.5	1.90	0.70	12	10	-1.30
7	Linggi	12.5	3.2	2.00	0.61	12	9	-14.00
8	Rompin	110	6.1	2.50	0.61	12	9	-33.40
9	Ulu Sedili Besar	49	4.1	2.50	0.77	12	11	-25.50
10	Maputo	16	4.1	3.29	0.91	12	13	2.00
11	Corantijn	48	6.7	3.10	0.77	12	11	-1.70
12	Mae Klong	150	4.6	3.30	0.55	24	15	-4.20
13	Lalang	94	10.3	2.60	1.05	24	29	-0.50
14	Limpopo	130	6.3	1.90	0.56	12	8	1.70
15	Tha Chin	87	5.6	2.60	0.73	24	20	-5.50
16	Chao Phya	130	6.5	3.38	0.80	24	22	-2.20
17	Delaware	42	6.4	1.80	0.56	12	8	0.70
18	Pungue	18.5	2.8	6.70	1.12	12	16	-8.50
19	Incomati	40	2.8	3.29	0.63	12	9	-19.90
20	Eems	19	3.8	3.60	1.05	12	15	-0.70
21	Gambia	100	8.8	1.83	0.63	12	9	-0.40
22	Thames	40	9.2	5.30	0.98	12	14	1.10
23	Schelde	27	9.4	4.00	0.77	12	11	2.80

Considering a constant depth in the estuary region, it is assumed that the river regime depth near the landward boundary of the estuary determines the average tidal depth,  $h_b \approx \bar{h}$ . This assumption is subsequently applied in the development of the predictive formula for bankfull discharge by integrating Lacey's formula into an estuarine number.

### 6.3.3. REGIME EQUATIONS

The relationship between the river width and bankfull discharge just outside the tidal region has been applied based on Equation (6.20), to determine which discharge frequency is best to represent bankfull discharge. Savenije [2003], Castro and Jackson [2001], Williams [1978] and Dury [1976], among others, found that the recurrence interval of bankfull discharge is approximately 1.5 to 2 years. Therefore, Equation (6.20) was tested for a range of return periods (20, 10, 2, 1.5 and 1.1 years) to check if the bankfull discharge was indeed associated with a maximum flood frequency of once in 1.5 to 2 years. Selection of the best discharge frequency was done in accordance with Simon and Albertson [1963], who claimed that the coefficient  $k_s$  in Equation (6.20) has the values of 3.1 for coarse sand and 6.2 for sand.

Subsequently, a regression has been performed between the regime river discharge and the mean estuary depth to further test the validity of the hydraulic geometry relationship, using Equation (6.22). For the estuary depth, four different estimates have been taken into consideration: the observed depth  $h_{obs}$ , the hydraulic depth  $h_{hyd}$  (Equation (6.23)), the regime depth  $h_{reg}$  (Equation (6.25)), and the ideal depth  $h_{ideal}$  (Equation (6.26)). Additionally, the modified aspect ratio between the width and depth at the landward boundary of an estuary defined in Equation (6.21) has also been verified for the four different depth estimates.

### 6.3.4. ESTIMATING THE ESTUARINE FLOOD NUMBER $N$

Canter-Cremers' estuary number  $N_Q$ , represents the ratio between the fresh water discharge during a tidal period to tidal flood volume [Savenije, 2005]:

$$N_Q = \frac{Q_b T}{P_t} = \frac{Q_b T}{A_1 E} = \frac{Q_b}{B_1 \bar{h} v} \pi \quad (6.27)$$

where  $P_t$  is the tidal flood volume,  $A_1$  and  $B_1$  are the cross-sectional area and width of an estuary of an estuary the inflection point  $x_1$ , respectively. Savenije [1992, 1993b] showed that the tidal flood volume equals the product of the tidal excursion  $E$  and cross-sectional area  $A$ . Since it is difficult to measure the discharge accurately due to the tidal influence, a new approach to calculate the estuary number has been developed by the relation mentioned in the hydraulic geometry theory. Substituting Equation (2.20) into the Canter-Cremers number leads to:

$$N_Q = \left( \frac{B_b}{B_1} \right) \cdot \left( \frac{h_b U_b}{\bar{h} v} \right) \cdot \pi \quad (6.28)$$

In accordance with the findings of Bretting [1958] and Bruun and Gerritsen [1960], velocity amplitude of tidal flow is assumed to be  $1 \text{ ms}^{-1}$  during spring tide. Hence, the velocity amplitude of  $1 \text{ ms}^{-1}$  is like a regime equation for alluvial estuaries. However, the value for the bankfull velocity  $U_b$  in the river regime is unknown although the order of magnitude generally ranges between  $1 \text{ m/s}$  to  $2 \text{ m/s}$  in a low-lying alluvial stream [Savenije, 2003].

Additionally, the estuary depth  $\bar{h}$  is assumed to be governed by the regime depth  $h_b$ . In order to combine all the unknowns in one variable, the specific discharge ratio  $k_b$  is introduced as the proportion of the bankfull flow per unit width (near the landward end

Table 6.4: Summary of the data and parameters used in predicting the Canter-Cremers flood number  $N$ .

No	River	$B_1$ (m)	$B_b$ (m)	$\bar{h}_1$ (m)	$v$ (m/s)	$Q_{1.5}$ (m <sup>3</sup> /s)
1	Kurau	130	20	6.30	0.66	113
2	Perak	2070	130	6.30	0.88	598
3	Bernam	1270	45	5.30	0.98	134
4	Selangor	270	35	3.70	0.89	111
5	Muar	280	55	8.20	0.77	180
6	Endau	310	72	6.50	0.70	331
7	Linggi	320	25	3.20	0.61	60
8	Rompin	140	50	6.10	0.61	223
9	Ulu Sedili Besar	140	35	4.10	0.77	50
10	Maputo	1150	100	4.10	0.91	280
11	Corantijn	5000	400	6.70	0.77	4090
10	Mae Klong	240	150	4.60	0.55	2000
11	Lalang	360	130	10.30	1.05	2500
12	Limpopo	180	90	6.30	0.51	1100
13	Tha Chin	260	45	5.60	0.47	600
14	Chao Phya	470	200	6.50	0.72	3620
15	Delaware	37655	120	6.40	0.56	2000
16	Pungue	5200	50	2.80	1.12	930
17	Incomati	380	22	2.80	0.56	500
18	Eems	31623	55	3.80	1.05	300
19	Gambia	3700	110	8.80	0.63	2000
22	Thames	780	50	9.20	0.98	304
23	Schelde	16000	50	9.40	0.77	500

of the estuary) to the tidal flow amplitude per unit width (near the estuary mouth) of which the order of magnitude is considered to be close to unity. Hence we obtain:

$$N_b = k_b \left( \frac{B_b}{B_1} \right) \cdot \pi \quad (6.29)$$

where  $N_b$  is the estuary number that primarily depends on the ratio between the bank-full width and the estuary width at the inflection point. The magnitude of  $B_b$  and  $B_1$  can be easily estimated from Google Earth. With this method, it would be possible to obtain the Canter-Cremers number even when the fresh water discharge is unknown. The summary of the data utilized in this analysis is presented in Table 6.4.

## 6.4. RESULTS AND DISCUSSION

### 6.4.1. DEPTH ESTIMATES

Before verifying the applicability of the regime theory in estuaries, we first need to calculate the various depth estimates according to the data available as described in Equation (6.23) to (6.26). The comparison between the different depth estimates is presented in Figure 6.4. Since this study is based on the condition during spring tide (spring tidal range with velocity amplitude of  $1 \text{ ms}^{-1}$ ), the regime depth is taken as reference on the horizontal axis, while on the vertical axis are the observed, hydraulic and ideal depths.

The two lines parallel to the line of perfect agreement differ by a factor 2. As can be seen from the graph, most estimated depths plot above the line of perfect agreement, particularly the hydraulic and ideal depth. For the observed depth, there are several that lie below the reference line. Despite a few significant outliers (deeper depth), the depth estimates fall within a range of a factor 2 compared to the regime depth.

The large scatter between the observed and the regime depth can be explained by the uncertainty in the geometry data. In the analytical tidal dynamic solution, the computed width and depth is actually referred to the effective stream width  $B_e$  and depth  $h_e$ , respectively as shown in 6.5. The effective cross-sectional area  $A_e$  is hatched in blue. However, the observed geometry obtained in this study takes into account the entire cross-sectional area in reference to the tidal average (see dotted lines). This may lead to underestimation of the estuary average depth as the inactive cross-sectional storage area has a shallower depth than the effective stream area.

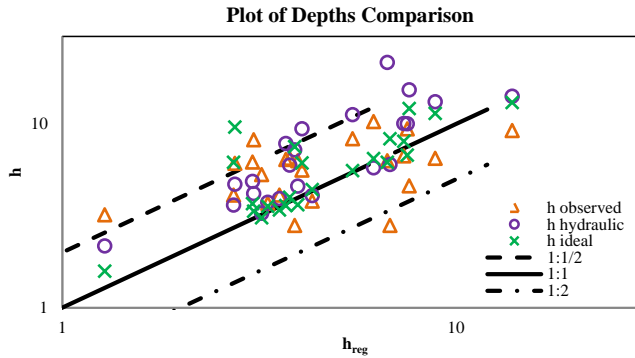


Figure 6.4: Comparison between the observed depth and computed depths of the estuaries.

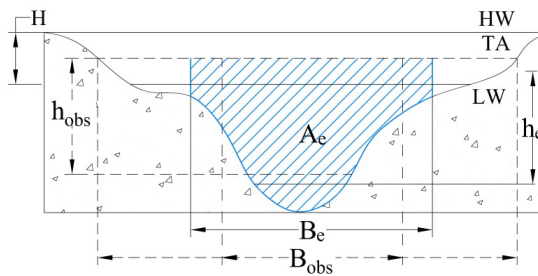


Figure 6.5: Cross-sectional sketch of the hydraulic and observed geometry.

One the other hand, an overestimation of the observed depth may be explained by the inability to measure the depth at the exact boundary of the banks especially during low flow, which may neglect part of the effective cross-section. In the coastal part of estuaries, the banks are often covered with plantations such the Nipah palm or mangroves.

This limits the accessibility to the bank boundary by boat. Furthermore, the depth captured during measurement may not fully represent the bankfull condition. Increasing depth landward as shown in the geometry result in Figure 4.5 also resulted in a deeper average value of the observed depth. The cross-sectional data for most of the estuaries studied, particularly the Malaysian estuaries, have been collected only until the salt limit. It may be possible that the tidal depth becomes shallower when it reaches the tidal limit.

### 6.4.2. VERIFICATION OF THE REGIME THEORY FOR WIDTH

The bankfull discharge was determined by comparing the plots of the regime width against different discharge frequency of 20, 10, 2, 1.5 and 1.1 years return period. From the plots, we found that the bankfull discharge is indeed best represented by 1.5 to 2 years discharge frequency (see Appendix A.4). This is because the coefficient of the regression obtained for these two discharge frequencies were the closest to the one defined by Simon and Albertson [1963], and had the most data points falling within the range.

The relation between the channel width  $B_b$  at the landward boundary and the bankfull discharge  $Q_b$  was also examined to validate the relation described in Equation (6.20). In Lacey's theory, it is generally agreed that the width is proportional to the bankfull discharge to the power of 1/2. Here, the best fit is obtained with an exponent of 0.47 and  $R^2$  of 0.66 as shown in Figure 6.6. There appears to be a good agreement with Lacey's regime theory, which can be clearly seen by comparing the dashed-dotted line with a fixed exponent of 0.5 to the regression line (solid red), which has a constant of 3.1. The value 3.1 is completely in line with the result for sandy bed material, which is generally found in a river regime. Thus, our findings support the hypothesis that the regime theory is applicable to the landward boundary of an alluvial estuary.

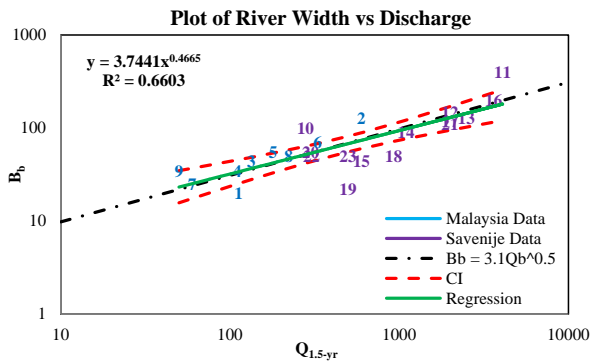


Figure 6.6: Power function relationship between the channel width at the upstream boundary of the estuary and bankfull discharge. Confidence interval (CI) of 95% is presented in dotted lines.

### 6.4.3. VERIFICATION OF THE REGIME THEORY FOR DEPTH

The observed and estimated depths from the tidal dynamics analyses were subsequently plotted against the bankfull discharge to investigate if there is a significant relationship.

Hereby it is implicitly assumed that the estuary depth and river depth at the head of the estuary is equal, which is a further constraining assumption. The plots in Figure 6.7 indicate a general agreement with the regime theory described in Section 6.2.2. In these plots, the data of four estuaries including Rompin (8), Ulu Sedili Besar (9), Thames (22), and Schelde (23) have been excluded from the regression, but are plotted as outliers. The reason is that the Thames and Schelde Estuary are not alluvial: they are heavily dredged and lined for navigation purposes. Hence their depth is not in agreement with the regime depth. As for the Rompin and Ulu Sedili Besar, the data obtained from the literature may not be very reliable due to the following reasons:

1. All the information was taken from a report.
2. The datum used refers to the Mean Sea Level for the cross-sectional area, while for the rest of the estuaries the cross-section is in reference to the tidal average.
3. A lot of the discharge data collected over the 29 years is incomplete which led to uncertainty in the discharge analysis.
4. It is difficult to determine whether the tide should be considered as diurnal or semi-diurnal.
5. The water level observations between stations are not entirely consistent, with one station showing different patterns.

## 6

According to Lacey [1930], the exponent of the power function for the depth should be about 1/3. Here we found that the average depth of the estuaries is proportional to the bankfull discharge to the power of 0.12 to 0.35 for different depth estimates. The variation in the exponent indicates that the hydraulic geometry relationship is sensitive to the depth estimation. The correlation between discharge and depth is reflected by  $R^2$  which varies between 0.18 and 0.74, with the observed depth giving the worst correlation. The regime depth with the assumption that the velocity amplitude is equivalent to  $1 \text{ ms}^{-1}$  gives the best correlation with an exponent of 0.30. The relatively poor correlation for the observed depth is probably caused by the large observational uncertainty due to the high spatial variability of the bottom level, which subsequently affects the performance of the results. For the condition where only the width geometry and tidal information are known, the ideal depth estimated from the tidal dynamics equation shows reasonably good correlation of about 62%. From the results, it can be seen that in a situation where data is limited, it is still possible to provide an estimate of the average depth at bankfull discharge. The summary of the equations is listed in Table 6.5.

It is a fascinating finding that the regime depth turns out to be the most reliable indicator for the hydraulic geometry theory in estuaries. This indicates that part of the uncertainty in estimating the tidal velocity amplitude may be reduced by the assumption that the velocity amplitude is near to unity during spring tide. In this study, the observed velocity amplitude is estimated from salinity measurements on the day of observation, which was not necessarily during extreme spring tide. The very low velocity in some of the estuaries listed in Table 6.3 may be caused by the timing of the measurements, being carried out too far apart from the highest spring tide. This may also explain the less satisfactory correlation for the observed and hydraulic depth.

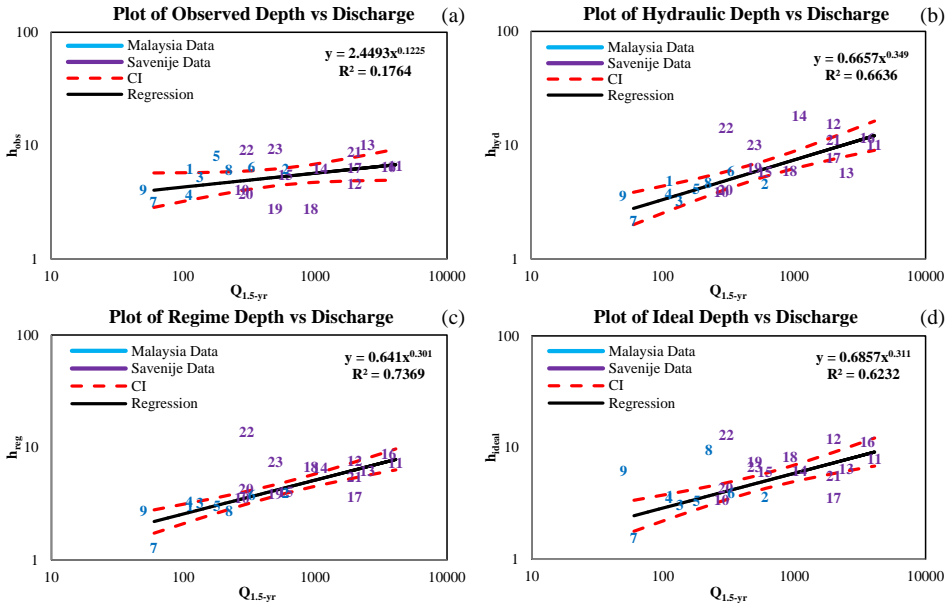


Figure 6.7: Power function relationship between the averaged depth and bankfull discharge in estuary with different depth conditions: a) Observed depth; b) Hydraulic depth; c) Regime depth; and d) Ideal depth, depending on amount of data available. Confidence interval (CI) of 95% is presented in dotted lines.

Table 6.5: Summary of the power function relationship between the averaged estuary depth and bankfull discharge in estuary.

Depth	Coefficient, $c$	Exponent, $y$	$R^2$
Observed, $h_{obs}$	2.45	0.12	0.15
Hydraulic, $h_{hyd}$	0.67	0.35	0.14
Regime, $h_{reg}$	0.64	0.30	0.10
Ideal, $h_{ideal}$	0.69	0.31	0.14

Furthermore, the tidal damping may also contribute to the uncertainty in this study. This can be seen from the decrease in the results performance for the ideal depth where the damping was neglected. Cai and Savenije [2013] found that if there is no (or a very small) river discharge, then alluvial estuaries have an equilibrium tidal amplitude that is reached asymptotically in inland direction. This constant tidal amplitude corresponds to an ideal estuary. Hence all estuaries tend towards an ideal condition. At the upstream end, where there is always river discharge, this situation is never reached (and the tide finally damps out), but in the tide dominated part of the estuary it can be clearly seen that at low river discharge the tidal amplitude tends to an equilibrium condition. This may be the reason why the ideal depth equation performs so well, even if some tidal damping or amplification was observed when the surveys were made.

One would expect the observations to be more accurate, but our result show otherwise. Apparently the vertical positioning, and the separation between stream profile and

storage profile is not trivial. The fact that the hydraulic and regime depths give the best correlation with bankfull discharge indicates that direct observation of the stream depth is very tricky. Interesting to note is that the hydraulic depth is always higher than the regime depth. This is probably due to the cross-sectional profile, where the deeper part dominates the flow, while the shallower parts contribute to storage. Here, the hydraulic equations determine the stream depth (assuming a rectangular profile) while accounting for the storage width through  $r_s$ . This leads to the estimation of a larger depth. It also appears that the ideal depth is close to the regime depth, but sometimes also larger (due to the same effect). Finally, the observed depth shows the largest scatter, due to errors of observation, difficulty of observation, and a variety of methods used to determine the depth. Additionally, velocity observations are notoriously inaccurate, which may also contribute to the scatter and uncertainty.

From the analysis, the regime depth appears to be the most reliable estimate. Moreover, if no water level observations are available (no information on damping) the ideal depth may be used as a prior estimate. This is particularly valuable for an ungauged estuary where only width data is available. Subsequently, an estimate can be made of the bankfull river discharge. It is worth noting that the methods established in this study may be applied to natural alluvial estuaries, but will be less reliable in non-alluvial, man-made or strongly modified estuaries.

## 6

#### 6.4.4. VERIFICATION OF THE DEPTH TO WIDTH RATIO

Finally we verified the depth to width ratio in the estuarine region. According to the theory by Cao and Knight [1996, 2002], as explained in Section 6.2.2, the average depth is proportional to the river width to a power of  $2/3$ . Making use of the results from Section 6.4.2 and 6.4.3, the ratio between the exponents obtained for the width over the depth yield an exponent of 0.26, 0.74, 0.64 and 0.66 for the observed, hydraulic, regime and ideal depth, respectively. The power for the observed depth is far off, but the power for the regime and ideal depth is close to the theoretical value of 0.67 in Equation (6.21). This again supports the hypothesis that the hydraulic geometry is applicable in alluvial estuaries.

#### 6.4.5. DETERMINING THE SPECIFIC DISCHARGE RATIO $k_b$ FROM CANTER-CREMERS'S ESTUARY FLOOD NUMBER $N$

In the same process, the specific discharge ratio (coefficients for the velocity and depth ratio)  $k_b$  has been determined on the basis of linear regression for different depth estimates. Figure 6.8 displays the relations between the estuarine number based on the width ratio  $N_b$  and the Canter-Cremers numbers  $N_Q$  for different depth estimates. Markers in blue are the data from field observations, while the data marked in purple were taken from Savenije [2005], which were claimed to be at bankfull state. The Canter-Cremers number in Figure 6.8(a) uses observed depth and velocity amplitude; Figure 6.8(b) uses hydraulic depth and observed velocity amplitude; Figure 6.8(c) uses regime depth and a velocity amplitude of  $1 \text{ ms}^{-1}$ ; Figure 6.8(d) uses the ideal depth and a velocity amplitude of  $1 \text{ ms}^{-1}$ . Table 6.8 lists the calibrated specific discharge ratios and the performance indicators for the various depth estimates.

In order to determine the specific discharge ratio  $k_b$ , linear regression was performed

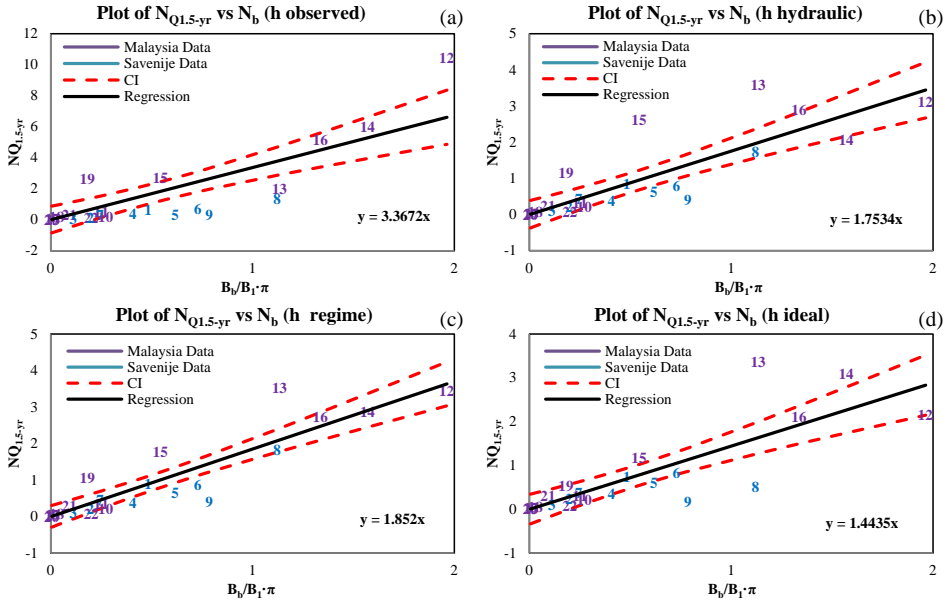


Figure 6.8: The relation of the estuary flood number computed from the basic equation  $N_Q$  to the one derived from the width ratio  $B_b/B_1 \cdot \pi$ , with comparison between different depths condition: a) Observed depth; b) Hydraulic depth; c) Regime depth; and d) Ideal depth. Discharge frequency of 1.5-year return period and confidence interval (CI) of 95% are applied. The linear regression coefficients represent  $k_b$  (equalling 1.85 for the regime depth).

Table 6.6: Results of the calibrated specific discharge ratio  $k_b$  and the performance of the new established equations in predicting the Canter-Cremers number  $N$ .

Depth	Coefficient, $k_b$	RMS	$R^2$
Observed, $h_{obs}$	3.37	1.42	0.77
Hydraulic, $h_{hyd}$	1.75	0.63	0.82
Regime, $h_{reg}$	1.85	0.49	0.89
Ideal, $h_{ideal}$	1.44	0.56	0.80

for the plots of  $N_Q$  against the width ratio  $B_b/B_1 \cdot \pi$  forcing zero intercept. The value of  $k_b$  obtained for each depth estimates appear to vary in the range of 1.5 – 3.5. If the prior assumption that the estuary depth has the same order of magnitude with the regime depth is true, the bankfull river regime velocity estimated (after multiplying the value of  $k_b$  with the tidal velocity amplitude) is in the order of 1 – 2  $ms^{-1}$ , which is in agreement with the claim made by Savenije [2003]. The regression obtained between the Canter-Cremers number using discharge measurement and width ratio (for all cases) shows good correlation with  $R^2$  value of 0.77, 0.82, 0.89 and 0.80 for the observed, hydraulic, regime and ideal depth estimate, respectively. The good fit supports the assumption that the estuary depth is governed by the depth of the river at bankfull discharge. The relation obtained between the bankfull discharge, tidal flood volume and estuary shape,

through the Canter-Cremers number, appears to have great potential to predict bankfull discharge from estuary shape and vice versa.

#### 6.4.6. DISCUSSION

Apparently, the bankfull river depth in the river regime agrees well with the average depth of an estuary. This is a fascinating conclusion, because it implies that the estuary depth is actually determined by the bankfull river discharge and not by the tide. The width convergence, on the other hand is determined by the balance between bankfull discharge and tide, which is reflected in the Canter-Cremers number. Additionally, the constant depth indicates that there is a balance between the tidal energy lost in friction and the energy gained due to convergence. However, this only applies to long alluvial estuaries, where the estuary morphology and shape are fully governed by the hydraulics of the flow. Here, the flow is governed by both the tide and the river discharge, whereby the tidal flow is dominant on the seaward end, while the river flow becomes gradually more dominant as one moves landward. It is worth noting that the analyses were carried out with data from a wide variety of natural alluvial estuaries around the world, which indicates that the relationship found is of a general nature.

### 6.5. CONCLUSION AND RECOMMENDATION

This study has shown that there is indeed a physical relationship between the shape of an estuary, tidal dynamics and the flood discharge. This relation can be expressed by a simple combination of empirical hydraulic geometry and analytical hydrodynamics equations, linking the Canter-Cremers estuarine number for bankfull discharge to estuary shape. The flood discharge frequency of 1.5-years return period has been shown to be the most representative for bankfull discharge in an estuary. It appears that the estuary width is determined by the tidal discharge, while the estuary depth appears to be governed by the river regime. Though the accuracy is still modest, the regime equation, considering tidal velocity amplitude of  $1 \text{ ms}^{-1}$ , provides remarkably consistent depth estimates for a wide range of estuaries. In order to improve the outcome, more detailed data especially on the cross-sectional area and discharge are required to minimize the uncertainty from the measurements.

Although the uncertainty in the depth estimator may still be high, with this simple tool, water managers and engineers should be able to obtain first order estimates of flood discharge characteristics based on simple estuary shape indicators. In this way a first estimate of estuary depth and flood discharge can be obtained for ungauged estuaries on the basis of readily available data.

# 7

## CONCLUSIONS AND RECOMMENDATIONS

## 7.1. CONCLUSIONS

THIS thesis has stressed the importance of the development of predictive methods for the analysis of the interaction between tides and fresh water flow in estuaries. Predictive methods are principally useful in ungauged basins where the availability of hydrological is minimal. Other than that, compiling the essential data required in the estuarine studies into a database will allow other researchers to make a quick search on the estuary of interest – provided that the estuary is already in the database. If researchers wish to contribute their work to expand the database particularly on salt intrusion studies, they can do so by performing the salinity analysis using the available templates. Here, we have drawn the main conclusions with regard to the objectives stated in Chapter 1.

1. Field surveys have been successfully carried out for the estuaries in Malaysia, and ample amount of data has been collected for the salt intrusion study in the area. The one dimensional analytical salinity model in combination with the exponential theory for the geometry of Savenije [1989] has been proven valid in analysing the salt intrusion condition of the Malaysian estuaries. It is also found that the predictive equations for the Van der Burgh coefficient  $K$  and dispersion coefficient at the mouth  $D_0$  for HWS condition performed rather well in comparison to calibrated ones.
2. From the study, we know that the discharge data obtained from the nearest upstream station underestimates the total amount of fresh water drained into the estuary. A rather rough area-wise compensation of the river discharge proposed for the case study in Malaysia has shown a much better correlation in the performance of the  $K$  and  $D_1$  predictive equations. This indicates that a simple projection method is applicable in the region where the climate, topography and hydrological characteristics are homogeneous. Moreover, this approach can be very useful especially for the case where on-site discharge measurement at the upper boundary of the estuary is unavailable. In Chapter 4, 5 and 6, the projection method for the discharge has been improved by accounting only for the sloped area instead of the total area.
3. In Chapter 5, we have improved and simplified the existing predictive equations for  $K$  and  $D_1$ , by changing to the TA tidal condition and adjusting the downstream boundary to the inflection point  $x_1$ . One of the advantages found in the new predictive equations is that the parameters selected are fully independent and easy to measure. Furthermore, the adjustment of the downstream boundary has solved the problem of selecting the appropriate geometry parameters to apply in the predictive analysis. The datasets selection process helped to reduce the uncertainties in developing the predictive methods by omitting the less reliable dataset from the calibration. Conducting the analyses based on TA condition has enabled the consistency in all the information used, and reduced possible model and data error. From TA condition, the results for dispersion and salt intrusion length can be converted to HWS situation by a translation over half of the tidal excursion.

4. Chapter 6 has laid out the most important findings in the relation between the river and estuary. One of the findings shows that the relation can be expressed by a simple combination of the regime theory and analytical tidal dynamics solutions, linking the Canter-Cremers estuarine number for bankfull discharge at 1.5-years return period to the estuary shape (represented by the width ratio at the inflection point and upstream boundary of the tidal limit). The empirical results of the exponent close to 1/3 for the relationship between the estuary depth and bankfull discharge has proved that the downstream hydraulic geometry theory can also be applied in the estuary region. Furthermore, the outcome also indicates that the tidal discharge shapes the estuary width, whereas river discharge determined the estuary depth. It is as well interesting to find that the assumption of tidal velocity amplitude of 1 m/s (which occurs in natural alluvial estuary at spring tide), provides the best correlation with the bankfull discharge.

It is obvious that some of the less reliable data are not suitable to be included in the calibration process. From the results obtained in this thesis, we believe the reasons for the low reliability can be explained as below.

1. The discharge data used are very uncertain because they are most of the time unavailable or estimated (e.g. the Incomati which has very low discharge).
2. Some estuaries are in an unsteady state condition at low flow (e.g. the Gambia, Incomati, and Pungue Estuary).
3. The data on the depth is uncertain which is confirmed in the analyses performed in Chapter 6.
4. There may be a residual slope effect between the neap-spring tidal cycle.
5. Errors may have occurred during salinity measurements, particularly if it was done too close to a bank or at a point where a fresh water pocket remained. Additionally, too few measurement points also affects the accuracy of the data.

Nevertheless, the new predictive equations appeared to perform very well for the other less reliable estuaries, despite there being some significant outliers.

The advancement in information technology has subsequently enabled us to obtain data through an online official database. Using the collectable basic data from the links discussed in Chapter 3 into the predictive relations proposed in this thesis, we can now at least perform some preliminary analyses to get the first estimates of the important parameters which determine the estuary characteristics. Moreover, it can be done without field measurements especially in ungauged estuaries.

## 7.2. LIMITATIONS AND RECOMMENDATIONS

As we know, there is no perfect model in this world and this also applies to the predictive methods proposed in this study. However, having limitations in the established methods is not entirely negative; it provides the opportunity for improvements and better understanding. In the following, we have listed the limitations of this study and suggested recommendations for future improvements.

1. In this thesis, the estuaries considered in the predictive solutions are all single branched estuaries, neglecting the influence from nearby tributaries. Most of them are also in steady state condition (except for the Incomati, Pungue and Gambia Estuaries during low flow). One of the reasons is because some data of the multi-network estuaries are not available especially for the tidal-dynamics analysis. It would be an advantage if the required data can be obtained for these types of estuaries so as to examine how they fit in the predictive methods.
2. It is described in Chapter 5 that nearly half of the data for the salinity measurements are grouped in the less reliable dataset. This indicates that these data are not very useful. Hence, it is recommended to carry out more field surveys in a wide range of estuaries to ensure the reliability of the data used and subsequently strengthen the predictive methods.
3. In Chapter 6, the comparison between the observed and estimated estuary depths does not seem highly satisfactory. This means that either the uncertainties are contributed by the depth observations or the tidal-dynamics model. In order to determine the root of the errors, it would be useful if detail surveys on the cross-sectional area and water level measurements could be conducted. However, this can only be done if it is financially permitted.
4. The variations in the geometry and tidal characteristics during high and low water and between neap and spring tide as investigated by Nguyen et al. [2012] may also influence the results in this study. The difference in cross-sectional area convergence length and tidal set-up due to the shift from high to low tide should be observed and taken into consideration. By comparing the results, we can determine how far the variations actually affected the predictive methods.
5. In the discharge adjustment analysis, we are aware that the simple area-wise projection method is only applicable in a region with homogeneous climate, topography and hydrological characteristics. For better estimates on the discharge data, it is recommended to set up a hydrological model for the intermediate catchments making use of the hydrological data available of the nested catchments within the basins. Moreover, it would be even better if a universal solution could be developed to estimate the discharge in the estuary.
6. Revisiting Lacey's hydraulic geometry theory, Savenije [2003] mentioned that the coefficient in the power relation formula is referred to as the sediment material coefficient. This has been proven by the development of his empirical relation between grain size  $D_{50}$  and the natural angle of repose  $\tan \phi$  (see Savenije [2003] for more explanation). Thus, information on sedimentation may be included in the solutions to predict the estuary depth and bankfull discharge.
7. The tidal excursion  $E$  used in this thesis is not localized. Hence, it would also be interesting to observe the effect of varying  $E$  on the results. This can be done by using the method introduced by Cai et al. [2014b].

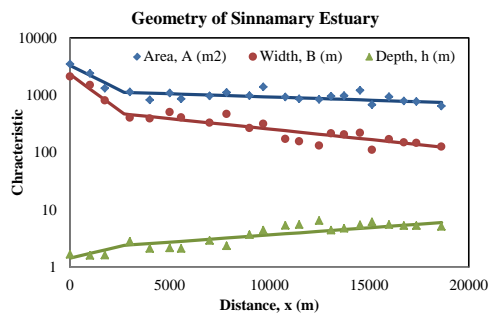
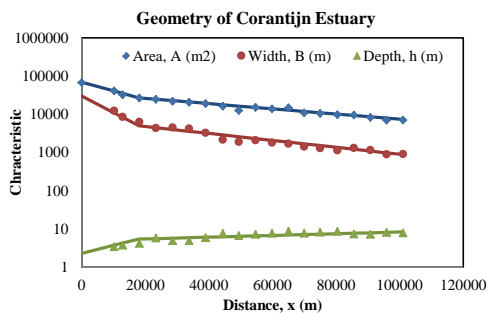
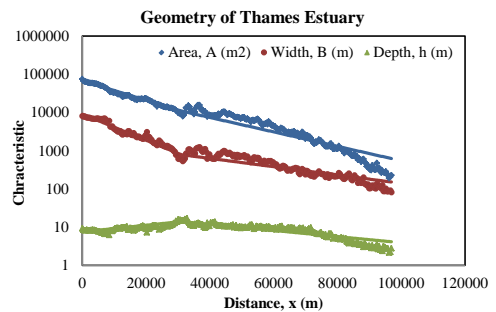
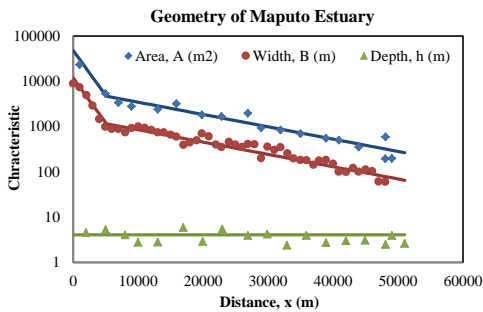
Despite the improvements to be considered in the future works, we believe that the findings of the studies described in this thesis are very useful for water resources management in the estuary region. Water managers or engineers are now able to make a first estimate of the shape, depth, bankfull discharge, and the salinity distribution in the estuary.

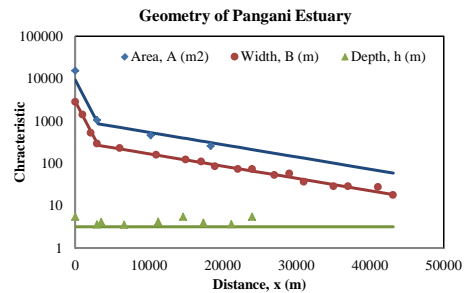
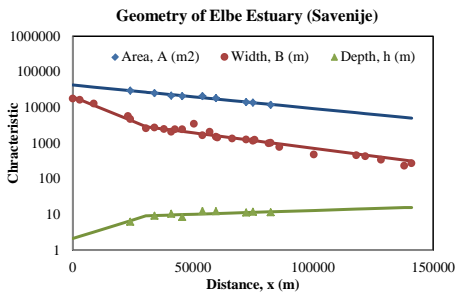
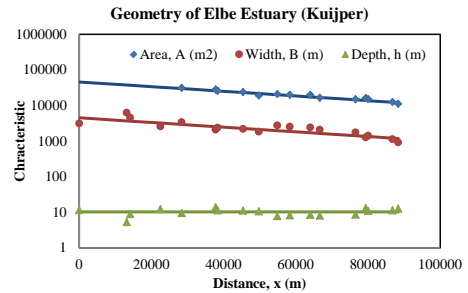
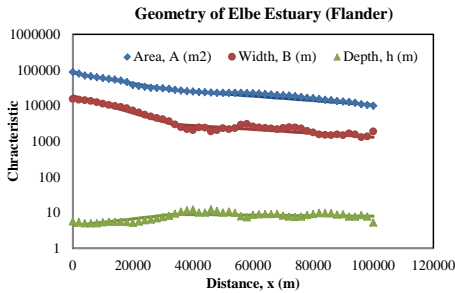
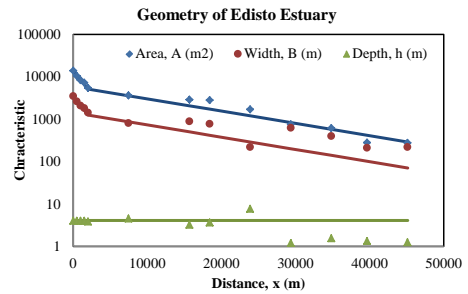
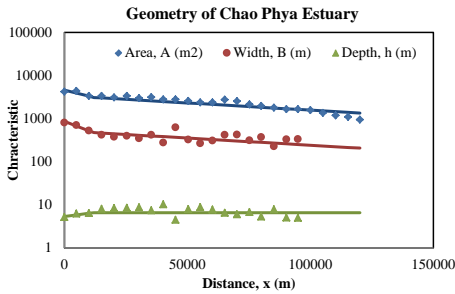
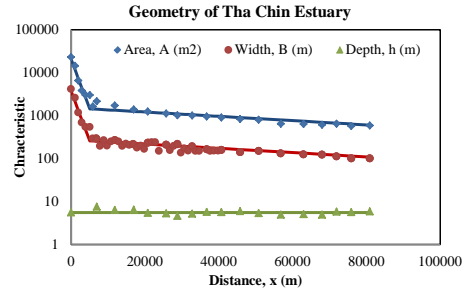
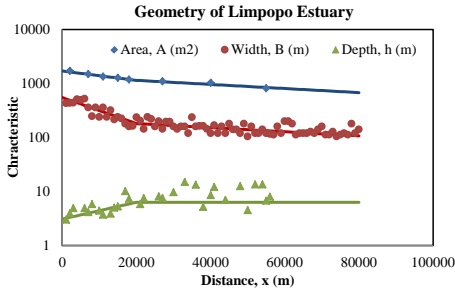
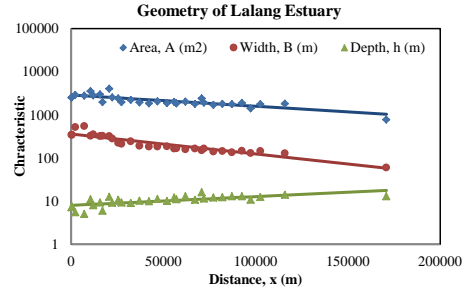
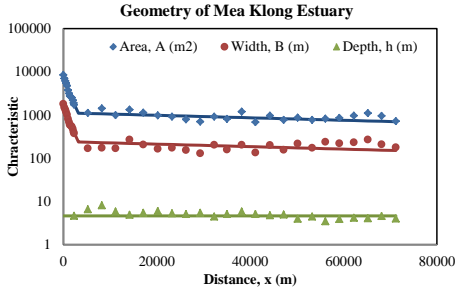


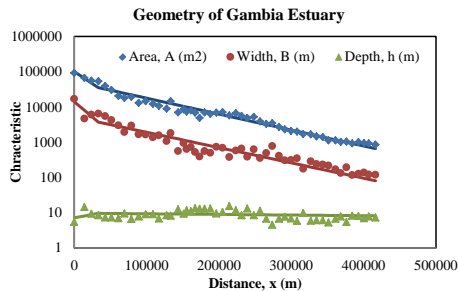
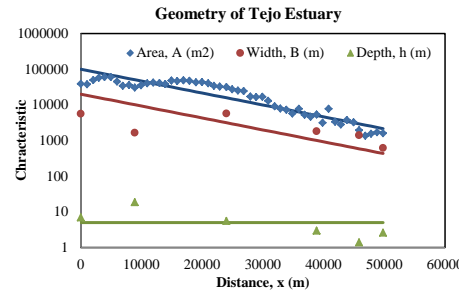
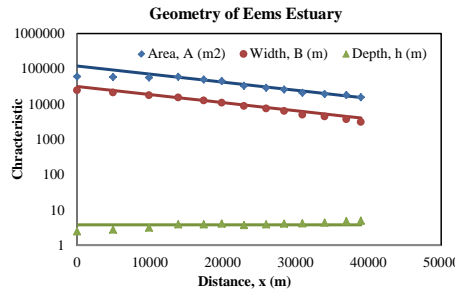
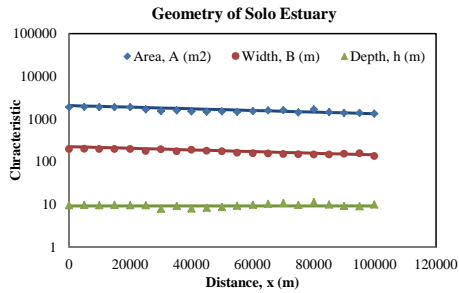
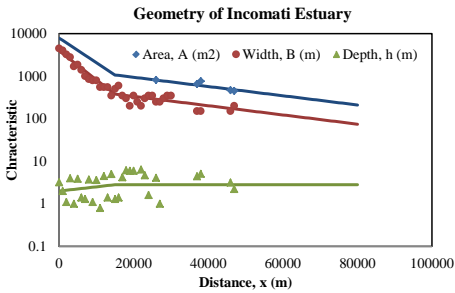
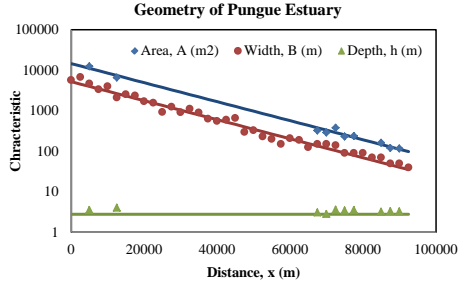
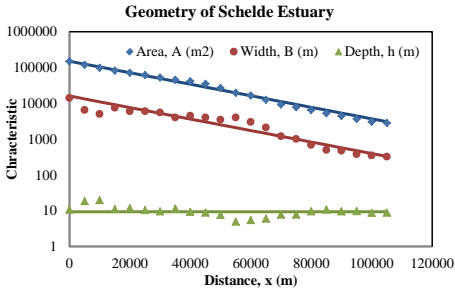
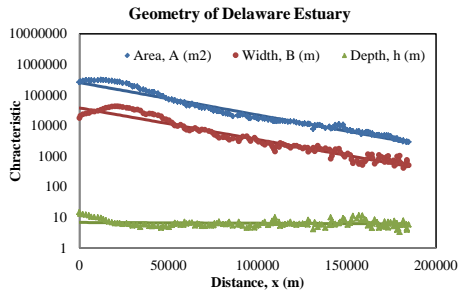
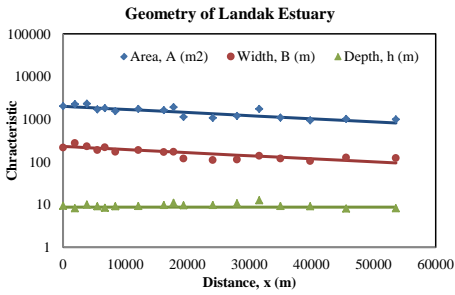
# A

## APPENDIX

### A.1. Compilation of the geometry analysis for the estuaries collected from existing resources (mainly from Savenije [2005, 2012]).







## A.2. Data used to develop the predictive equation for the dispersion coefficient $D$ .

(a) Reliable sets for calibration														
No	Estuary	Date	$A_1$ ( $m^2$ )	$h_1$ (m)	$H_0$ (m)	$E_0$ (km)	T (hr)	Q ( $m^3/s$ )	$K_m$	$\delta_H$ ( $10^{-6} m^{-1}$ )	$D_1$ ( $m^2/s$ )	$D_1$ [2]	$D_1$ [4]	$D_1$ [9]
1a	Kurau	27/02/13	660	5.2	2.0	9.4	12	50	30	-6.3	443	514	572	443
1b		28/02/13	660	5.2	2.0	9.4	12	50	30	-6.3	456	529	587	456
2	Perak	13/03/13	9210	4.5	2.5	12.5	12	316	65	3.0	235	199	159	235
3	Bernam	21/06/12	4460	3.5	2.9	14.0	12	42	70	1.7	169	141	116	169
4	Selangor	24/07/12	1000	3.6	4.0	12.7	12	41	40	-3.7	326	349	381	326
5	Muar	03/08/12	1580	5.6	2.0	11.0	12	35	45	-2.7	283	273	252	283
6	Endau	28/03/13	2000	6.5	1.9	10.0	12	54	45	-1.3	329	321	293	329
7	Maputo	28/04/82	4700	4.1	2.8	13.0	12	25	58	2.0	139	127	122	139
7a		15/07/82	4700	4.1	1.5	7.0	12	8	58	2.0	64	59	53	64
7b		19/04/84	4700	4.1	3.3	13.0	12	120	58	2.0	293	267	236	293
7c		17/05/84	4700	4.1	3.3	13.0	12	50	58	2.0	187	170	158	187
7d		29/05/84	4700	4.1	2.8	13.0	12	40	58	2.0	171	156	146	171
8	Thames (New)	07/04/49	10900	13.9	5.3	14.0	12	40	45	1.1	209	202	206	209
9	Corantijn	09/12/78	26800	5.4	1.8	10.0	12	120	40	-1.7	91	94	104	91
9a		14/12/78	26800	5.4	2.3	13.0	12	130	40	-1.7	91	94	111	91
9b		20/12/78	26800	5.4	1.6	9.0	12	220	40	-1.7	105	109	117	105
10	Sinnamary	12/11/93	1120	2.4	2.6	8.6	12	168	40	-5.0	293	312	315	293
10a		27/04/94	1120	2.4	2.9	9.6	12	148	40	-5.0	302	321	331	302
10b		02/11/94	1120	2.4	2.7	7.8	12	112	40	-5.0	385	408	392	385
10c		03/11/94	1120	2.4	2.9	9.5	12	112	40	-5.0	341	363	368	341
11	MaeKlong	08/03/77	1100	4.6	1.5	10.0	12	60	40	-4.2	466	490	478	466
11a		09/04/77	1100	4.6	2.0	9.0	12	36	40	-4.2	347	365	359	347
12	Lalang	20/10/89	2880	8.0	2.6	29.0	24	120	84	-0.5	762	557	358	762
13	Limpopo	04/04/80	1140	6.3	1.1	7.0	12	150	43	1.7	140	140	135	140
13a		31/12/82	1140	6.3	1.1	8.0	12	2	43	1.7	70	71	76	70
13b		14/07/94	1140	6.3	1.0	7.0	12	5	43	1.7	91	92	92	91
13c		24/07/94	1140	6.3	0.9	6.8	12	5	43	1.7	101	102	101	101
13d		10/08/94	1140	6.3	1.0	7.1	12	3	43	1.7	81	82	84	81
14	Tha Chin (New)	16/04/81	1440	5.6	1.6	12.0	24	55	50	-5.5	653	615	479	653
14a		27/02/86	1440	5.6	2.6	20.0	12	40	50	-10.6	410	390	380	410
14b		01/03/86	1440	5.6	1.8	14.0	24	40	50	-5.5	648	611	492	648
14c		13/08/87	1440	5.6	2.0	15.0	12	39	50	-10.6	320	303	286	320
15	ChaoPhya	05/06/62	3100	6.5	2.2	22.0	24	63	65	-2.2	509	428	328	509
15a		16/01/87	3100	6.5	2.5	14.0	24	180	65	-2.2	389	326	234	389
15b		23/02/83	3100	6.5	1.6	19.0	24	100	65	-2.2	574	481	353	574
15c		29/01/83	3100	6.5	2.4	26.0	24	90	65	-2.2	681	572	441	681
16	Edisto	12/07/10	5150	4.1	2.3	10.0	12	15	30	-8.8	120	144	195	120
16a		13/07/10	5150	4.1	2.3	10.0	12	14	30	-8.8	109	131	180	109
16b		14/07/10	5150	4.1	2.3	10.0	12	25	30	-8.8	156	187	247	156
16c		15/07/10	5150	4.1	2.3	10.0	12	25	30	-8.8	156	187	246	156
17	Elbe_Flanders	21/09/04	27300	9.0	3.0	18.0	12	200	32	2.0	168	188	254	168
17a	Elbe_Kuijper	21/09/04	46000	10.2	3.0	18.0	12	200	32	2.0	216	238	303	216
17b	Elbe_Savenije	21/09/04	43000	9.3	3.0	18.0	12	200	32	2.0	213	233	292	213
18	Pangani	27/10/07	860	3.2	4.2	17.0	12	15	42	10.0	254	271	321	254
18a		11/12/07	860	3.2	3.0	15.0	12	11	42	10.0	203	216	256	203
19	Rembau Linggi	05/07/12	1500	4.6	2.0	8.7	12	26	30	-14.0	253	308	384	253
20	Landak	15/09/09	2000	8.7	1.6	15.0	24	10	45	-6.7	176	169	163	176

Note:  $H_0$ ,  $E_0$ ,  $\delta_H$  and  $Q$  reflect the condition at the time of observation.



(b) Less Reliable Sets for Verification

No	Estuary	Date	$A_1$ ( $m^2$ )	$h_1$ (m)	$H_0$ (m)	$E_0$ (km)	T (hr)	Q ( $m^3/s$ )	$K_m$	$\delta_H$ ( $10^{-6} m^{-1}$ )	$D_1$ ( $m^2/s$ )	$D_1$ [2]	$D_1$ [4]	$D_1$ [9]
21	Delaware	23/08/32	255000	6.8	1.7	8.0	12	120	55	0.7	42	38	37	42
21a		04/10/32	255000	6.8	1.7	8.0	12	72	55	0.7	31	28	28	31
22	Westerschelde	01/07/87	150000	9.4	3.0	10.0	12	90	46	2.8	61	58	61	61
22a		02/11/00	150000	9.4	4.0	12.0	12	220	46	2.8	111	105	107	111
23	Pungue	26/05/82	14500	2.8	5.0	9.0	12	50	31	-8.5	79	97	137	79
23a		06/08/82	14500	2.8	5.2	10.0	12	36	31	-8.5	71	86	127	71
23b		22/09/82	14500	2.8	5.2	15.0	12	26	31	-8.5	66	81	131	66
23c		29/10/82	14500	2.8	6.0	15.0	12	60	31	-8.5	105	129	197	105
23d		31/01/02	14500	2.8	6.2	19.0	12	262	31	-8.5	213	261	389	213
23e		27/02/02	14500	2.8	6.1	21.0	12	200	31	-8.5	191	234	362	191
23f		01/03/02	14500	2.8	6.7	27.0	12	150	31	-8.5	170	209	345	170
23g		26/09/80	14500	2.8	6.3	17.0	12	22	31	-8.5	62	76	127	62
23h		03/10/93	14500	2.8	5.3	11.0	12	10	31	-8.5	36	45	72	36
23i		12/10/93	14500	2.8	3.8	15.0	12	10	31	-8.5	40	49	83	40
23j		16/10/93	14500	2.8	6.4	16.0	12	10	31	-8.5	40	49	85	40
24	Incomati	05/09/82	1070	2.8	1.4	7.0	12	2	56	-19.9	41	39	37	41
24a		23/06/93	1070	2.8	1.4	8.0	12	4	56	-19.9	53	50	47	53
24b		07/07/93	1070	2.8	2.6	9.0	12	4	56	-19.9	52	49	48	52
25	Solo	26/07/88	2070	9.2	0.8	9.0	24	50	31	3.0	727	805	743	727
25a		08/09/88	2070	9.2	0.4	5.0	24	7	31	3.0	218	242	224	218
26	Eems	-	120000	3.8	3.6	15.0	12	10	31	-0.7	14	17	31	14
27	Tejo	18/08/81	100000	5.0	3.4	10.0	12	29	56	2.2	31	28	30	31
27a		21/10/81	100000	5.0	1.9	6.0	12	149	56	2.2	68	62	54	68
28	Elbe_Flanders	09/07/02	27300	9.0	3.3	10.0	12	100	32	2.0	25	28	41	25
28a		04/04/04	27300	9.0	3.7	22.0	12	211	32	2.0	51	57	92	51
28b		01/11/04	27300	9.0	3.4	10.0	12	100	32	2.0	28	31	45	28
29a	Elbe_Kuijper	09/07/02	46000	10.2	3.3	10.0	12	100	32	2.0	75	83	104	75
29b		04/04/04	46000	10.2	3.7	21.0	12	211	32	2.0	167	185	250	167
29c		01/11/04	46000	10.2	3.4	10.0	12	100	32	2.0	70	77	97	70
30a	Elbe_Savenije	09/07/02	43000	9.3	3.3	10.0	12	100	32	2.0	75	81	101	75
30b		04/04/04	43000	9.3	3.7	21.0	12	211	32	2.0	165	181	242	165
30c		01/11/04	43000	9.3	3.4	10.0	12	100	32	2.0	69	75	94	69
31a	Rompin	10/07/98	840	6.1	1.7	8.7	12	20	15	-33.4	107	167	283	107
31b		11/07/98	840	6.1	1.8	8.7	12	20	15	-33.4	100	155	265	100
31c		12/07/98	840	6.1	1.9	8.7	12	20	15	-33.4	96	150	257	96
32a	Ulu Sedili Besar	24/06/98	670	4.7	1.1	11.0	12	8	30	-25.5	160	192	252	160
32b		25/06/98	670	4.7	1.2	11.0	12	8	30	-25.5	161	193	253	161
32c		26/06/98	670	4.7	1.3	11.0	12	8	30	-25.5	170	204	266	170

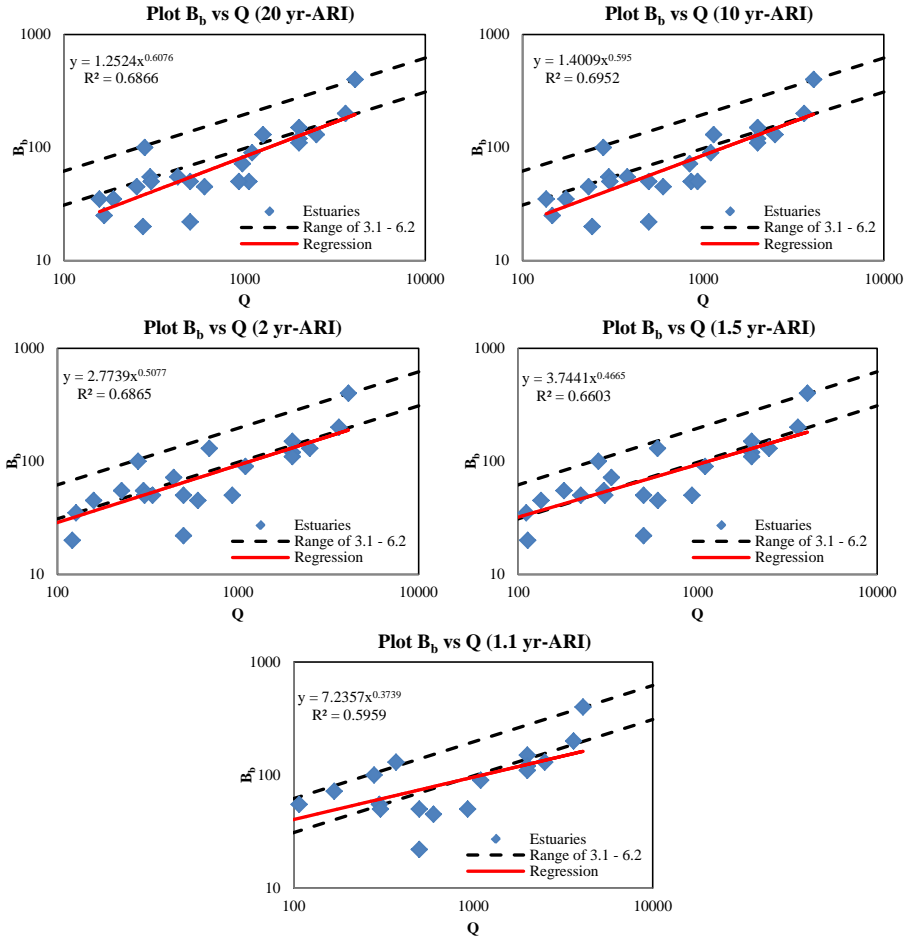
Note:  $H_0$ ,  $E_0$ ,  $\delta_H$  and  $Q$  reflect the condition at the time of observation.

### A.3. Data and results of the maximum salt intrusion length $L^{HWS}$ .

(a) Reliable Sets for Calibration													
No	Estuary	Date	$A_1$ ( $m^3$ )	$a_2$ (km)	$x_1$ (m)	$E_0$ (km)	$Q$ ( $m^3/s$ )	K Pre	$N_r$	$L^{HWS}$ (km)	$L^{HWS}$ [2]	$L^{HWS}$ [4]	$L^{HWS}$ [9]
1a	Kurau	27/02/13	660	46	3600	9.4	50	0.35	0.4530	17	23	24	26
1b		28/02/13	660	46	3600	9.4	50	0.35	0.4765	18	23	25	26
2	Perak	13/03/13	9210	37	4000	12.5	316	0.24	0.0493	29	31	29	26
3	Bernam	21/06/12	4460	25	4300	14.0	42	0.22	0.0190	58	48	44	41
4	Selangor	24/07/12	1000	13	2800	12.7	41	0.42	0.0891	22	21	22	22
5	Muar	03/08/12	1580	100	3900	11.0	35	0.32	0.1150	51	43	42	40
6	Endau	28/03/13	2000	44	4800	10.0	54	0.33	0.2050	29	39	39	37
7	Maputo	28/04/82	4700	16	5100	13.0	25	0.32	0.0173	30	41	39	39
7a		15/07/82	4700	16	5100	7.0	8	0.32	0.0389	36	43	41	40
7b		19/04/84	4700	16	5100	13.0	120	0.32	0.0635	27	30	29	28
7c		17/05/84	4700	16	5100	13.0	50	0.32	0.0289	28	35	34	33
7d		29/05/84	4700	16	5100	13.0	40	0.32	0.0248	32	37	36	35
8	Thames (New)	07/04/49	10900	23	31000	14.0	40	0.24	0.0250	100	94	93	93
9	Corantijn	09/12/78	26800	64	18000	10.0	120	0.27	0.0237	86	73	74	78
9a		14/12/78	26800	64	18000	13.0	130	0.27	0.0095	93	71	73	78
9b		20/12/78	26800	64	18000	9.0	220	0.27	0.0445	87	58	59	61
10	Sinnamary	12/11/93	1120	39	2700	8.6	168	0.46	0.2923	10	11	11	11
10a		27/04/94	1120	39	2700	9.6	148	0.46	0.2090	12	12	12	13
10b		02/11/94	1120	39	2700	7.8	112	0.46	0.6594	17	14	15	14
10c		03/11/94	1120	39	2700	9.5	112	0.46	0.2689	14	14	15	15
11	MaeKlong	08/03/77	1100	150	3200	10.0	60	0.48	0.3871	32	25	26	25
11a		09/04/77	1100	150	3200	9.0	36	0.48	0.3335	47	28	29	29
12	Lalang	20/10/89	2880	167	0	29.0	120	0.57	0.0677	34	44	36	29
13	Limpopo	04/04/80	1140	115	20000	7.0	150	0.38	0.1406	27	26	26	26
13a		31/12/82	1140	115	20000	8.0	2	0.38	0.0264	72	99	99	103
13b		14/07/94	1140	115	20000	7.0	5	0.38	0.0665	53	68	68	69
13c		24/07/94	1140	115	20000	6.8	5	0.38	0.0881	58	72	72	72
13d		10/08/94	1140	115	20000	7.1	3	0.38	0.0515	65	85	85	86
14	Tha Chin (New)	16/04/81	1440	87	5000	12.0	55	0.31	1.2382	72	54	52	44
14a		27/02/86	1440	87	5000	20.0	40	0.31	0.0316	51	53	51	51
14b		01/03/86	1440	87	5000	14.0	40	0.31	0.7125	57	66	64	56
14c		13/08/87	1440	87	5000	15.0	39	0.31	0.0559	46	44	43	41
15	ChaoPhya	05/06/62	3100	130	12000	22.0	63	0.71	0.0963	50	54	50	44
15a		16/01/87	3100	130	12000	14.0	180	0.71	0.2913	26	28	27	25
15b		23/02/83	3100	130	12000	19.0	100	0.71	0.1981	43	44	41	36
15c		29/01/83	3100	130	12000	26.0	90	0.71	0.0894	52	54	50	45
16	Edisto	12/07/10	5150	15	2000	10.0	15	0.31	0.0366	43	41	44	48
16a		13/07/10	5150	15	2000	10.0	14	0.31	0.0312	45	41	43	48
16b		14/07/10	5150	15	2000	10.0	25	0.31	0.0580	44	38	40	44
16c		15/07/10	5150	15	2000	10.0	25	0.31	0.0579	43	38	40	44
17	Elbe_Flanders	21/09/04	27300	70	33000	18.0	200	0.27	0.0064	92	98	102	115
17a	Elbe_Kuijper	21/09/04	46000	66	0	18.0	200	0.25	0.0125	93	101	106	118
17b	Elbe_Savenije	21/09/04	43000	66	0	18.0	200	0.28	0.0122	94	91	95	107
18	Pangani	27/10/07	860	15	3100	17.0	15	0.41	0.0181	29	30	30	32
18a		11/12/07	860	15	3100	15.0	11	0.41	0.0189	25	30	30	32
19	Rembau Linggi	05/07/12	1500	8	500	8.7	26	0.36	0.2123	20	19	20	22
20	Landak	15/09/09	2000	60	0	15.0	10	0.69	0.0522	36	44	43	42

(b) Less Reliable Sets for Verification													
No	Estuary	Date	$A_1$ (m <sup>2</sup> )	$a_2$ (km)	$x_1$ (m)	$E_0$ (km)	$Q$ (m <sup>3</sup> /s)	K Pre	$N_r$	$L^{HWS}$ (km)	$L^{HWS}$ [2]	$L^{HWS}$ [4]	$L^{HWS}$ [9]
21	Delaware	23/08/32	255000	41	0	8.0	120	0.09	0.0120	147	136	132	131
21a		04/10/32	255000	41	0	8.0	72	0.09	0.0072	160	145	141	141
22	Westerschelde	01/07/87	150000	27	0	10.0	90	0.10	0.0107	120	104	102	104
22a		02/11/00	150000	27	0	12.0	220	0.10	0.0159	124	97	96	96
23	Pungue	26/05/82	14500	19	0	9.0	50	0.22	0.0242	59	40	43	48
23a		06/08/82	14500	19	0	10.0	36	0.22	0.0138	65	43	47	53
23b		22/09/82	14500	19	0	15.0	26	0.22	0.0030	73	50	54	62
23c		29/10/82	14500	19	0	15.0	60	0.22	0.0067	63	44	47	55
23d		31/01/02	14500	19	0	19.0	262	0.22	0.0100	50	35	37	44
23e		27/02/02	14500	19	0	21.0	200	0.22	0.0059	47	38	41	48
23f		01/03/02	14500	19	0	27.0	150	0.22	0.0020	56	43	47	55
23g		26/09/80	14500	19	0	17.0	22	0.22	0.0017	82	53	56	65
23h		03/10/93	14500	19	0	11.0	10	0.22	0.0031	86	54	58	66
23i		12/10/93	14500	19	0	15.0	10	0.22	0.0012	86	58	61	71
23j		16/10/93	14500	19	0	16.0	10	0.22	0.0010	98	58	62	72
24	Incomati	05/09/82	1070	40	15000	7.0	2	0.34	0.0528	67	57	56	54
24a		23/06/93	1070	40	15000	8.0	4	0.34	0.0506	53	47	46	45
24b		07/07/93	1070	40	15000	9.0	4	0.34	0.0326	57	48	47	46
25	Solo	26/07/88	2070	226	0	9.0	50	0.64	3.6975	29	47	51	48
25a		08/09/88	2070	226	0	5.0	7	0.64	3.5219	39	86	93	88
26	Eems	-	120000	19	0	15.0	10	0.11	0.0002	83	91	94	106
27	Tejo	18/08/81	100000	13	0	10.0	29	0.16	0.0032	60	56	55	56
27a		21/10/81	100000	13	0	6.0	149	0.16	0.0771	50	44	43	41
28	Elbe_Flanders	09/07/02	27300	70	33000	10.0	100	0.27	0.0018	49	60	62	71
28a		04/04/04	27300	70	33000	22.0	211	0.27	0.0004	57	65	67	78
28b		01/11/04	27300	70	33000	10.0	100	0.27	0.0022	58	62	64	73
29a	Elbe_Kuijper	09/07/02	46000	66	0	10.0	100	0.25	0.0154	52	80	84	95
29b		04/04/04	46000	66	0	21.0	211	0.25	0.0046	68	87	92	107
29c		01/11/04	46000	66	0	10.0	100	0.25	0.0134	63	76	81	92
30a	Elbe_Savenije	09/07/02	43000	66	0	10.0	100	0.28	0.0151	52	71	75	85
30b		04/04/04	43000	66	0	21.0	211	0.28	0.0046	67	79	83	96
30c		01/11/04	43000	66	0	10.0	100	0.28	0.0131	61	68	72	81
31a	Rompin	10/07/98	840	110	19000	8.7	20	0.64	0.4240	43	30	34	40
31b		11/07/98	840	110	19000	8.7	20	0.64	0.3722	42	30	33	39
31c		12/07/98	840	110	19000	8.7	20	0.64	0.3515	41	29	33	39
32a	Ulu Sedili Besar	24/06/98	670	38	4300	11.0	8	0.45	0.0600	28	32	35	40
32b		25/06/98	670	38	4300	11.0	8	0.45	0.0606	29	32	35	40
32c		26/06/98	670	38	4300	11.0	8	0.45	0.0668	32	33	36	42

**A.4. Determining the bankfull discharge by comparing the discharge frequency of 20, 10, 2, 1.5 and 1.1 years in relation to the width hydraulic geometry theory based on Simon and Albertson [1963]**



## REFERENCES

- Bauer, J. E., Cai, W.-J., Raymond, P. A., Bianchi, T. S., Hopkinson, C. S., and Regnier, P. A. G.: The changing carbon cycle of the coastal ocean, *Nature*, 504, 61–70, 2013.
- Bechle, A. J. and Wu, C. H.: An entropy-based surface velocity method for estuarine discharge measurement, *Water Resources Research*, 50, 6106–6128, 2014.
- Blench, T.: Regime theory for self-formed sediment-bearing channels, *Trans. ASCE*, 117, 383–400, 1952.
- Bowden, K. F. and Gilligan, R. M.: Characteristic features of estuarine circulation as represented in the Mersey estuary, *Limnol. Oceanogr.*, 16, 490–502, 1971.
- Bretting, A. E.: *Stable channels*, Moolers Bogtrykkeri, Copenhage, 1958.
- Bruun, P. and Gerritsen, E.: *Stability of coastal inlets*, North Holland, Amsterdam., 1960.
- Cai, H. and Savenije, H. H. G.: Asymptotic behavior of tidal damping in alluvial estuaries, *Journal of Geophysical Research: Oceans*, 118, 6107–6122, 2013.
- Cai, H., Savenije, H. H. G., and Toffolon, M.: A new analytical framework for assessing the effect of sea-level rise and dredging on tidal damping in estuaries, *Journal of Geophysical Research: Oceans*, 117, C09 023, 2012.
- Cai, H., Savenije, H. H. G., and Jiang, C.: Analytical approach for predicting fresh water discharge in an estuary based on tidal water level observations, *Hydrol. Earth Syst. Sci.*, 18, 4153–4168, hESS, 2014a.
- Cai, H., Savenije, H. H. G., and Gisen, J. I. A.: A coupled analytical model for salt intrusion and tides in convergent estuaries, *Hydrological Sciences Journal*, (under review), 2014b.
- Cameron, W. and Pritchard, D.: *Estuaries, The Composition of sea-water : comparative and descriptive oceanography*, Vol 2, Wiley, New York, 1963.
- Cao, S. and Knight, D. W.: *Regime Theory of Alluvial Channels Based Upon The Concepts of Stream Power and Probability*, 1996.
- Cao, S. and Knight, D. W.: Review of regime theory of alluvial channel, *Journal of Hydrodynamics*, Ser B, 1–7, 2002.
- Castro, J. M. and Jackson, P. L.: Bankfull Discharge Recurrence Intervals and Regional Hydraulic Geometry Relationships: Patterns In the Pacific Northwest, USA, *JAWRA Journal of the American Water Resources Association*, 37, 1249–1262, 2001.

- Chiras, D.: Environmental Science, Jones and Bartlett Learning, 2013.
- Chong, S. E.: The width, depth and velocity of Sungei Kimla, Perak, *Geographica*, 6, 72–63, 1970.
- Dalrymple, R. W., Zaitlin, B. A., and Boyd, R.: Estuarine facies models: conceptual basis and stratigraphic implications, *Journal of Sedimentary Petrology*, 62, 1130–1146, 1992.
- Daniels, D. G.: A laboratory study of estuarine salinity intrusion in a rectangular channel of large aspect ratio., Univ. Calif., Berkeley, *Hydraul. Eng. Lab. Rep. WHM-17*, 1974.
- Davies, G. and Woodroffe, C. D.: Tidal estuary width convergence: Theory and form in North Australian estuaries, *Earth Surface Processes and Landforms*, 35, 737–749, 2010.
- Davies, J. L.: A morphogenic approach to world shorelines, *Zeitschrift fur Geomorphologie*, 8, 1964.
- Day, J., Kemp, W., Yáñez-Arancibia, A., and Crump, B.: *Estuarine Ecology*, Wiley, 2012.
- de Swart, H. E., de Jonge, V. N., and Vosbeek, M.: Application of the Tidal Random Walk Model to Calculate Water Dispersion Coefficients in the Ems Estuary, *Estuarine, Coastal and Shelf Science*, 45, 123–133, 1997.
- Dionne, J. C.: Towards a more adequate definition of the St. Lawrence estuary, *Z. Geomorphol.*, 7, 36–44, 1963.
- Dronkers, J.: Conditions for gradient-type dispersive transport in one-dimensional, tidally averaged transport models, *Estuarine, Coastal and Shelf Science*, 14, 599–621, 1982.
- Dunne, T. and Leopold, L. B.: *Water in environmental planning*, Earth Surface Processes, W. H. Freeman and Co., San Francisco., 1978.
- Dury, G. H.: Discharge prediction, present and former, from channel dimensions, *Journal of Hydrology*, 30, 219–245, 1976.
- Dyer, K. R.: *Estuaries; a physical introduction*, John Wiley, Chichester, 2nd edn., 1997.
- Economic Planning Unit Malaysia, E. P. U.: *National Water Resources Study Malaysia Volume 5, Sectoral Report, River Conditions*, 1982.
- Ervine, D. A., Bekic, D., and Glasson, L.: Vulnerability of two estuaries to flooding and salinity intrusion, *Water Science and Technology: Water Supply*, 7, 125, 2007.
- Fairbridge, R.: The estuary: its definition and geodynamic cycle, pp. 1–35, Wiley, New York, 1980.
- Faridah-Hanum, I., Latiff, A., Hakeem, K., and Ozturk, M.: *Mangrove Ecosystems of Asia: Status, Challenges and Management Strategies*, Springer, 2013.
- Fischer, H. B.: Mass transport mechanisms in partially stratified estuaries, *Journal of Fluid Mechanics*, 53, 671–687, 1972.

- Fischer, H. B.: Discussion of "Minimum Length of Salt Intrusion in Estuaries" by Ben P. Rigter., *Journal of the Hydraulics Division*, 100, 708–713, 1974.
- Fischer, H. B.: Mixing and Dispersion in Estuaries, *Annual Review of Fluid Mechanics*, 8, 107–133, 1976.
- Friedrichs, C. T., Armbrust, B. D., and de Swart, H. E.: Hydrodynamics and equilibrium sediment dynamics of shallow funnel - shaped tidal estuaries, 1998.
- Gisen, J. I. A. and Savenije, H. H. G.: Estimating bankfull discharge and depth in ungauged estuaries., *Water Resources Research*, (under review), 2014.
- Gisen, J. I. A., Savenije, H. H. G., Nijzink, R. C., and Abd. Wahab, A. K.: Testing a 1-D Analytical Salt Intrusion Model and its Predictive Equations in Malaysian Estuaries, *Hydrological Sciences Journal*, p. (accepted), 2014a.
- Gisen, J. I. A., Savenije, H. H. G., and Nijzink, R. C.: New predictive Van der and dispersion equations and methods for their determination., *Hydrol. Earth Syst. Sci.* (submitted), 2014b.
- Hansen, D. V. and Rattray, M.: Gravitational circulation in straits and estuaries., *J. Mar. Res.*, 23, 104–122, 1965.
- Harleman, D. R. F. and Abraham, G.: One-dimensional analysis of salinity intrusion in the Rotterdam waterway, *Hydraulics Laboratory Publ. No. 44*, Delft, 1966.
- Harleman, D. R. F. and Ippen, A. T.: Two dimensional aspects of salinity intrusion in estuaries : analysis of salinity and velocity distributions., *US Army Corps Eng., Comm. Tidal Hydraul., Tech. Bull. No. 13.*, 1967.
- Hoitink, A. J. F., Buschman, F. A., and Vermeulen, B.: Continuous measurements of discharge from a horizontal acoustic Doppler current profiler in a tidal river, *Water Resources Research*, 45, W11 406, 2009.
- Ibrahim, Z. Z., Moi, L. S., Abdullah, R., and Arshad, A.: Classification of Malaysian estuaries for development planning, *Aquatic Conservation: Marine and Freshwater Ecosystems*, 6, 195–203, 1996.
- Ippen, A. T. and Harleman, D. R. F.: One-dimensional analysis of salinity intrusion in estuaries, *US Army Corps Eng., Waterways Experiment Station, Vicksburg, Miss. Tech. Bull. No. 5*, 1961.
- Kuijper, K. and van Rijn, L. C.: Analytical and numerical analysis of tides and salinities in estuaries; part II: salinity distributions in prismatic and convergent tidal channels, *Ocean Dynamics*, 61, 1743–1765, 2011.
- Lacey, G.: Stable channels in alluvium, in: *Minutes of the Proceedings ICE*, vol. 229, pp. 259–292, 1930.
- Lane, E. W.: Design of stable canals, *Trans. ASCE*, 120, 1234–1260, 1955.

- Langbein, W. B.: The hydraulic geometry of a shallow estuary, *International Association of Scientific Hydrology. Bulletin*, 8, 84–94, 1963.
- Lee, J. and Julien, P.: Downstream Hydraulic Geometry of Alluvial Channels, *Journal of Hydraulic Engineering*, 132, 1347–1352, 2006.
- Leopold, L. B. and Maddock, T.: The hydraulic geometry of stream channels and some physiographic implications, *Professional Paper No. 252*, USGS, Washington, DC, 1953.
- Lindley, E. S.: Regime Channels, in: *Punjab Engineering Congress*, vol. 7, pp. 63–74, 1919.
- Moftakhari, H. R., Jay, D. A., Talke, S. A., Kukulka, T., and Bromirski, P. D.: A novel approach to flow estimation in tidal rivers, *Water Resources Research*, 49, 4817–4832, 2013.
- Nguyen, A. D. and Savenije, H. H. G.: Salt intrusion in multi-channel estuaries: a case study in the Mekong Delta, Vietnam, *Hydrol. Earth Syst. Sci.*, 10, 743–754, hESS, 2006.
- Nguyen, A. D., Savenije, H. H. G., van der Wegen, M., and Roelvink, D.: New analytical equation for dispersion in estuaries with a distinct ebb-flood channel system, *Estuarine, Coastal and Shelf Science*, 79, 7–16, 2008.
- Nguyen, D. H., Umeyama, M., and Shintani, T.: Importance of geometric characteristics for salinity distribution in convergent estuaries, *Journal of Hydrology*, 448–449, 1–13, 2012.
- Ong, J. E., Gong, W. K., Wong, C. H., Din, Z., and Kjerfve, B.: Characterization of a Malaysian mangrove estuary, *Estuaries*, 14, 38–48, 1991.
- Perillo, G. M. E.: *Geomorphology and sedimentology of estuaries*, *Developments in sedimentology* 53, Elsevier, Amsterdam, 1995.
- Pethick, J.: *An Introduction to Coastal Geomorphology*, Edward Arnold, London, 1984.
- Pickard, G.: Physical features of British Columbia inlets, *Trans. Roy. Soc. Canada*, 50, 47–58, 1956.
- Pickard, G. L.: Oceanographic Features of Inlets in the British Columbia Mainland Coast, *Journal of the Fisheries Research Board of Canada*, 18, 907–999, 1961.
- Pond, S. and Pickard, G. L.: 13 - Tides, pp. 253–281, *Butterworth-Heinemann*, Oxford, 1983.
- Prandle, D.: Salinity Intrusion in Estuaries, *Journal of Physical Oceanography*, 11, 1311–1324, 1981.
- Pritchard, D.: Salinity Distribution and Circulation in the Chesapeake Bay Estuarine System, *J. Mar. Res.*, 11, 106–123, 1952b.
- Pritchard, D.: Estuarine Circulation Patterns, *Proc. Am. Soc. Civ. Eng.*, 81, No. 717, 1955.
- Pritchard, D. W.: *Estuarine Hydrography*, vol. Volume 1, pp. 243–280, Elsevier, 1952a.

- Pritchard, D. W.: A study of the salt balance in a coastal plain estuary, *J. Mar. Res.*, 13, 133–144, 1954.
- Rigter, B. P. .: Minimum Length of Salt Intrusion in Estuaries, *Journal of the Hydraulics Division*, 99, 1475–1496, 1973.
- Risley, J., Guertin, D., and Fogel, M.: Salinity Intrusion Forecasting System for Gambia River Estuary, *Journal of Water Resources Planning and Management*, 119, 339–352, 1993.
- Sassi, M. G., Hoitink, A. J. F., Vermeulen, B., and Hidayat, H.: Discharge estimation from H-ADCP measurements in a tidal river subject to sidewall effects and a mobile bed, *Water Resources Research*, 47, W06 504, 2011a.
- Sassi, M. G., Hoitink, A. J. F., de Brye, B., and Deleersnijder, E.: Downstream hydraulic geometry of a tidally influenced river delta, *Journal of Geophysical Research: Earth Surface*, 117, F04 022, 2012.
- Savenije, H. H. G.: A one-dimensional model for salinity intrusion in alluvial estuaries, *Journal of Hydrology*, 85, 87–109, 1986.
- Savenije, H. H. G.: Influence of Rain and Evaporation on Salt Intrusion in Estuaries, *Journal of Hydraulic Engineering*, 114, 1509–1524, 1988.
- Savenije, H. H. G.: Salt intrusion model for high-water slack, low-water slack, and mean tide on spread sheet, *Journal of Hydrology*, 107, 9–18, 1989.
- Savenije, H. H. G.: Lagrangian Solution of St. Venant's Equations for Alluvial Estuary, *Journal of Hydraulic Engineering*, 118, 1153–1163, 1992.
- Savenije, H. H. G.: Composition and driving mechanisms of longitudinal tidal average salinity dispersion in estuaries, *Journal of Hydrology*, 144, 127–141, 1993a.
- Savenije, H. H. G.: Determination of Estuary Parameters on Basis of Lagrangian Analysis, *Journal of Hydraulic Engineering*, 119, 628–642, 1993b.
- Savenije, H. H. G.: Predictive model for salt intrusion in estuaries, *Journal of Hydrology*, 148, 203–218, 1993c.
- Savenije, H. H. G.: A simple analytical expression to describe tidal damping or amplification, *Journal of Hydrology*, 243, 205–215, 2001.
- Savenije, H. H. G.: The width of a bankfull channel; Lacey's formula explained, *Journal of Hydrology*, 276, 176–183, 2003.
- Savenije, H. H. G.: *Salinity and Tides in Alluvial Estuaries*, Elsevier, New York, 2005.
- Savenije, H. H. G.: *Salinity and Tides in Alluvial Estuaries*, <http://salinityandtides.com/>, 2 edn., 2012.

- Savenije, H. H. G. and Veling, E. J. M.: Relation between tidal damping and wave celerity in estuaries, *Journal of Geophysical Research: Oceans*, 110, C04 007, 2005.
- Savenije, H. H. G., Toffolon, M., Haas, J., and Veling, E. J. M.: Analytical description of tidal dynamics in convergent estuaries, *Journal of Geophysical Research: Oceans*, 113, C10 025, 2008.
- Schultz, E. A. and Simmons, H. B.: Fresh water-salt water density currents : a major cause of siltation in estuaries, *US Army Corps Eng., Comm. Tidal Hydraul., Tech., Bull. No. 2*, 1957.
- Shaha, D. C. and Cho, Y. K.: Comparison of empirical models with intensively observed data for prediction of salt intrusion in the Sumjin River estuary, Korea, *Hydrol. Earth Syst. Sci.*, 13, 923–933, hESS, 2009.
- Simon, D. B. and Albertson, M. L.: Uniform water conveyance channel in alluvial material, *Trans. ASCE*, 128, 65–107, 1963.
- Singh, V.: On the Theories of Hydraulic Geometry, *International Journal of Sediment Research*, 18, 196–218, 2003.
- SMHB, Ranhill, and Zaaba: Salinity studies for Sg. Rompin and Sg. Sedili Besar, vol. 5 of *Malaysia National Water Resources Study*, DID Malaysia, Malaysia, 2000.
- Smith, R.: Buoyancy Effects upon Longitudinal Dispersion in Wide Well-Mixed Estuaries, *Philosophical Transactions of the Royal Society of London. Series A, Mathematical and Physical Sciences*, 296, 467–496, 1980.
- Thatcher, M.: A mathematical model for the prediction of unsteady salinity intrusion in estuaries, Phd., Sea Grant Project Office, Massachusetts Institute of Technology, 1972.
- Toffolon, M. and Savenije, H. H. G.: DBest: a database of estuarine morphology, 2009.
- Townend, I.: The estimation of estuary dimensions using a simplified form model and the exogenous controls, *Earth Surface Processes and Landforms*, 37, 1573–1583, 2012.
- van Breemen, M.: Salt intrusion in the Selangor estuary in Malaysia: model study with Delft3D., Master, University of Twente, 2008.
- van der Burgh, P.: Ontwikkeling van een methode voor het voorspellen van zoutverdelingen in estuaria, kanalen en zeeen., Tech. rep., 1972.
- Van Os, A. and Abraham, G.: Currents and Salt Intrusion. Lecture Note for the Hydraulic Engineering Course at IHE-Delft, Delft Hydraulics,, 1990.
- van Rees, A. J. and Rigter, B. P.: Flume study on salinity intrusion in estuaries, *Hydraulics Laboratory, Delft*, 1969.
- Volta, C., Arndt, S., Savenije, H. H. G., Laruelle, G. G., and Regnier, P.: C-GEM (v 1.0): a new, cost-efficient biogeochemical model for estuaries and its application to a funnel-shaped system, *Geosci. Model Dev.*, 7, 1271–1295, gMD, 2014.

- West, J. and Broyd, T.: Dispersion coefficients in estuaries, in: ICE Proceedings, vol. 71, pp. 721–737, 1981.
- Williams, G.: Hydraulic geometry of river cross-section- Theory of minimum variance, Professional paper 1029, USGS, Washington DC, 1978.
- Yu, B. and Wolman, M. G.: Some dynamic aspects of river geometry, *Water Resources Research*, 23, 501–509, 1987.
- Zhang, E., Savenije, H. H. G., Wu, H., Kong, Y., and Zhu, J.: Analytical solution for salt intrusion in the Yangtze Estuary, China, *Estuarine, Coastal and Shelf Science*, 91, 492–501, 2011.
- Zimmerman, J. T. F.: Mixing and flushing of tidal embayments in the Western Dutch Wadden Sea, part II: Analysis of mixing processes, *Netherlands Journal of Sea Research*, 10, 397–439, 1976.



## SUMMARY

**E**STUARIES have been used for settlement by humans since 5000-9000 years ago [Day et al., 2012]. The calm environment and nutrient-rich soil encouraged the development of ports and agriculture. Over-development however has put estuaries in unhealthy condition, where the water is polluted (excessive nutrient or salt intrusion problem) and natural morphodynamic equilibrium is disturbed. This implies that the need for effective estuarine management is crucial. Unfortunately, most of the estuaries around the globe are still ungauged, limiting the understanding and knowledge of the underlying hydrological process. Hence, the aims of this study are to: 1) collect and reorganize the existing information available from various sources such as the literature, engineering reports, and open access databases shared by researchers and authorities; 2) conduct field surveys in 7 Malaysian estuaries to expand the database; and 3) develop predictive measures to estimate the two important calibration parameters in salt intrusion (the Van der Burgh and dispersion coefficients), the estuary depth, and the bankfull discharge.

Data collection was carried out in 7 previously un-surveyed Malaysian estuaries during the dry season and near spring tide, from June to August 2012 and February to March 2013. Fundamental data such as cross-sectional area, water level, and salinity were surveyed, starting from the estuary mouth moving landward until a few kilometres beyond the salt intrusion limit. Subsequently, the fully analytical 1-D salt intrusion model of Savenije [1986] was tested on all the newly surveyed estuaries making use of the data collected. Here, the geometry was analysed following a branched exponential function. The cross-sectional data were adjusted in reference to the mean tidal level. The results obtained from the salt intrusion model show that the model is capable of simulating the salinity distribution in comparison to the observed data.

Although the existing predictive equations for the Van der Burgh and dispersion coefficients appeared reliable, there were still some issues to deal with. In this study, several modifications were made to improve the predictive equations. Geometry and salinity data of 30 estuaries worldwide including the newly surveyed were collected and re-analysed to create a consistence data base. Selection of data was made to ensure that only the reliable dataset was applied in the derivation of the predictive equations, using various combinations of dimensionless parameters. Moreover, the seaward boundary location was moved to the inflection point (determined by the geometry analysis) where the system becomes tide dominated. Another reason for shifting the boundary location was to eliminate the dilemma of the downstream boundary location. From analyses, it is found that the predictive coefficients are strongly related to the geometry, tidal strength, friction and the Canter-Cremers estuarine number. The new equation obtained for the dispersion is very satisfying and reliable. On the other hand, the correlation for the Van der Burgh coefficient is slightly lower, implying the equation has to be used with caution. Nevertheless, these predictive equations are adequate to be applied for obtaining a first order estimate of the salt intrusion.

In cases where data are strictly limited, more parameters have to be predicted. In salt intrusion analysis, discharge data is crucial because the salt intrusion length is strongly dependent on the amount of river flow draining into the estuary. Apart from the discharge, the estuary depth is also an important parameter to determine the salt intrusion. Without an extensive field survey, it is nearly impossible to obtain these parameters, especially the discharge. In this study, an effort has been made to find predictive measures that can be applied to estimate depth and discharge. This was done by relating the hydraulic geometry theory of river regime [Lacey, 1930] with the estuary depth estimated using the analytical tidal dynamics solutions of Savenije et al. [2008]. Subsequently, the relation was verified by linking the Canter-Cremers estuarine flood number for bankfull discharge at 1.5-years return period to the estuary shape (represented by the width ratio at the infection point and upstream boundary of the tidal limit). Results show that the relationship between the estuary depth and bankfull discharge can be expressed by a power function with an exponent near to  $1/3$ , in agreement with Lacey's theory. Furthermore, the results obtained from the Canter-Cremers flood number analysis imply that the estuary depth is determined by the bankfull discharge, while the width is determined by the tide. This analysis has demonstrated that the downstream hydraulic geometry theory can also be applied in the estuary region.

In spite of the fact that predictive measures established are useful in making first order estimates of salt intrusion, they are still open for improvements. It is hope that in future more reliable data can be collected and used to strengthen the predictive methods.

# SAMENVATTING

**E**STUARIA worden sinds 5000-9000 jaar geleden door mensen gebruikt [Day et al., 2012]. De rustige omgeving en voedselrijke bodem moedigde de ontwikkeling aan van havens en landbouw. Over-ontwikkeling heeft de estuaria echter ongezond gemaakt, waarbij het water is vervuild (overmatig nutriënt of zoutindringing probleem) en het natuurlijke morfodynamische evenwicht is verstoord. Dit impliceert dat de behoefte aan effectief estuariumbeheer cruciaal is. Helaas zijn de meeste van de estuaria wereldwijd nog ungauged, wat het begrip en de kennis van het onderliggende hydrologische proces beperkt. Vandaar dat de doelstellingen van dit onderzoek zijn: 1) het verzamelen en reorganiseren van de bestaande informatie uit verschillende bronnen, zoals de literatuur, technische rapporten, en open toegankelijke databanken voor gebruik door onderzoekers en overheden; 2) het uitvoeren van veldonderzoek in 7 Maleisische estuaria om de database uit te breiden; en 3) het ontwikkelen van voorspellende vergelijkingen om de twee belangrijkste kalibratieparameters voor zoutindringing in te schatten (de Van der Burgh coëfficiënt en de dispersiecoëfficiënten), de diepte, en de bankfull rivierafvoer.

Gegevens zijn verzameld in 7 niet eerder bemeten Maleisische estuaria tijdens het droge seizoen en in de buurt van springtij, in de periode van juni 2012 tot maart 2013. Fundamentele gegevens zoals de oppervlakte van de dwarsdoorsnede, waterpeil, en zoutgehalte werden gemeten, vanaf de monding landwaartse, tot een paar kilometer voorbij de zoutlimiet. Vervolgens werd het volledig analytische 1-D zoutindringingsmodel van Savenije [1986] getest en toegepast op de nieuw onderzochte estuaria. Hier werd de geometrie geanalyseerd middels een vertakte exponentiële functie. De dwarsprofielgegevens werden aangepast aan het gemiddelde getijniveau. Uit de verkregen modelresultaten blijkt dat het model de zoutverdeling goed kan simuleren.

Hoewel de bestaande voorspellende vergelijkingen voor de Van der Burgh en dispersiecoëfficiënt betrouwbaar schenen, waren er nog een aantal zaken te verbeteren. Geometrie en zoutgehalte gegevens van 30 estuaria wereldwijd, waaronder de onlangs bemeten estuaria, werden verzameld en opnieuw geanalyseerd om een consistente database te creëren. Door selectie van gegevens werd ervoor gezorgd dat alleen de betrouwbare dataset toegepast werd bij de afleiding van de voorspellende vergelijkingen, gebruik makend van verschillende combinaties van dimensieloze parameters. Bovendien werd de zeewaartse randvoorwaarde verplaatst naar het knikpunt (bepaald uit de geometrische analyse) vanwaaraf het systeem getij-gedomineerd is. Een andere reden voor het verschuiven van de randvoorwaarde was de moeilijkheid om de benedenstroomse randvoorwaarde te localiseren. Uit analyses is gebleken dat de voorspellende coëfficiënten sterk gerelateerd zijn aan de geometrie, getijverschil, wrijving en het Canter-Cremers getal. De nieuwe verkregen vergelijking voor de dispersie is zeer bevredigend en betrouwbaar. Aan de andere kant, is de correlatie voor de Van der Burgh coëfficiënt iets lager, wat impliceert dat de vergelijking met zorg moet worden toegepast. Toch zijn deze voorspellende vergelijkingen toereikend om een eerste orde schatting van de zoutindringing

te verkrijgen.

Wanneer er nog minder gegevens beschikbaar zijn, moeten nog meer parameters moeten worden geschat. Voor zoutindringingsanalyse, zijn afvoergegevens cruciaal omdat de zoutindringing sterk afhankelijk is van de rivierafvoer naar het estuarium. Daarnaast is de diepte een belangrijke parameter om de zoutindringing te bepalen. Zonder een uitgebreid veldonderzoek, is het bijna onmogelijk deze parameters te verkrijgen. In deze studie is een poging gedaan om voorspellende vergelijkingen te ontwikkelen om diepte en afvoer in te schatten. Dit werd gedaan door de regime theory van [Lacey, 1930] te gebruiken om de estuarium diepte te bepalen gebruik makend van de analytische oplossingen van Savenije et al. [2008]. Vervolgens werd de relatie geverifieerd door het koppelen van het Canter Cremers getal aan de bankfull afvoer met 1,5 jaar return period. De resultaten tonen aan dat de relatie tussen de diepte en bankfull afvoer door een power-functie kan worden beschreven met een exponent in de buurt van  $1/3$ , in overeenstemming met Lacey's theorie. De resultaten laten zien dat de estuarium diepte wordt bepaald door de bankfull afvoer, terwijl de breedte wordt bepaald door het getij. Deze analyse heeft aangetoond dat de regime theorie ook in estuaria kan worden toegepast.

Ondanks het feit dat de voorspellende vergelijkingen nuttig zijn voor het maken van een eerste orde schatting van de zoutindringing, zijn ze nog open voor verbeteringen. Het is de hoop dat in de toekomst meer betrouwbare gegevens kunnen worden verzameld om de voorspellende methoden te versterken.

# CURRICULUM VITÆ

## Jacqueline Isabella Anak GISEN

02-03-1983 Born in Sarawak, Malaysia.

### EDUCATION

- 1996–2000 Secondary School  
SMK. DPHA Gapor Stampin, Malaysia
- 2001–2006 Undergraduate in Civil Engineering  
University of Technology Malaysia, Malaysia
- 2006–2007 Master in Hydrology and Water Resources  
University of Technology Malaysia, Malaysia
- 2010–2015 PhD. in Water Resources (Estuary)  
Delft University of Technology, the Netherlands  
*Thesis:* Prediction in ungauged estuaries  
*Promoter:* Prof. dr. Ir. Hubert H. G. Savenije

### EXPERIENCES

- 2007–2008 Hydrology and hydraulic engineer  
Sepakat Setia Perunding Sdn. Berhad.  
*Activities:* Hydrology and hydraulic modelling  
River basin and flood management study
- 2008–2010 Structural engineer  
HL Yong Engineering Consultant (civil and structure)  
*Activities:* Structural design and drafting
- 2010–2015 PhD. researcher  
Delft University of Technology  
*Activities:* Developing predictive methods for salt intrusion in ungauged estuaries.  
Leading site measurements in Malaysian estuaries.  
Supervising master students (thesis and field work).



# LIST OF PUBLICATIONS

4. **Gisen, J.I.A.**, Savenije, H.H.G., Nijzink, R.C. and Abd. Wahab, A.K. (2014), *Testing a 1-D Analytical Salt Intrusion Model and its Predictive Equations in Malaysian Estuaries.*, Hydrological Sciences Journal (accepted).
3. **Gisen, J.I.A.**, Savenije, H.H.G., *Estimating bankfull discharge and depth in ungauged estuaries.*, Water Resources Research (under review).
2. **Cai, H.**, Savenije, H.H.G., Gisen, J.I.A., *A coupled analytical model for salt intrusion and tides in convergent estuaries.*, Hydrological Sciences Journal (under review).
1. **Gisen, J.I.A.**, Savenije, H.H.G., Nijzink, R.C., *New predictive Van der Burgh and dispersion equations and methods for their determination.*, Hydrol. Earth Syst. Sci. (submitted).



# ACKNOWLEDGEMENTS

I Am taking this opportunity to express my sincerest gratitude to my promoter, Prof. Dr. Ir. Hubert H.H.G. Savenije for the aspiring guidance and boundless patience he has given to me throughout my PhD journey. I will keep the knowledge that you have shared and passed down to me preciously. Without them, I could never have achieved this mission.

I would like to convey my gratefulness to the Malaysian Ministry of Education and University Malaysia Pahang for giving me this opportunity to pursue my PhD. This could never have happened without the fellowship funding awarded to me. I also like to express my appreciation to the committee members of my PhD defense for sparing your precious time to assess my thesis and attend my defense.

Additionally, many thanks to Kees Kuijper (Deltares), Department of Irrigation and Drainage Malaysia (DID), and National Hydraulic Research Institute of Malaysia (NAHRIM) for their kindness in sharing and providing the survey and hydrological data. Not to forget University Technology Malaysia (UTM) for their support and assistance in completing the field work in Malaysia.

I would like to thank everyone who supported me throughout this PhD journey – my new best buddies in the Netherlands (you know who you are), my officemates, colleagues, and Malaysian friends. Thank you for making my life here more colourful with nice food and keeping me company. Also thanks to my dentist for fixing my missing tooth beautifully.

My warmest thanks to my family members: my parents, sisters, brother, nephews and nieces. Finally, I like to convey my infinitely gratitude to my dearest husband Lim Liang Jin for your unconditional support and unfailing love. Thanks for being there when I needed you the most, especially when I am too busy to cook!

*Jacqueline Isabella Anak Gisen  
Delft, December 2014*